miR-34a negatively regulates alveolarization in a bronchopulmonary dysplasia mouse model

Inaugural Dissertation

submitted to the

Faculty of Medicine

in partial fulfilment of the requirements

for the PhD-Degree

of the Faculties of Veterinary Medicine and Medicine

of the Justus Liebig University Giessen

by

Ruiz Camp, Jordi

of

Barcelona, Catalonia, Spain

Giessen (2017)

From the Institute of Max Planck Insitute for Heart and Lung Research

Director / Chairman: Prof. Dr. Werner Seeger

of the Faculty of Veterinary Medicine or Medicine of the Justus Liebig University Giessen

First Supervisor and Committee Member: Prof. Dr. Klaus-Dieter Schlüter

Second Supervisor and Committee Member: Prof. Dr. Thomas Braun

Committee Members: Prof. Dr. Werner Seeger

Date of Doctoral Defense: 29th of September 2017

1. Table of contents

1. Table of contents 1
2. List of figures 4
3. List of tables 6
4. List of abbreviations 7
5. Introduction 11
5.1 Human lung development 11
5.2 Myofibroblasts during mouse post-natal late lung development 12
5.3 Bronchopulmonary dysplasia 15
5.4 Bronchopulmonary dysplasia animal models 15
5.5 microRNA biology 16
5.6 microRNA in lung development 17
5.7 The miR-34 family 19
6. Hypothesis 21
7. Materials and methods 22
7.1 Materials 22
7.1.1 Technical equipment 22
7.1.2 Chemicals and reagents 24
7.2 Methods 27
7.2.1 Animal experiments 27
7.2.1.1 AntagomiR-34a and target-site blocker injections *in vivo* 27
7.2.1.2 Transgenic animals 27
7.2.2 Cell culture 28
7.2.2.1 Primary fibroblast isolation, seeding and transfection 28
7.2.2.2 Seeding and transfection of mouse lung fibroblast cell line 29
7.2.2.3 Target-site blockers and miR-34a mimic co-transfection 29
7.2.3 Confocal microscopy 29

7.2.3.1.1 Lung fixation and embedding 29
7.2.3.1.2 Staining 30
7.2.4 Design-based stereology 30
7.2.4.1.1 Lung fixation followed by plastic embedding 30
7.2.4.1.2 Stereological measurements 31
7.2.5 Fluorescence-activated cell sorting 31
7.2.5.1.1 Whole-lung cell suspension preparation 31
7.2.5.1.2 Staining 33
7.2.5.2 PDGFRα^{+} cell sorting followed by amplification of miR-34a by real-time quantitative PCR 34
7.2.6 Real-time quantitative PCR analyses 34
7.2.6.1.1 Real-time quantitative PCR of cDNA from mRNA 34
7.2.6.1.2 microRNA real-time quantitative PCR 35
7.2.7 Statistical analysis 36
7.2.8 Western blot 36
7.2.9 β-galactosidase activity detection 37
7.2.10 Elastin visualization 38
8. Results 39
8.1 miR-34a expression in the bronchopulmonary dysplasia animal model 39
8.2 miR-34a global deletion improved the lung structure in the bronchopulmonary dysplasia animal model 39
8.3 Cellular localization of miR-34a in the mouse lung 42
8.4 miR-34a interacts with *Pdgfra* mRNA in the bronchopulmonary dysplasia animal model 43
8.5 The role of miR-34a in PDGFRα^{+} cells in the bronchopulmonary dysplasia animal model 44
8.6 miR-34a, interacting with *Pdgfra* mRNA, is capable of partially impairing alveoli formation 47

8.7 Therapeutic intervention to block miR-34a function in the bronchopulmonary dysplasia animal model 48

8.8 miR-34a negatively regulates the PDGFRα^{+} cell population in the lungs of mice maintained under hyperoxic conditions 52

8.9 miR-34a is partially responsible for the increased apoptosis observed in the bronchopulmonary dysplasia animal model 56

8.10 Dysfunctionality of miR-34a under hyperoxic conditions leads to a decrease in apoptosis in almost every cell-type evaluated. 58

8.11 miR-34a is responsible for the thickened septa: what cells constitute the thickened alveolar septum? 61

9. Discussion 63

10. Summary 71

11. Zusammenfassung 72

12. Bibliography 74

13. Acknowledgements 81

14. Declaration 822

15. Appendix 83

2. List of figures

Figure 1. Human lung developmental stages 12

Figure 2. Post-natal late lung development 14

Figure 3. Lung structure when aberrant mouse late lung development is caused by hyperoxia exposure 16

Figure 4. miR synthesis in the cell 18

Figure 5. Comparison of the *Mus musculus* miR-34 family members. 20

Figure 6. Stereological measurements in mouse lungs employing Visiopharm® software 32

Figure 7. miR-34a expression is strongly up-regulated in mouse lungs under hyperoxic conditions 40

Figure 8. miR-34a plays an important role during aberrant secondary septation caused by hyperoxia 41

Figure 9. miR-34a is highly expressed in PDGFRα^{+} cells *in vivo* in mouse lungs undery hyperoxic conditions....44

Figure 10. The *Pdgfra* expression is down-regulated in mouse lungs under hyperoxic conditions 45

Figure 11. Deletion of miR-34a enhanced alveologenesis in the lungs of mice under hyperoxic conditions 46

Figure 12. The miR-34a-*Pdgfra* mRNA interaction is partially responsible for the worsening of the lung structure in mouse pups maintained under hyperoxic conditions 49

Figure 13. The miR-34 family is involved in the blunted secondary septation in the lungs of mice maintained under hyperoxic conditions....51

Figure 14. Analysis of mesenchymal cells by FACS....53

Figure 15. Myofibroblast abundance in the lung is partially restored in mice treated with antagomiR-34a in the bronchopulmonary dysplasia animal model 54

Figure 16. Better organised elastin foci were observed in the developing lungs of mice treated with antagomiR-34a in the bronchopulmonary dysplasia animal model.....55

Figure 17. Gating strategy for annexin V^+ or $Ki67^+$ cells by FACS analysis.....56

Figure 18. AntagomiR-34a administration reduced apoptosis but not cell proliferation levels in mouse lungs in the bronchopulmonary dysplasia animal model 57

Figure 19. Reduction of apoptosis in different cell-types of the lung after blockade of miR-34a in mice maintained under hyperoxic conditions 59

Figure 20. Quantification of apoptotic epithelial and myofibroblast cells in the lung of mice treated with antagomiR-34a under hyperoxic conditions 60

Figure 21. The cell composition of the septa after anatagomiR-34a injection in mice maintained under hyperoxic conditions 62

Figure 22. Comparison between the different treatments which blocked miR-34a function in mice maintained under hyperoxic conditions 66

3. List of tables

Table 1. List of the different locked nucleic acids injected to mouse pups.....27

Table 2. List of primers employed to assess gene expression 35

Table 3. List of primers employed to assess miR expression 36

Table 4. Stereological analysis of lungs from miR-34a$^{-/-}$ mice maintained under normoxic or hyperoxic conditions compared to wild-type controls 42

Table 5. Structural parameters of mouse lungs carrying a deletion of miR-34a in PGDFRα^{+} cells in the bronchopulmonary dysplasia animal model 47

Table 6. Structural parameters of lungs from mice treated with scrambled antagomiR or target-site blocker maintained under hyperoxic conditions.....50

Table 7. Structural parameters of lungs from mice treated with scrambled antagomiR or antagomiR-34a in the bronchopulmonary dysplasia animal model 52

4. List of abbreviations

AEC1	alveolar epithelial cell-type 1
AEC2	alveolar epithelial cell-type 2
Ago	argonaute
alv	alveoli
alv air	alveolar airspaces
alv epi	alveolar epithelium
AntmiR34a	antagomiR-34a
APC	allophycocyanin
APS	ammonium persulfate
AQP5	aquaporin 5
B	bridge
Bcl-2	B cell lymphoma-2
bp	base pair(s)
BPD	bronchopulmonary dysplasia
BSA	bovine serum albumin
CD31	cluster of differentiation 31
CD45	cluster of differentiation 45
CD140a	cluster of differentiation 140a
Chr	chromosome
CV	coefficient of variation
CY3	cyanine 3
CY7	cyanine 7
DAPI	4',6-diamidino-2-phenylindole
DMEM	Dulbecco’s modified Eagle medium

DMSO	dimethyl sulfoxide
E	embryonic day
ECM	extracellular matrix
EDTA	Ethylenediaminetetraacetic acid
EGTA	Triethylene glycol diamine tetraacetic acid
EMEM	Eagle's minimum essential medium
EpCAM	epithelial cell adhesion molecule
FACS	fluorescence-activated cell sorting
FCS	fetal calf serum
FITC	fluorescein
g	gram
h	hour
HEPES	hydroxyethyl-piperazineethane-sulfonic acid
HRP	horseradish peroxidase
iΔPC	inducible deletion in platelet-derived growth factor receptor α^+ cells
IL-6-R	interleukin 6 receptor
LNA	locked nucleic acid
M	mark
mg	milligram
miR	microRNA
ml	mililliter
MLI	mean linear intercept
mmu	*Mus musculus*
µg	microgram

µl	microliter
µm	micrometer
µM	micromolar
N	number
nm	nanometer
non-par	non-parenchyma
Nv	numerical density
P	point in stereology counting
P	post-natal day
P	to document significances in data analysis
par	parenchyma
PFA	paraformaldehyde
PCR	polymerase chain reaction
PBS	phosphate buffered saline
PDGFA	platelet derived growth factor ligand a
PDGFB	platelet derived growth factor ligand b
PDGFC	platelet derived growth factor ligand c
PDGFD	platelet derived growth factor ligand d
PDGFRα	platelet derived growth factor receptor α
PDGFRβ	platelet derived growth factor receptor β
Polr2a	RNA polymerase II
proSP-C	prosurfactant protein c
P/S	penicillin and streptomycin
qPCR	quantitative PCR
rpm	revolutions per minute

RT	reverse transcription
s	seconds
S	surface area
SCR	scrambled
SEM	standard error of the mean
sep	septa
SP-C	surfactant protein-c
S_v	surface density
αSMA	α smooth muscle actin
TEMED	N,N,N´,N´-tetramethylethane-1,2-diamine
TRBP	human immunodeficiency virus transactivating response RNA-binding protein
TSB	target-site blocker
τ (sep)	mean septal wall thickness
UTR	untranslated region
V	volume
Vv	volume density
WT	wild-type
X-Gal	5-bromo-4-chloro-3-indolyl β-D-galactopyranoside

5. Introduction

5.1 Human lung development

The main function of the lung is to be the organ where atmospheric oxygen is transported into the bloodstream and, at the same time, carbon dioxide is directed towards the outside of the body. This gas exchange takes place across the alveolo-capillary barrier, composed of several types of cells interacting with each other, located inside the alveolar unit (32). To facilitate proper gas exchange function, the lung is organised into tubular networks to achieve the maximum surface area possible within the organ (44). Using an analogy, the lung could be compared to a tree that branches in a fractal way trying to optimize the surface area to carry out the maximum amount of gas exchange in the minimum possible space.

Mammalian lung development is a temporally and spatially organised process which can be divided into two main periods: early lung development, during the embryonic stage; and, late lung development, which occurs after birth until the lung is ultimately mature. Human lung development can be described by a sequence of different developmental stages (**Fig. 1**). In first instance, lung buds form from the ventral wall of the foregut and this will result in the lung lobar division. This is the initial step known as embryonic stage which starts at week four and lasts until week five of the embryonic period. Then, the pseudoglandular stage, which starts at week five and ends at week 17th of the fetal period, is characterized by major airway branching and epithelial tube formation, in close contact with the mesenchymal cells. The canalicular stage follows the pseudoglandular stage from week 16 to week 25 of the fetal period. In this canalicular stage, respiratory bronchioles are formed leading to an increased number of capillaries surrounding the cuboidal epithelium, which initiates alveolar development. Then, alveolar ducts and air sacs originate during the saccular stage, from week 24 to week 40 before birth. Finally, both alveoli and capillary number increase after secondary septation takes place, which consists of growing crests of cells that will cross from one side to another side of the alveolar walls, closing the alveolar space to form the small but functional alveoli units. Secondary septation occurs during the late fetal stage until eight years of life after birth, and this stage is known as the alveolar stage, in which the lung reaches maturity (13, 66).

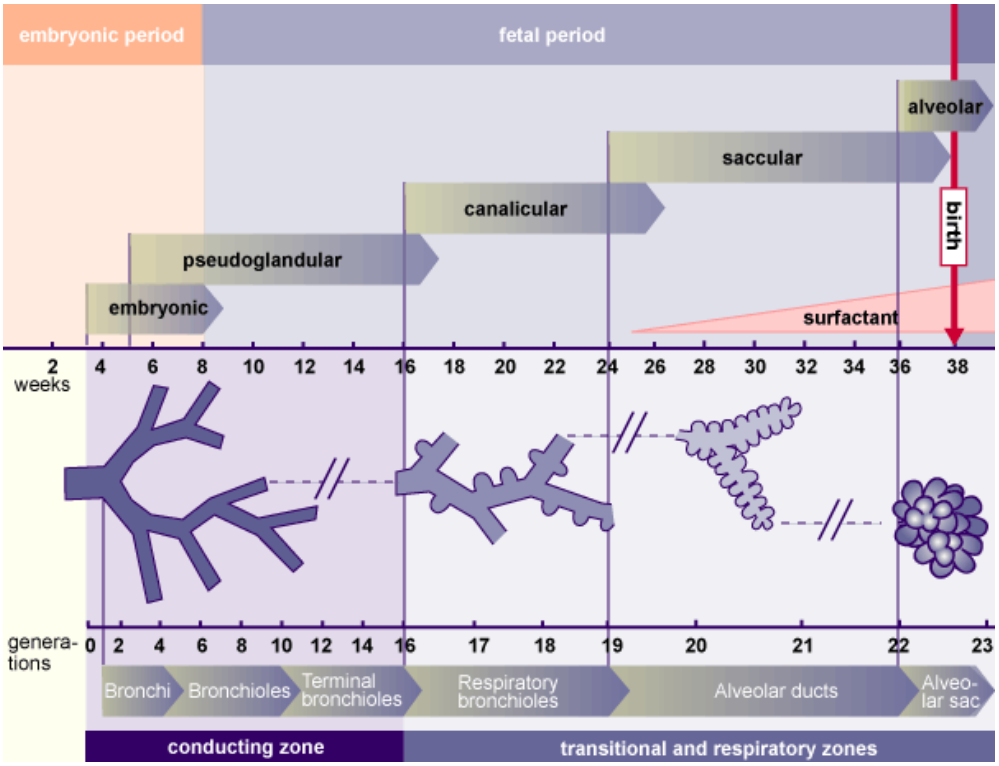

Figure 1. Human lung developmental stages. The five stages of human lung development: the embryonic, pseudoglandular, canalicular, saccular and alveolar developmental stages. Picture from (62).

5.2 Myofibroblasts during mouse post-natal late lung development

Human and mouse lung development are similar except for the timing of the developmental stages, since the gestation period is different between mouse and human. The mouse lung starts developing at embryonic day (E)8 and finishes at post-natal day (P)21.5 which is considered the beginning of adulthood (22). It is in the saccular stage (E17.5-P5.5) where the lung forms the alveolar sacs within which secondary septation occurs during the alveolar stage (P5.5-P21.5) (16). The main difference between mouse and human lung development is that the mouse lung undergoes the saccular stage after birth, which continues until P3.5.

During the saccular stage, epithelial bipotential cells in the distal tubules transdifferentiate into two different mature alveolar epithelial cell types, cell-type 1 (AEC1) cells or into alveolar epithelial cell-type 2 (AEC2) cells (**Fig. 2**) (61) which is crucial for proper alveoli formation. In the alveolar stage, secondary septation starts

from ridges on the alveolar wall, and stromal cells migrate towards the septal wall and differentiate into perycites, lipofibroblasts, and myofibroblasts, amongst other uncharacterized cell lineages (28, 29, 55). Lipofibroblasts, which are fibroblasts containing lipid droplets, are described to reside close to AEC2 cells forming a niche supporting surfactant phospholipid synthesis by AEC2 cells (60) and producing ECM compounds (43). On the other hand, myofibroblasts are located at the tips of the growing septa (**Fig. 2**) where myofibroblasts will become the main elastin and collagen producers, creating a proper ECM for cells to grow up on, and to migrate through [9, 18]. Thus, the growing septa, composed of epithelial and mesenchymal cells interacting with each other, close the alveolar sacs into smaller and functional alveolar units, thereby increasing the gas exchange surface area which takes place at the epithelial-endothelial interface.

The mesenchymal α smooth muscle actin $(SMA)^+$ myofibroblast abundance reaches a maximum level during secondary septation (P5.5-P12.5) (42) but this myofibroblast abundance slowly decreases as the lung matures, with myofibroblasts becoming a very rare cell-type in the adult lung with primarily homeostatic and tissue repair functions. These αSMA^+ myofibroblasts are characterized by the expression of the platelet-derived growth factor receptor (PDGFR)α (41) that together with PDGFRβ interact with the platelet-derived growth factor (PDGF) family of ligands, which is formed by four ligands, PDGFA, PDGFB, PDGFC and PDGFD. These ligands need to form dimers in order to bind the receptors and form the dimers AA, AB, BB, CC and DD. The PDGFA ligand solely interacts with the PDGFRα; the PDGFB and the PDGFC interact with both PDGFRα and PDFGRβ; while, PDGFD interacts only with the PDFGRβ (6). All these ligands and receptors are important molecules for the proper development of many organs in mammals.

In the lung, PDGFs play important roles in regulating the proliferation, migration and transdifferentiation of mesenchymal cells during embryonic and late lung development (5). Particularly, PDGFA is expressed in the epithelial cells of the alveolar sacs and PDGFRα is expressed in myofibroblasts (6). This PDGFA-PDGFRα signalling is required for a proper myofibroblast transdifferentiation during secondary septation, and, subsequently, for a proper lung alveolarization. The first study reporting the need for the activation of the PDGFA-PDGFRα signalling pathway was based on genetic abrogation of PDGFA expression in developing mice

(11). The lack of PDGFA in epithelial cells translated into a lack of alveolar myofibroblasts specifically in the alveolar air spaces, thus impairing secondary septation in mouse lungs (10). Additionally, very low levels of elastin were detected in the PDGFA-null mouse lungs since myofibroblasts were absent. These data revealed a pivotal role for the PDGFRα signalling pathway in epithelial mesenchymal cross-talk during secondary septation, which facilitates proper cell migration and differentiation leading to correct lung maturation.

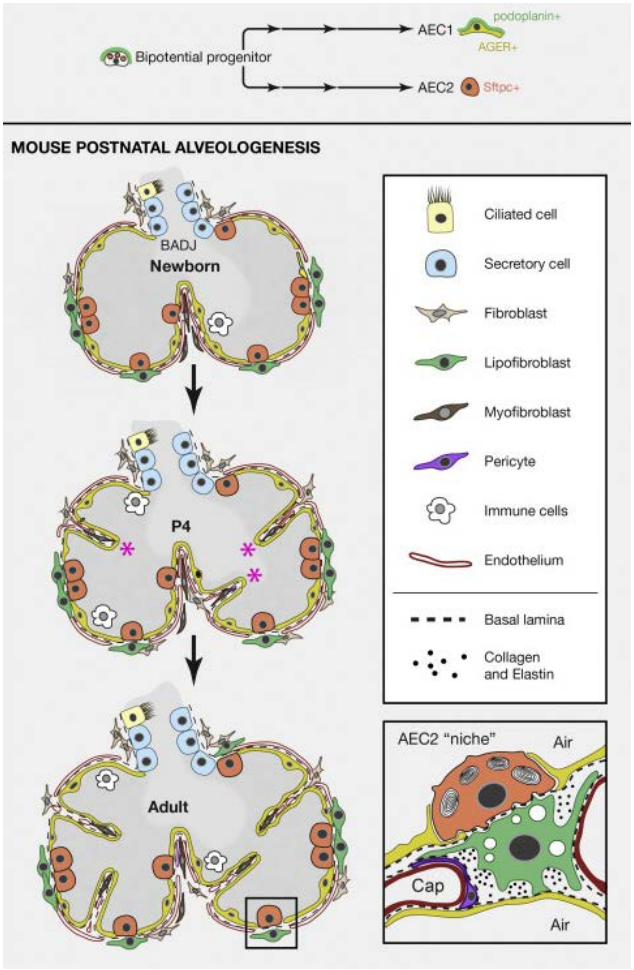

Figure 2. Post-natal late lung development. Upper panel, cell lineages of a bipotential progenitor which can differentiate into alveolar epithelial cell-type 1 (AEC1) or alveolar epithelial cell-type 2 (AEC2) cells. Lower panel, formation of secondary crests during late lung development in mice. At P4.5, the epithelial-mesenchymal cross-talk leads the formation of bridges that will close the alveolar spaces into small functional alveoli. Myofibroblasts are located at the tips of the growing septa and will lead the migration and differentiation of the different cells of the alveolar region by producing extracellular matrix compounds, such as elastin or collagen, and secreting growth factors. BADJ, bronchoalveolar duct junction; Cap, capillary. Image adapted from (29).

5.3 Bronchopulmonary dysplasia

Despite the fact that the scientific community still poorly understands the mechanisms of new alveoli generation, there is one fact certainly well accepted: secondary septation can be blunted in preterm newborns resulting in a poorly-alveolarized adult lung which performs poorly in terms of gas exchange function. This rare disease was firstly described by Northway et al. in 1967 and received the name bronchopulmonary dysplasia (BPD) (51).

Bronchopulmonary dysplasia is a long-term lung complication with high prevalence in preterm infants, particularly those with birth weights <1,250 g (2). Phenotypically, this disease can be divided into two categories: “old” and “new” BPD, with the “new” variant being the prevalent variant today. This different prevalence between the “old” and “new” BPD is due to the evolution of interventions to reduce the morbidity and mortality in preterm infants. Today, the intervention emphasises reduced mechanical ventilation with a lower concentration of oxygen (40%), in contrast to the initial protocol that triggered the “old” and more severe BPD (47). The development of BPD is multifactorial, and includes lung immaturity, volutrauma, inflammation, and oxygen toxicity (38). The aim of studying the biology behind lung development is to solve the enigma of how the tightly regulated process of creating functional alveoli works under normal conditions and why this process is arrested in BPD.

5.4 Bronchopulmonary dysplasia animal models

Different animal models are employed to mimic human BPD, and are based on different stimuli (such as hyperoxia exposure or mechanical ventilation, or both combined), which will lead to a BPD-like phenotype, in order to study human BPD (58). In our laboratory, the BPD animal model is based on hyperoxia (85% O_2) exposure of newborn mouse pups from the day of birth (39, 46, 57). This excess of oxygen triggers a failure of secondary septation and, subsequently, a failure of alveologenesis, a thickening of the alveolar septa, and irregular vascular growth (**Fig. 3**).

The aim of modelling BPD in mice is to unravel responsible mechanisms that lead to blunted secondary septation. Although these mechanisms are poorly understood, previous studies have reported some mechanisms that might explain the failure of

alveolarization in newborn mice exposed to hyperoxia. The abundance of PDGFRα protein was decreased in neonatal lung mesenchymal stromal cells from infants who developed BPD (54). Others have reported that elastic fibres are irregularly distributed and elastin deposition is decreased in mice exposed to 85% O_2 due to aberrant lysyl oxidase expression (46). Interestingly, the intervention with the broad-spectrum lysyl oxidase inhibitor, β-aminopropionitrile, in mice exposed to hyperoxia could not reverse the diminished number of alveoli observed. Furthermore, there is clear evidence that lungs of mice maintained under hyperoxic conditions express higher levels of pro-inflammatory interleukin-6 and lower levels of anti-inflammatory interleukin-10 in comparison to healthy pups (39). Studies performed on baboons ventilated with 100% O_2 reported increased levels of nuclear p53 and p21, a downstream target of p53, probably due to increased oxidant DNA damage (40). Despite these observations, the main mechanisms of the normal late lung development and aberrant late lung development caused by hyperoxia remain unclear. Thus, BPD animal models have identified perturbations to fibroblast subpopulation, ECM metabolism, inflammation, and cell proliferation and death as candidate pathomechanisms at play in BPD.

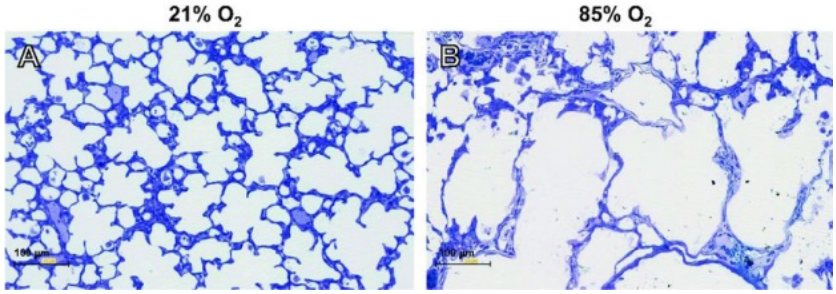

Figure 3. Lung structure when aberrant mouse late lung development is caused by hyperoxia exposure. A) Normal late lung development where the lung is fully alveolarized. **B**) Aberrant late lung development caused by hyperoxia exposure where the lung did not develop proper alveoli. Image adapted from reference (39).

5.5 microRNA biology

In the last decade, the field of microRNA (miR) began to be explored in order to understand the molecular biology of organ development with some studies addressing early lung development (58). The miRs are short (20-23 nucleotide), endogenous regulators of gene expression during development, as well as in tissue

homeostasis, and disease. Evolutionarily, miRs have been identified in plants and animals, and are conserved between species. The miR clusters are transcribed in the nucleus and pre-miRs are exported to the cytoplasm where Dicer, in complex with the human immunodeficiency virus transactivating response RNA-binding protein (TRBP), will cleave the miR hairpin into two mature strands: the 5p and the 3p strands. Then, the mature miR together with argonaute (Ago) will carry out the main function of miRs which is the inhibition of protein translation by targeting several mRNA species at the same time, in the same or different cells (**Fig. 4**) (64). This capability to inhibit different targets at once confers to the miRs importance as molecules holding a proximal rank in a gene regulation hierarchy.

5.6 microRNA in lung development

Although miR function is not completely understood, the involvement of miRs in the physiology and different pathologies of the lung has recently been reported in normal lung development, the inflammatory response, smoking-related disease, and lung cancer (48). Related to lung development, the expression of the enzyme Dicer was observed in the distal branching regions while Ago1 and Ago2 were expressed in the epithelium and mesenchyme, respectively, at E11.5 (36). Interestingly, the abrogation of Dicer expression in the epithelium resulted in defective lung branching and large fluid-filled alveolar sacs exhibiting a detached epithelium from the mesenchyme at E15.5 in developing mouse lungs (26). These findings highlighted the importance of miRs in the epithelial-mesenchymal cross-talk required for proper secondary septation. Additionally, miRs encoded by the miR-17-92 cluster promoted proliferation and inhibited differentiation of the epithelial progenitor cells at E18.5 in the lung, revealing that miRs can regulate cell fate during development (37).

In the BPD context, certain studies have claimed a correlation between the dysregulated expression level of several miRs and the lack of secondary septation in rodent lungs. For example, it has been reported that miR-489 expression level was upregulated, and, after antagomiR-489 injection (to block miR-489) the lung structure of those mice exposed to hyperoxia improved (53). Other studies aimed at a more broad detection of miRs that changed in expression during normal and aberrant late lung development by performing microarrays. In this line, a miR microarray

performed with rat lungs exposed to hyperoxia revealed the expression of miR-335-5p, miR-150-5p, miR-126-3p and miR-151-5p down-regulated, whereas the expression of miR-21-5p and miR-34a-5p was up-regulated (7). However, none of these dysregulated miRs were further characterized and it is still is not well understood what function these miRs exert in the lung, as the studies lack functional experiments *in vivo*.

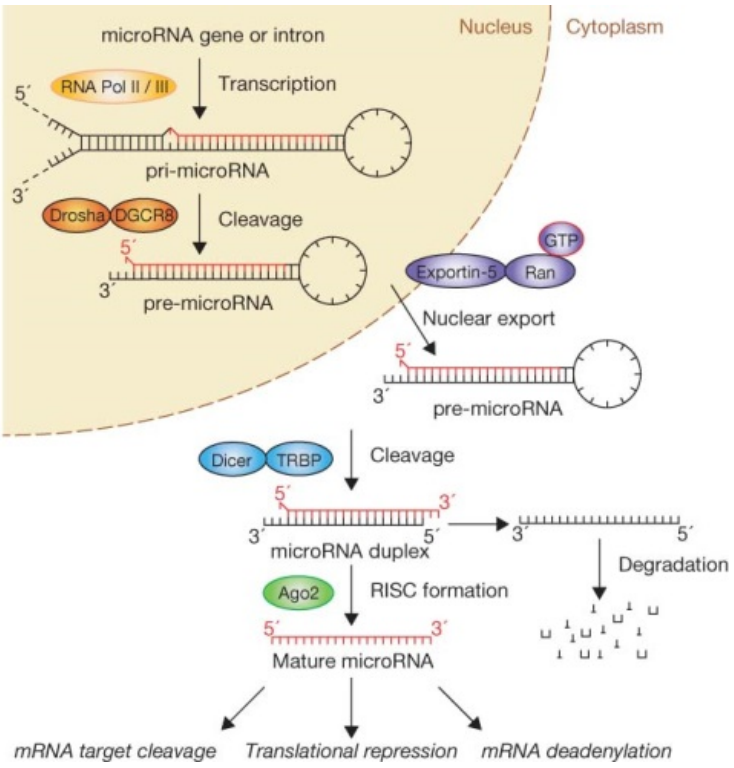

Figure 4. miR synthesis in the cell. The biogenesis of miRs is a multistep process starting in the nucleus where miRs are transcribed as “normal” genes under the control of a promoter. In general, miRs are transcribed by RNA polymerase II or III and this will generate the pri-miR which is cleaved by the Drosha in complex with DiGeorge syndrome critical region 8 (DGCR8) protein in the nucleus, generating the pre-miR. This pre-miR is exported to the cytoplasm by Exportin-5-Ran-GTP where RNase Dicer in complex with double-stranded RNA-binding protein (TRBP) will cleave the pre-miR hairpin achieving mature length. In these processes, every miR has two complementary strands: the leading (named 5p), believe to exert the function, and the complementary strand (named 3p), believed to be degraded. As a result, the functional miR will be part of the RNA-induced silencing complex (RISC) formation, together with argonaute 2 (Ago2) protein, for a subsequent silencing of mRNA targets by means of cleavage, translational repression or deanylation. Image adapted from (64).

5.7 The miR-34 family

In our laboratory, a miR microarray comparing whole-lung homogenates from mice exposed either to normoxia or hyperoxia, with total RNA isolated at different time-points (P3.5, P5.5 and P14.5) was carried out. The analysis revealed several dysregulated miRs when the normoxia and hyperoxia groups were compared, particularly during secondary septation, at P5.5. From these data, a single miR exhibited up-regulated expression levels at both P5.5 and P14.5: miR-34a.

The miR-34 family consists of several members, miR-34a, miR-34b and miR-34c (**Fig. 5**) which shares the seed sequence with the miR-449 family. The location of miR-34a is on chromosome (Chr) 4 whereas miR-34b and miR-34c are located on Chr 9, and are regulated by the same promoter, forming a gene cluster called *mirc21* (25). Both the miR-34 and miR-449 families are implicated in important biological functions such as cell proliferation and differentiation. For example, miR-449 suppresses cell proliferation and promotes apoptosis once activated by E2F transcription factor 1 (35) and miR-449a is involved in mucociliary airway cell differentiation during normal lung development (34). Conversely, miR-34a is proposed as a new anti-cancer weapon (45) since miR-34a is reported to play a role in a variety of cancers (not only in the lung) as miR-34a is a downstream transcriptional target of P53, the apoptotic mediator. It has been described that ectopic expression of miR-34a induces cell cycle arrest in tumor cells (27). A different study revealed that transient miR-34a transfection in glioma and medulloblastoma cell-lines triggered inhibition of cell proliferation, arresting the cell cycle and decreasing cell survival and cell invasion (33). This tumor-suppressor action is explained by the function of miR-34a mRNA targets. To give some examples, some of the validated miR-34a targets are: B cell lymphoma-2 (Bcl-2) which is involved in apoptosis (17); cyclin E and cyclin D which are involved in cell cycle arrest (20); and, Notch1 which is a relevant signalling molecule involved in several cell functions (56). However, the role that miR-34a plays in normal and aberrant late lung development remains unknown.

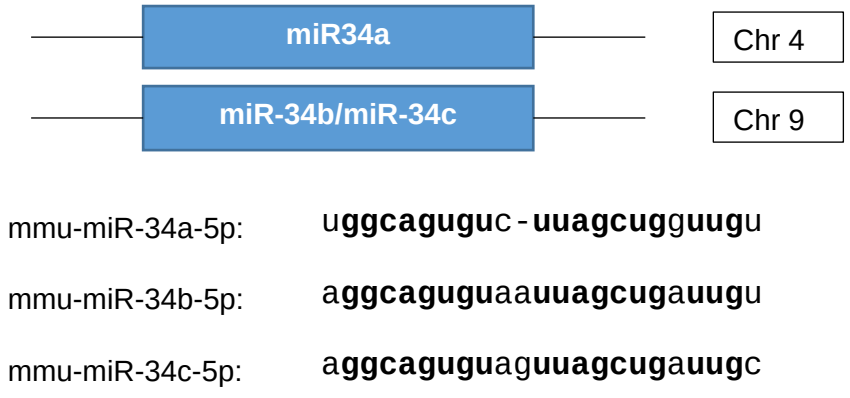

Figure 5. Comparison of the *Mus musculus* miR-34 family members. While miR-34a is located in chromosome (Chr) 4, miR-34b and miR-34c, regulated by the same promoter, are located in the chromosome 9. The sequence of each miR-34 family member is compared and the shared nucleotides are highlighted in bold letters. mmu, *Mus musculus*

In this project, the aim was to study the function of a miR which we demonstrated to be dysregulated in developing mouse lungs under hyperoxic conditions. In detail, we selected the miR-34 family that targeted *Pdgfra* mRNA, an interaction that was informatically predicted (23) and validated in lung cancer cells (24). The general deletion of miR-34a, the deletion of miR-34a in PDGFRα^{+} cells and the abolished interaction between miR-34a and *Pdgfra* mRNA in mice exposed to hyperoxia all resulted in a better alveolarization of developing mouse lungs. On the other hand, myofibroblast abundance was increased, and this correlated with better secondary septation when miR-34a function was blocked in mice exposed to hyperoxia. Overall, blocking miR-34a under hyperoxic conditions triggered better cell organization in the lung and a generalized decrease in apoptosis. Summing up, miR-34a negatively modulated the fate of PDGFRα^{+} cells, therefore, diminishing myofibroblast transdifferentiation and interrupting epithelial-mesenchymal cross-talk, leading to alveologenesis failure in a BPD mouse model.

6. Hypothesis

Bronchopulmonary dysplasia (BPD) was first described in 1967 as a chronic respiratory condition that developed in premature infants after mechanical ventilation with elevated oxygen levels (13). Although BPD is considered a rare lung disease, many preterm infants develop this lung disease and treatments for BPD are still not fully established. For this purpose, a better comprehension of lung biology, in terms of normal or altered late lung development, is required.

Over the past decades, it has been reported that lung development is time- and spatial-dependent and that there are some rare but relevant cell-types required for proper alveoli formation, named myofibroblasts. Myofibroblasts, regulated by a key receptor named platelet-derived growth factor receptor (PDGFR)α, are essential for proper epithelial-mesenchymal cross-talk. Epithelial and mesenchymal cells communicate with one another to form the secondary crests which will grow and divide the alveolar sacs into smaller alveolar units. Regarding aberrant late lung development, it has been reported that PDGFRα protein levels are down-regulated in patients suffering from BPD (53). Along these lines, a remarkable study where PDGFRα signalling was impaired, myofibroblast abundance was low and alveolarization failed in mouse lungs under normal conditions (11), positioning PDGFRα as a key regulator of late lung development. In addition, other studies regarding BPD revealed a down-regulation of tropoelastin expression (12), and a dysfunctional extracellular matrix (ECM) deposition in the growing secondary crests in mouse lungs under hyperoxic conditions (46). Therefore, it was hypothesised that miR-34a played a role in lung alveolarization by interacting with *Pdgfra* mRNA and modulating the PDGFRα^{+} cell lineage in normal and aberrant late lung development caused by hyperoxia.

Objective of the project:

This project attempted to delineate the role of miR-34a in both normal late lung development and aberrant late lung development caused by hyperoxia. To this end, several *in vivo* approaches based on modulating miR-34a function were carried out, such as antagomiR-34a (AntmiR34a) or target-site blocker (TSB) administration, or the use of miR-34a global knockout transgenic mice.

7. Materials and methods

7.1 Materials

7.1.1 Technical equipment

BD LSRII flow cytometers run by DIVA software, BD Biosciences, USA

BD FACSAriaIII run by DIVA software, BD Biosciences, USA

Cell culture sterile working bench, Thermo Scientific, USA

Cell strainers: 100, 40 and 20 µm, Fisher Scientific, USA

Countess® cell counter, Invitrogen, UK

Espresso personal microcentrifuge, VWR, USA

GentleMACS dissociator; Miltenyi Biotech, Germany

InoLab® pH meter, WTW, Germany

Isoplate™ B&W 96-well plate, PerkinElmer, USA

Leica microscope DM6000B, Leica, Germany

Laser scanning microscope (LSM) 710, Zeiss, Germany

MicroAmp® FAST 96-well reaction plate, Applied Biosystems, USA

Microcentrifuge tubes: 0.5, 1.5 and 2 ml, Eppendorf, Germany

Minispin® centrifuge, Eppendorf, Germany

Multifuge 3 S-R centrifuge, Heraeus, Germany

NanoZoomer XR C12000 Digital slide scanner, Hamamatsu, Japan

NanoDrop® ND 1000, PeqLab, Germany

Pipetboy, Eppendorf, Germany

Pipetmans P2, P10, P100, P200 and P1000, Eppendorf, Germany

Pipetman filter tips: 10, 20, 100, 200 and 1000 µl. Greiner Bio-One, Germany

Precellys®24 Homogenizer, PeqLab, Germany

Refrigerated microcentrifuge CT15RE, VWR, USA

Serological pipettes of 2, 5, 10, 25 and 50 ml, Falcon, USA

StepOnePlus™ PCR system, Applied Biosystems, USA

Vortex mixer, VWR, USA

Microtome LEICA SM 2500, Leica, Germany

Microtome LEICA CM 3050, Leica, Germany

7.1.2 Chemicals and reagents

Agarose; Promega, Germany

Bovine serum albumin; Sigma-Aldrich, Germany

Bromophenol blue; Sigma-Aldrich, Germany

5-Bromo-4-chloro-3-indolyl β-D-galactopyranoside; Sigma-Aldrich, Germany

Calcium chloride; Sigma-Aldrich, Germany

Collagenase; Sigma-Aldrich, Germany

Complete™ protease inhibitor cocktail; Roche, Germany

Dimethyl sulfoxide; Sigma-Aldrich, Germany

Dispase; BD Biosciences, USA

Dithiothreitol; Sigma-Aldrich, Germany

DNase I; Serva, Germany

dNTP mix; Promega, USA

Dulbecco's modified Eagle medium; Sigma-Aldrich, Germany

Dulbecco's phosphate buffered saline 10×; PAA Laboratories, Austria

Phosphate-buffered saline 1×; PAA Laboratories, Austria

Eosin; Sigma-Aldrich, Germany

Eagle's minimum essential medium; ATCC, USA

Ethanol 70% (v/v); SAV-LP, Germany

Ethanol 99% (v/v); J.T. Baker®, Netherlands

Ethanol absolute; Honeywell Riedel-de Haën™, Germany

Ethidium bromide; Promega, USA

Ethylenedinitrilo-tetraacetic acid; Sigma-Aldrich, Germany

Triethylene glycol diamine tetraacetic acid; Sigma-Aldrich, Germany

Fetal bovine serum; ATCC, USA

Fluorescence-activated cell sorting staining buffer, eBioscience, USA

Formamide; Fluka, Germany

Gamunex; Bayer Healthcare, Germany

Giemsa's azur eosin methylene blue solution; Merck, Germany

Glutaraldehyde 50% (v/v); Sigma-Aldrich, Germany

Glycol methacrylate; Heareus Kulzer, Germany

Hydroxyethyl-piperazineethane-sulfonic acid buffer; PAA Lab, Austria

HiPerFect reagent; Qiagen, USA

Hydrochloric acid; Sigma-Aldrich, Germany

Isoflurane; CP-Pharma, Germany

Laemmli buffer; Bio-rad, Germany

Lipofectamine 2000®; Thermo-Fisher, Germany

Magnesium chloride; Sigma-Aldrich, Germany

Magnesium chloride, 25 mM; Applied Biosystems, USA

Methanol; Fluka, Germany

Miglyol 812; Cäesar & Lorentz, Germany

miRNeasy® Mini kit; Qiagen, USA

miScript®II RT kit; Qiagen, USA

miScript SYBR® Green PCR Kit; Qiagen, USA

MuLV reverse transcriptase; Applied Biosystems, USA

Nonidet™ P-40; Sigma-Aldrich, Germany

Nuclease-free water; Ambion, USA

Reduced serum media (Opti-mem™); Thermo-Fisher, Germany

Osmium tetroxide; Sigma-Aldrich, Germany

Paraformaldehyde; Sigma-Aldrich, Germany

PCR buffer II, 10×; Applied Biosystems, USA

PERTEX®, Histolab, Sweden

Penicillin and streptomycin; Thermo-Fisher, Germany

Proteinase K; Promega, USA

2-Propanol; Merck, Germany

Quick Start™ Bradford dye reagent; Bio-rad, USA

Random hexamers; Applied Biosystems, USA

RNase inhibitor; Applied Biosystems, USA

Saponin; Calbiochem, Germany

Select agar; Sigma-Aldrich, Germany

Sodium azide; Sigma-Aldrich, Germany

Sodium cacodylate trihydrate; Sigma-Aldrich, Germany

Sodium chloride; Merck, Germany

Sodium orthovanadate; Sigma-Aldrich, Germany

SuperSignal® West Femto chemiluminescent substrate; Thermo-Fisher, Germany

Tamoxifen; Sigma-Aldrich, Germany

Technovit 7700, Heraeus Kulzer, Germany

Total RNA kit peqGOLD kit; PeqLab, Germany

Tissue-Tek® O.C.T.; Sakura® Fine Tek, USA

Trypan blue; Fluka, Germany

Uranyl acetate; Sigma-Aldrich, Germany

7.2 Methods

7.2.1 Animal experiments

All animal experiments were approved by the *Regierungspräsidium Darmstadt* under approval numbers B2/1002 and B2/1060.

7.2.1.1 AntagomiR-34a and target-site blocker injections *in vivo*

The C57BL/6 pregnant mice were ordered from Charles River and Janvier. Wild-type (WT) newborn mice were injected with AntmiR34a, TSB or scrambled antagomiR (SCR) (**Table 1**) and placed under normoxic (21% O_2) or hyperoxic (85% O_2) conditions on the day of birth, P1.5. Pups were injected twice with the locked nucleic acid (LNA) sequences (AntmiR34a or SCR: 10 mg/kg; mixture of TSB1,2: 5 mg/kg each), first at P1.5 and again at P3.5, ensuring a sustained concentration of LNA until the end of experiment, P14.5. Mice were euthanized by pentobarbital overdose (500 mg/kg) injected intraperitoneally. The interesting fact of using this LNA^{TM} technology is that the chemical structure contains phosphorothioate backbone modifications protecting the LNA from degradation and making the LNA able to perform longer in the organism and easy to incorporate into the cell by gymniosis (59). The AntmiR34a is designed to block miR-34-5p whereas SCR is a nonspecific LNA sequence employed as control. Both TSBs were designed to interfere with the interaction between miR-34a and the 3' UTR *Pdgfra* mRNA in mice.

Table 1. List of the different locked nucleic acids injected to mouse pups:

Name of LNA	Sequence
SCR	5'-ACGTCTATACGCCCA-3'
AntmiR34a	5'-AGCTAAGACACTGCC-3'
TSB1	5'-TTGGCAGTATTCTCCA-3'
TSB2	5'-AGGCAGTGATACAGCT-3'

7.2.1.2 Transgenic animals

The transgenic animals used were purchased from Jackson Laboratory except the *Pdgfra*-Cre^{ERT2} mouse line which was provided by Prof. Dr. William Richardson (UC London). The strain B6(Cg)-*Mir34a*^{tm1Lhe}/J contains an insertion of the *lacZ* gene in the miR-34a locus, which results in β-galactosidase translation and miR-34a

truncation (18). For experiments, miR34a::*lacZ*$^{+/-}$ mice were crossed in order to obtain the control and the experimental miR34a::*lacZ* homozygous (named miR-34a$^{-/-}$ for lung structure assessment and miR-34a::*lacZ* for the β-galactosidase activity staining) subjects in the same litter. The strain mir34a$^{tm1.2Aven}$/J contains two *loxP* sites, one up- and the other down-stream of the pre-miR34a (19). Thus, this strain was crossed with the *Pdgfra*-Cre^{ERT2} mouse line which contains a tamoxifen-inducible Cre insertion in exon 2 of the *Pgdfra* gene (31). The mice *Pdgfra*-Cre^{ERT2} heterozygous and miR-34a$^{fl/fl}$ homozygous lost miR-34a expression only in PDGFRα^{+} cells upon injection with tamoxifen. In this study, these mice lacking miR-34a expression in PDGFRα^{+} cells were named miR34a$^{iΔPC/iΔPC}$ mice, where iΔPC stands for inducible deletion in PDGFRα^{+} cells. Tamoxifen was diluted in Miglyol 812, a caprylic/capric triglyceride mixture, to reach a final concentration of 20 mg/ml. Each newborn mouse received 0.2 mg of tamoxifen injected at P1.5, as tamoxifen at high doses is toxic in mice under hyperoxia stress, as previously observed in our laboratory (57). Importantly, the experimental set-up of hyperoxia exposure was modified for this case. These miR34a$^{iΔPC/iΔPC}$ and control miR34a$^{wt/wt}$ mice received a single injection at P1.5 and were kept under normoxic conditions for the first 24 h. Afterwards, the same mice were placed in the hyperoxia chambers until P14.5.

7.2.2 Cell culture

7.2.2.1 Primary fibroblast isolation, seeding and transfection

Lung primary fibroblasts were isolated from WT adult C57BL/6J mice. The lungs were perfused with PBS, instilled with preheated collagenase type I (2 mg/ml in Hank's buffer) and, after harvesting, incubated with 2 mg/ml collagenase at 37 °C for 1 h with gentle agitation at 70 rpm. After homogenizing and disrupting the tissue clusters, the whole-lung cell suspension was filtered through a 40 µm filter and centrifuged at 120 × *g* at 4 °C for 8 min. Then, the pellet (cells) was re-suspended and cultured in high-glucose DMEM supplemented with 10% (v/v) fetal calf serum (FCS), 100 U/ml penicillin and 100 µg/ml streptomycin. Fibroblasts were passaged with low-glucose DMEM supplemented with 10% (v/v) fetal calf serum (FCS), 100 U/ml penicillin and 100 µg/ml streptomycin (DMEM complete media). For primary cell transfection, cells were seeded 24 h prior to transfection in DMEM complete media and placed in the incubator at 37 °C. The mixtures of HiPerFect reagent

(Qiagen, 301704) and miR-34a mimic (80 nM) (Qiagen, MSY0000542) or scrambled mimic (80 nM) (Qiagen, SI03650318) were performed in Opti-mem™ for 10 min prior to transfection to allow the miR-34a mimic- or scrambled mimic-complexes to form. Thus, the mixtures were pipetted into the cells in DMEM complete media at 37 °C for 24 h.

7.2.2.2 Seeding and transfection of mouse lung fibroblast cell line

Mouse lung fibroblast immortalized cells (MLg; ATCC®, CCL-206™) were cultured in Eagle's minimum essential medium (EMEM) supplemented with 10% (v/v) fetal bovine serum (FBS) (EMEM complete media), following the manufacturer's indications. For cell line transfection, cells were seeded 24 h prior to transfection in EMEM complete media and placed into the incubator at 37 °C. Lipofectamine® 2000 was used as a transfection reagent (15) and the complexes between miR-34a mimic (80 nM) or scrambled mimic (80 nM) together with Lipofectamine® 2000 were performed in Opti-mem™ for 20 min prior to transfection. Afterwards, the mixtures were pipetted into the cell cultures which were incubated with Opti-mem™. After 4 h, media was replaced by EMEM complete media until the end of transfection. Cells were harvested 24 h post-transfection for protein isolation.

7.2.2.3 Target-site blockers and miR-34a mimic co-transfection

Co-transfection of TSB1 (80 nM) or TSB2 (80 nM) reagents together with miR-34a mimic (80 nM) or scrambled mimic (80 nM) in MLg cells was performed employing Lipofectamine® 2000, as previously described (section **7.2.2.2**). In each case, the final concentration of combined reagents per well was 160 nM. Cells were harvested 24 h post-transfection for protein isolation.

7.2.3 Confocal microscopy

7.2.3.1.1 Lung fixation and embedding

Confocal microscopy studies utilized 10-µm lung tissue sections obtained from mice at P5.5 and P14.5. For paraffin sections, mice were euthanized and the lungs were perfused transcardially with 1x PBS and then inflated until total lung capacity with 4% (m/v) paraformaldehyde (PFA), dissected out of the thoracic cavity and fixed in 4% (m/v) PFA overnight at 4 °C. Then, the lungs underwent a dehydration protocol based on 100%, 96% and 70% (v/v) alcohols to finally be embedded in paraffin. The

paraffin-embedded lungs were cut into 4 µm sections and mounted on glass slides at 37 °C overnight.

To obtain cryoblocks, mouse lungs were perfused transcardially with 1x PBS and inflated with a mixture of Tissue-Tek® O.C.T. and 1x PBS (1:1) prior to freezing in a bath of isomethylbutane. The frozen lung tissue was sliced into 10 µm sections using a cryostat and was mounted on glass slides.

7.2.3.1.2 Staining

Paraffin lung sections were dehydrated using a protocol based on a decreasing alcohol gradient [100%, 96% and 70% (v/v) ethanol] whereas cryosections were fixed with a cold acetone:methanol (1:1) solution. In both cases, the lung sections were blocked for 1 h with a blocking mixture containing 50% (v/v) goat serum, 1% (v/v) bovine serum albumin (BSA) and 0.5% (v/v) Triton-X. Primary antibodies were diluted with the primary antibody buffer [0.5% (v/v) Triton X-100 and 1% (v/v) BSA in 1x PBS] and incubated with tissue at 4°C overnight. The secondary antibody conjugated with a fluorophore was diluted in 1x PBS buffer and incubated (if required) with the tissue for 1 h followed by 4',6-diamidino-2-phenylindole (DAPI) diluted (1:1000) in 1x PBS staining. The antibodies used were rabbit anti-aquaporin 5 (1:100, Abcam, ab78486), rat anti-CD31-Cy7/PE (1:100, Biozol, BLD-102418), rabbit anti-proSP-C (1:100, Abcam, ab3786) and mouse anti-αSMA-CY3 (1:100, Sigma Aldrich, C6198). The antibodies employed for the IgG control were: rabbit IgG isotype control (1:100, Thermo Scientific, PA5-23090), rat IgG isotype control (1:100, Miltenyi, 130-106-548), mouse IgG2aκ isotype control (1:100, Biolegend, 401502) and rat IgG2a isotype control-PE (1:100, Biozol, 00508).

7.2.4 Design-based stereology

7.2.4.1.1 Lung fixation followed by plastic embedding

At P14.5 mice were euthanized and lungs were inflated with a fixative solution [1.5% (m/v) glutaraldehyde, 0.15 M HEPES, 1.5% (m/v) PFA in 1x PBS; pH 7.4] at a hydrostatic pressure of 20 cmH_2O. After 24 h in fixative solution at 4 °C, lungs were embedded in 2% agar and cut into slices of 3 mm thickness in order to calculate the lung volume using the Stepanizer© software (version 2b28off) with the lung images taken with a high resolution camera. To embed the lungs in plastic, lungs were incubated with 0.1 M sodium cacodylate for 20 min, 0.1% (m/v) osmium tetroxide for

2 h and 5% (m/v) uranyl acetate overnight followed by embedding in Technovit 7100 resin. Then, blocks were cut into 2 µm slices which were stained with Richardson's stain making the lungs visible and ready for scanning with a NanoZoomer-XR C12000 digital slide scanner (Hamamatsu).

7.2.4.1.2 Stereological measurements

The stereological analysis was carried out using the Visiopharm® NewCast computer-assisted stereology system (version VIS4.5.3). Alveolar and septal volume were assessed by point counting (**Fig. 6A**) while surface density was measured by counting line intersections within the lung parenchyma (**Fig. 6B**), as explained in former published work from our group (39). These densities were then multiplied by the lung volume and the volume of lung parenchyma to obtain the total surface area, mean linear intercept (MLI) or mean septal wall thickness according to standardized formulae (30). The surface density (S_v) was calculated using the formula: $Sv = 2 \times (\Sigma I) / (lp \times \Sigma P)$, where I refers to counted intersection; *lp* is the length of the line between two points in µm; and, *P* refers to counted reference points inside parenchyma. To obtain the total surface area (*S*): $S = Sv \times V \times Vv(par/lung)$, where *V* refers to lung volume, and, *Vv(par/lung)* to volume of parenchyma. From the surface area, septal wall thickness can be assessed: $\tau(sep)[\mu m] = 2V(sep/lung) / S$, where *V(sep/lung)* is the volume of septa in the parenchyma. The mean linear intercept (*lm*) can also be calculated using the formula $lm = 4V(alv/lung) / S$, where *V(alv/lung)* refers to volume of alveolar air space. In order to count the number (*N*) of alveoli, a physical dissector (dissector height 4 µm) was employed. Before use, the block advance microtome was calibrated. The formula to assess the total number of alveoli was: $N(alv/lung) = B \times V(par/lung)[cm3] / (2M \times h[cm] \times A[cm2])$, where *B* refers to counted bridges; *M* refers to counted marks; *h* is the dissector height; and, *A* is the counting frame surface (**Fig. 6C** and **6D**). To ensure the precision of the measurements, the coefficient of error (CE), the coefficient of variation (CV) and the ratio between squared (CE^2/CV^2) were measured for each parameter.

7.2.5 Fluorescence-activated cell sorting

7.2.5.1.1 Whole-lung cell suspension preparation

After mice were euthanized, the lungs were instilled through the trachea with approximately 300 µl of dispase (50 U/ml) followed by incubation at 37 °C for 30 min.

Then, lungs were homogenized using gentleMACS dissociator in 5 ml (per lung) DMEM supplemented with 0.15 M HEPES, 100 U/ml penicillin, 100 µg/ml streptomycin, and 2% (m/v) bovine pancreatic DNAse type I. Whole-lung cell suspensions were filtered through 100 µm and 40 µm pore filter, in the respective order.

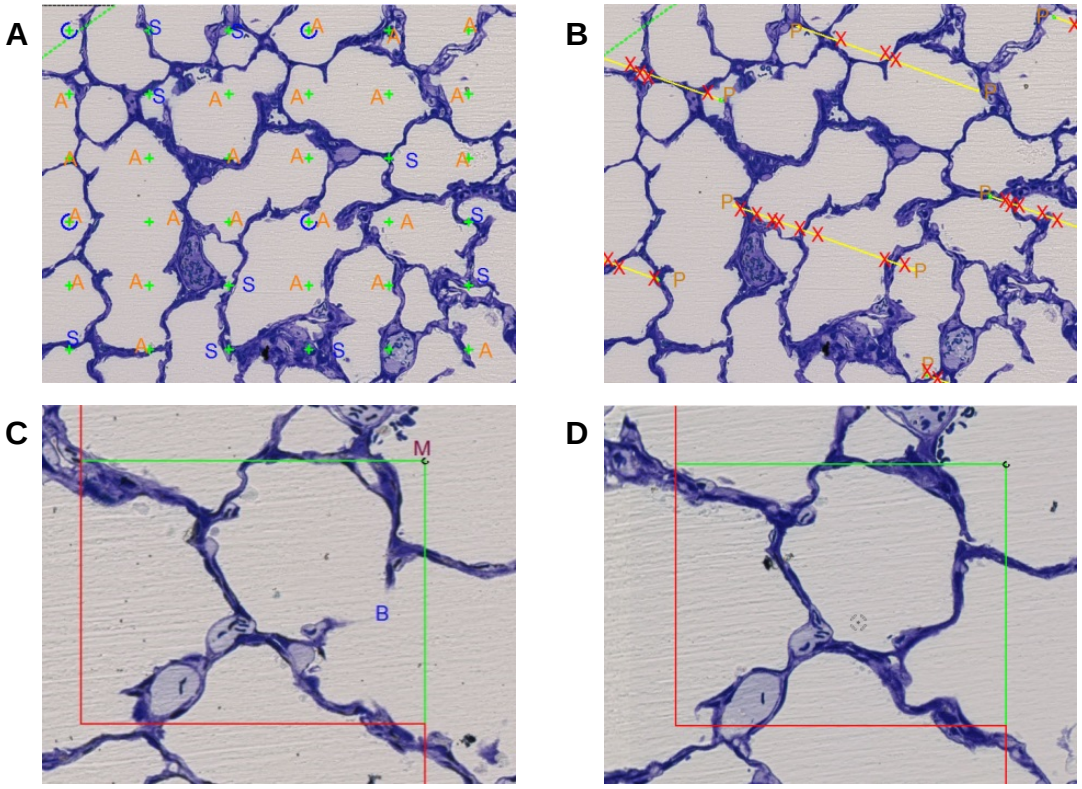

Figure 6. Stereological measurements in mouse lungs employing Visiopharm® software. (**A**) The volume of air spaces (point A) and septa (point S) are assessed by counting points that fall in the alveolar space or in the septa. (**B**) Lines are used to assess the surface density by counting each time that a line crosses the septal wall (X) together with the line points that fall in the parenchyma (orange P). Representative image of an opened alveolar space (**C**) closed by the formation of a bridge (**D**) which is counted (B) together with the marks (M) in order to assess the total number of alveoli in the lung.

This resulted in a whole-lung cell suspension that was fixed with a 0.05% (m/v) PFA solution at 4 °C for 10 min and after washing with PBS and centrifuging at 266 × *g* for 10 min at 4 °C, the cell pellet was re-suspended in Flow Cytometry Staining Buffer (FACS buffer). This procedure was applied for the FACS experiments carried out evaluating the PDGFRα^{+} and αSMA^{+} cell populations. Nevertheless, in the FACS

experiments for PDGFRα^{+} cell sorting or annexin V and Ki67 assessment, whole-lung cell suspensions were neither fixed with PFA nor permeabilized with saponin, as cells were required alive.

7.2.5.1.2 Staining

After centrifuging the tubes containing whole-lung cell suspensions at 266 × *g* for 10 min at 4 °C, pellets were re-suspended in 1 ml of DMEM supplemented with 0.15 M HEPES, 100 U/ml penicillin and 100 µg/ml streptomycin. Cells were pipetted into a 96-well plate in order to facilitate the staining and washing steps. Thus, cells were incubated with 10 µl of Gamunex (100 mg/ml), a blocking reagent, together with 20 µl of the primary antibodies solution or the corresponding isotypes at 4 °C for 20 min. This was followed by a washing step with FACS buffer to finally pipet the stained cells through a filter to remove the blood clots or aggregates from the stained cells. In the case of the assessment of the PDGFRα^{+} and αSMA^{+} cell populations, cells were permeabilized and incubated with 0.2% (m/v) saponin at 4 °C for 15 min prior to incubation with antibodies. This extra-step was not applied to the other FACS experiments since live cells were required.

In the 20 µl mixture of antibodies or respective antibody isotype, the following antibodies and isotypes were used: mouse anti-αSMA-FITC (1:100, Sigma-Aldrich, F3777), mouse anti-annexin V-647 (1:100 in annexin V buffer, Thermo Fisher, A23204), rat anti-CD31-Pacific Blue (1:500, Biolegend, 102422), rat anti-CD45-FITC (1:50, Pharmingen, 553079), rat anti-CD90.2-PE/Cy7 (1:300, Biolegend, 140309), rat anti-CD140a-APC (1:100, Biolegend, 135907), rat anti-CD140-PE (1:100, Biolegend, 135905), rat anti-EpCAM-APC/Cy7 (1:50, Biolegend, 118217), mouse anti-Ki67-PE and isotype control (undiluted, BD Pharmingen, 556027), Syrian hamster anti-T1α-PE/Cy7 (1:20, Biolegend, 127411); and, the isotypes, mouse IgG2aκ-FITC (Biolegend, 400207), mouse IgG1κ-Pacific Blue (Biolegend, 400131), mouse IgG1κ-FITC (Biolegend, 400109), rat IgG2aκ-PE/Cy7 (Biolegend, 400522), rat IgG2aκ-APC (Biolegend, 400511), rat IgG2aκ-PE (Biolegend, 400508), rat IgG2aκ-APC/Cy7 (Biolegend, 400523) and Syrian hamster IgG-PE/Cy7 (eBioscience, 25-4914-82).

7.2.5.2 PDGFRα$^+$ cell sorting followed by amplification of miR-34a by real-time quantitative PCR

The PDGFRα$^+$ cell sorting was carried out on whole-lung cell suspensions from P5.5 WT mice exposed either to 21% or 85% O_2 and on miR34a$^{i\Delta PC/i\Delta PC}$ mice exposed to 85% O_2. For sorting PDGFRα$^+$ cells, whole-lung cell suspensions were obtained and stained following the protocol formerly described for live cells (section **7.2.5.1.1**). The PDGFRα$^+$ cell population was stained with the CD140a-APC antibody whereas epithelial cells, leukocytes and αSMA$^+$ cells were stained with EpCAM-FITC, CD45-FITC and αSMA-FITC, respectively. In order to increase the purity of the isolated PDGFRα$^+$ cell population, FITC$^+$ cells were excluded. A low number of PDGFRα$^+$ cells could be collected (approximately 10,000 cells per mouse). Therefore, PDGFRα$^+$ sorted cells were pooled in one tube per group in order to obtain an acceptable RNA yield. The RNA isolation was performed using the miRNeasy® Mini kit and the reverse transcription (RT)-PCR was performed by means of a miScript®II RT kit, suitable for miR expression analysis.

7.2.6 Real-time quantitative PCR analyses

7.2.6.1.1 Real-time quantitative PCR of cDNA from mRNA

Around 70-90 mg of tissue from the mouse lungs were homogenized with a Precellys®24 Homogenizer and the RNA was extracted following the protocol of the Total RNA kit peqGOLD kit.

For cDNA synthesis, RT-PCR was performed in a 20-µl volume, containing 1,000 ng of RNA. These 20 µl of RNA were first denaturated at 70 °C for 10 min and placed on ice. The denatured RNA was mixed with 20 µl of a mixture containing 4 µl of 10x PCR buffer II; 8 µl of 25 mM $MgCl_2$; 1 µl H_2O; 2 µl of random hexamers; 1 µl RNase inhibitor; 2 µl of 10 nM dNTPs; and, 2 µl of MuLV reverse transcriptase. The mixture was first incubated at 21 °C for 10 min; then, followed by an RNA synthesis step at 43 °C for 1 h 15 min; and, finalized by incubation at 99 °C for 5 min to inactivate MuLV reverse transcriptase.

The real-time quantitative polymerase chain reaction (qPCR) was carried out using a Platinum SYBR® Green® qPCR SuperMix UDG kit and a StepOnePlus™ qPCR System. Intron-spanning primers specific to the mRNA target were designed using

the Primer-BLAST software (http://www.ncbi.nlm.nih.gov/tools/primer-blast/) (**table 2**).

Table 2. List of primers employed to assess gene expression:

Gene	Species	Sequences
Pdgfra	*Mus musculus*	Forward: 5'-CTAAGGGGCAGCCAAAGAAAC-3' Reverse: 5'-CCATTCAGCATACAACTCTAGGC-3'
Polr2a	*Mus musculus*	Forward: 5'-CTAAGGGGCAGCCAAAGAAAC-3' Reverse: 5'-CCATTCAGCATACAACTCTAGGC-3'

The thermal cycling conditions were as follows: 50 °C for 2 min, 95 °C for 5 min, 40 cycles of 95 °C for 5 s, 59 °C for 5 s, 72 °C for 30 s.

7.2.6.1.2 microRNA real-time quantitative PCR

The miRs were isolated with a miRNeasy® Mini kit according to the manufacturer's instructions.

For cDNA synthesis, RT-PCR was performed on 1,000 ng of total RNA. A total of 12 µl of RNA was mixed with 4 µl of 5x miScript buffer, 2 µl of 10x miScript nucleic mix and 2 µl of miScript Reverse transcriptase, following the of the miScript®II RT instructions kit. The mixture was incubated at 37°C for 1 h followed by an inactivating incubation at 95° C for 5 min.

The gene expression analysis of miRs by qPCR was carried out using the miScript SYBR® Green PCR Kit and a StepOnePlus™ qPCR System. The primers were designed, and purchased from Qiagen (**table 3**).

The cycling conditions were according to the manufacturer's instructions: 95 °C for 15 min; and, 40 cycles of a 3-step cycling consisting of 94 °C for 15 s, 55 °C for 30 s, 70 °C for 30 s.

In both cases, for mRNA and miR, the samples were then subjected to melting curve analysis to ensure amplification of a single and specific product. A reference gene (*Polr2a* for mRNA and RNU6-2 for miR amplification), constitutively expressed in all tissues and not affected by hyperoxia, was used as a reference gene for qPCR

reactions. The data were analysed with the comparative C_T method (ΔC_T method) and calculated with the equation: $\Delta C_T = C_T$ reference gene - C_T target gene.

Table 3. List of primers employed to assess miR expression:

Gene	Species	Catalogue number
miR-34a-5p	*Mus musculus*	MS00001428
miR-34a-3p	*Mus musculus*	MS00025697
miR-34b-5p	*Mus musculus*	MS00007910
miR-34b-3p	*Mus musculus*	MS00011900
miR-34c-5p	*Mus musculus*	MS00001442
miR-34c-3p	*Mus musculus*	MS00011907
RNU6-2	*Mus musculus*	MS00033740

7.2.7 Statistical analysis

Data are presented as the mean ± SD of the number of different replicates of each experiment. One-way ANOVA followed by Tukey's *post hoc* test was used to perform statistical analysis between the mean of multiple different groups. For the statistical analysis of two different groups, an unpaired Student's *t*-test was applied. Values of $P < 0.05$ were considered significant.

7.2.8 Western blot

Proteins were extracted using a protein lysis buffer containing 20 mM Tris pH 7.5, 150 mM NaCl, 1 mM EDTA, 1 mM EGTA and 1% (m/v) Nonidet™ P-40 supplemented with 1 mM sodium orthovanadate and Complete™ protease inhibitor cocktail (1 tablet per 25 ml of protein lysis buffer). After cell scraping or lung homogenization in combination with the complete protein lysis buffer, proteins were placed on ice for 30 min (vortexing every 10 min) and centrifuged at 13,249.6 × *g* for 15 min at 4° C. The supernatants were collected and protein quantification was achieved with Quick Start™ Bradford dye reagent. Thus, the protein quantification was determined by the measurement of the absorbance at a wavelength of 570 nm using a VersaMax micro-plate reader and extrapolating the results from a BSA standard curve. From the readout of the protein concentrations, 20-50 µg of proteins were combined with 5x Laemmli buffer containing 100 µM of dithiothreitol and incubated at 95 °C for 10 min for protein denaturation. Denatured proteins were then

loaded onto an 8% or 10% (v/v) SDS-PAGE gel and the electrophoresis was performed at 110 V for 90 min. Afterwards, the proteins that ran along the gel according to the size were blotted onto a nitrocellulose membrane at 90 V for 1 h. The membrane was blocked in 5% (m/v) skim milk diluted in 1x PBS (pH 7.4) at room temperature for 1 h followed by incubation with different primary antibodies at 4 °C overnight. The primary antibodies employed were rabbit anti-PDGFRα (1:1,000, Cell Signaling, 3174), rabbit anti-SIRT1 (1:1,000, Cell Signaling, 2493) or rabbit anti-βactin (1:4,000, Cell Signaling, 4967) and the incubation was with 5% (m/v) skim milk overnight. After incubation with primary antibodies, the membranes were washed (3x) with washing buffer (1x PBS and 1% (m/v) Tween-20) and incubated with HRP-conjugated anti-rabbit IgG (1:3,000, Thermo-Fisher, 31460) in 5% (m/v) skim milk for 1 h at room temperature. Later, the membrane was rinsed (3x) for 10 min with washing buffer and incubated with SuperSignal® West Femto chemiluminescent substrate for the corresponding time for each protein. The visualization of the protein bands was carried out by means of a LAS-4000 luminescent image analyser.

7.2.9 β-galactosidase activity detection

The miR-34a::*lacZ*$^{+/+}$ mice were exposed to hyperoxia from birth and the lungs were harvested at P5.5 to obtain cryoblocks, applying the protocol mentioned before (**section 6.2.3.1.1**). Cryosections were 10 µm thick and were mounted on a glass slide for fixation using 0.5% (v/v) glutaraldehyde in PBS at 4 °C for 10 min. Sections were washed with 1 mM $MgCl_2$ in PBS, 2 × 15 min at room temperature, and pre-incubated in 5-bromo-4-chloro-3-indolyl β-D-galactopyranoside (X-Gal) buffer [5 mM potassium ferrocyanide (II), 5 mM potassium ferricyanide (III), 1 mM MgCl2 in PBS, pH 7.0, at room temperature for 10 s]. This was followed by incubation with 1 mg/ml X-Gal in X-Gal buffer at 37 °C overnight. Slides were then washed with 1 mM $MgCl_2$ in PBS at room temperature for 15 min, fixed with 4% (m/v) PFA in PBS for 4 min, and dehydrated by incubation with 100% (v/v), 96% (v/v) and 70% (v/v) ethanol at room temperature for 5 min each. Finally, cryosections were washed with PBS, counterstained with 1% (m/v) eosin diluted in dH_2O:ethanol (20:80) at room temperature for 30 s. Slides were washed by immersion in dH_2O, mounted with PERTEX® and evaluated under bright field microscopy. [Note that macrophages have endogenous β-galactosidase activity and were considered as a background (14)].

7.2.10 Elastin visualization

Elastin deposition was visualized on P14.5 paraffin-embedded mouse lungs obtained as previously described (**section 6.2.3.1.1**). The paraffinized lungs were cut into 3-µm thick sections which were stained with Hart's elastin stain.

8. Results

8.1 miR-34a expression in the bronchopulmonary dysplasia animal model

Different studies have reported dysregulated expression of several miRs in newborn mouse lungs under hyperoxic conditions (7, 21, 37, 48, 52) leading to the idea that miRs might play a role during the aberrant secondary septation caused by hyperoxia. Thus, a miR microarray on normoxia-exposed developing mouse lungs compared to hyperoxia-exposed developing mouse lungs at different time-points was carried out to screen dysregulated miR expression. After the analysis of the microarray, only miR-34a expression was found up-regulated at two different time-points, P5.5 and P14.5. After validation by qPCR, miR-34a-5p exhibited up-regulated expression in whole-lung homogenates from mice exposed to 85% O_2 (**Fig. 7B**), from the earliest (P3.5) to the latest (P14.5) time-point screened including the phase of secondary septation (from P5.5 to P14.5). Interestingly, the magnitude of up-regulated expression of miR-34a increased with time, particularly at P14.5, under hyperoxic conditions whereas miR-34a expression decreases under normoxic conditions. Regarding the other miR-34 family members, the miR-34b (**Fig. 7D**) and miR-34c (**Fig. 7E**) expression was not significantly altered by hyperoxia except for miR-34b-3p (**Fig. 7C**) and miR-34c-5p (**Fig. 7F**) which were significantly up-regulated at P14.5 and at P3.5, respectively. These data suggested miR-34a-5p (from now on referred as miR-34a) expression the most significant up-regulated expression, among the miR-34 family members, in whole-lung homogenates from mice exposed to 85% O_2 that developed a BPD-like phenotype. Therefore, miR-34a became the target miR to study in the following experiments presented in this project.

8.2 miR-34a global deletion improved the lung structure in the bronchopulmonary dysplasia animal model

To assess the role of miR-34a during normal and aberrant late lung development, transgenic newborn mice carrying a miR-34a::*lacZ* gene trap (**Fig. 8A**) were exposed to 21% O_2 or 85% O_2 and the lung structure was evaluated at P14.5. This transgenic mouse line carries a miR-34a gene that is inactivated by *lacZ* gene insertion in the miR-34a locus without affecting the expression levels of miR-34b and miR-34c (**Fig. 8B**). The representative images of the lung structure after two weeks of

experiment are illustrated (**Fig. 8C**) and were subjected to stereological analysis. Mice deficient for miR-34a (miR-34a$^{-/-}$) and exposed to 21% O_2 did not exhibit any

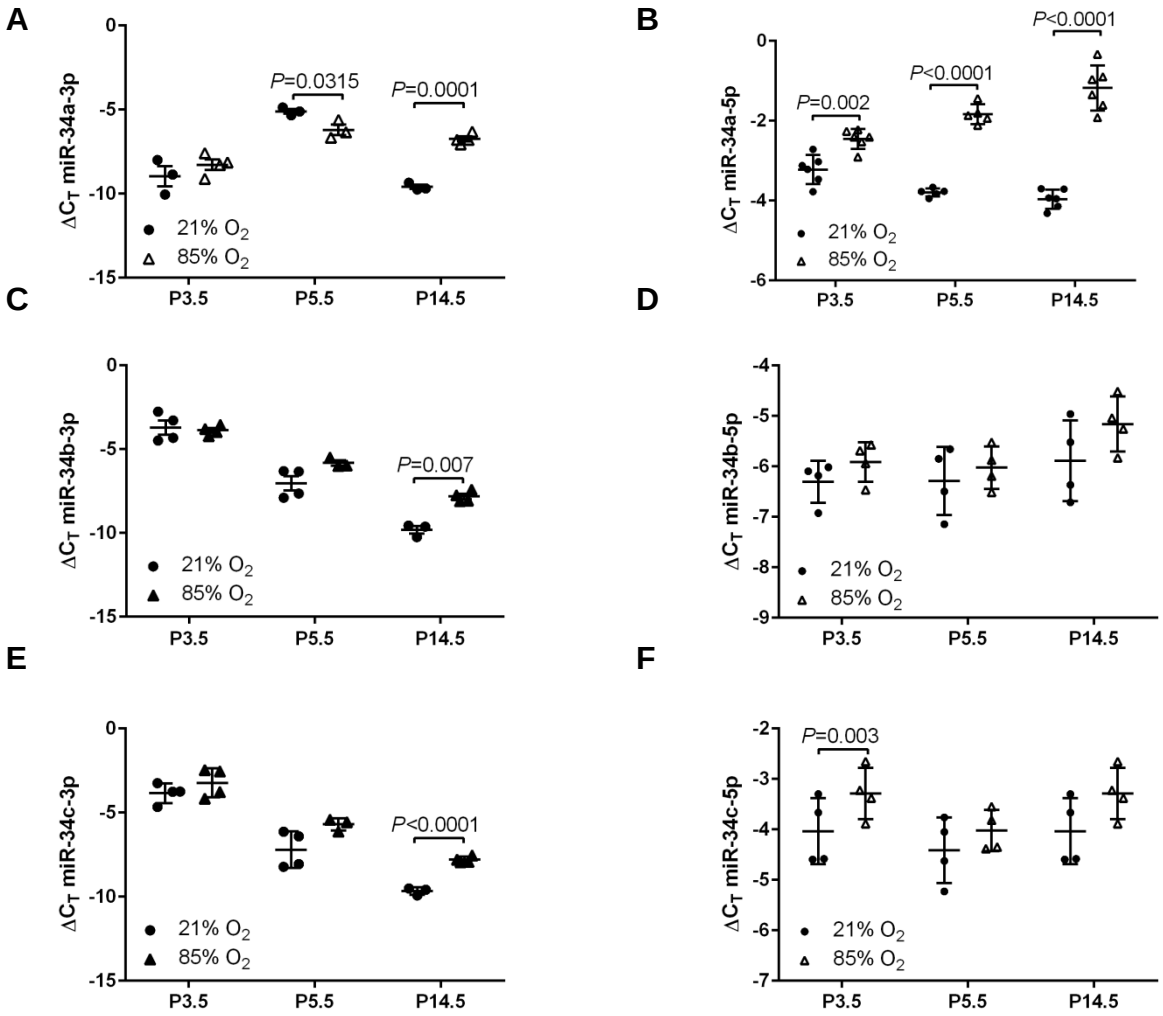

Figure 7. miR-34a expression is strongly up-regulated in mouse lungs under hyperoxic conditions. Newborn mice were exposed to 21% or 85% O_2 from the day of birth, P1.5. Lungs were harvested at P3.5, P5.5 and P14.5 in order to amplify miR-34a-3p (**A**), miR-34a-5p (**B**), miR-34b-3p (**C**), miR-34b-5p (**D**), miR-34c-3p (**E**) and miR-34c-5p (**F**) by real-time qPCR. Values are means ± SD; *n*=4-5. An unpaired Student's *t*-test was used to determine the *P* values.

altered lung structure, whereas miR-34a$^{-/-}$ mice exposed to 85% O_2 revealed an increase in the total number of alveoli (**Fig. 8D**) and a decrease in the mean septal wall thickness (**Fig. 8E**) compared to hyperoxia-exposed WT mice (**Table 4**). These findings supported two ideas: a) miR-34a is not required during normal late lung development for proper lung maturation; and, b) miR-34a strongly participates in the failure of alveolarization during aberrant late lung development caused by hyperoxia.

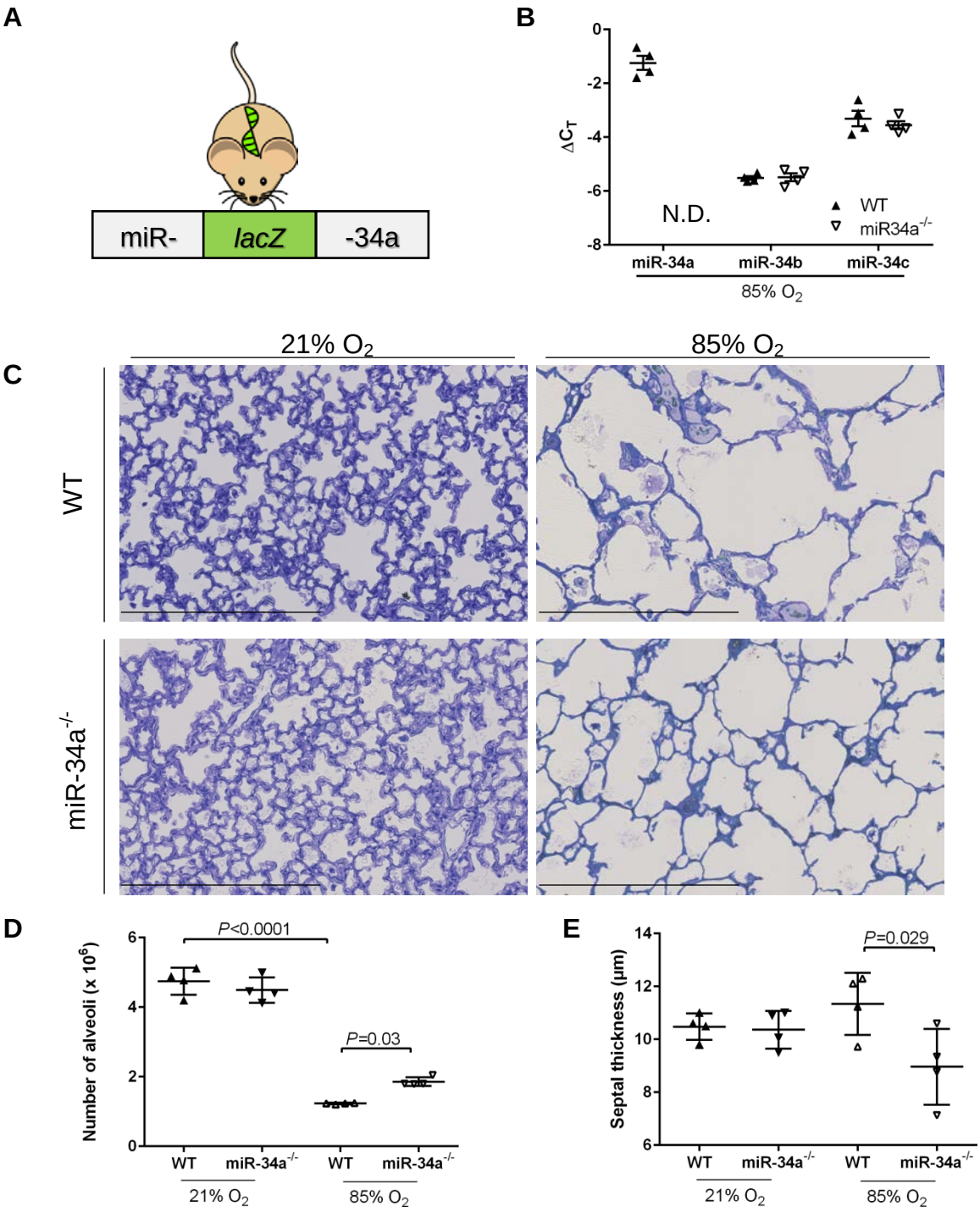

Figure 8. miR-34a plays an important role during aberrant secondary septation caused by hyperoxia. (**A**) Schematic view of the *lacZ* knock-in in the miR-34a gene locus. (**B**) miR-34a, miR-34b and miR-34c relative gene expression was assessed after amplification by real-time qPCR in whole-lung homogenates from P5.5 homozygous miR-34a$^{-/-}$ mice (triangles) compared to wild-type (WT) mice (squares) exposed to hyperoxia. (**C**) Representative images of plastic-embedded P14.5 mouse lungs from WT and homozygous miR-34a$^{-/-}$ mouse pups exposed either to 21% or 85% O_2. Scale bars, 800 µm. From the stereological analysis, the total number of alveoli in the lung (**D**) and the mean septal wall thickness (**E**) were determined. Values are means ± SD; *n*=5. A one-way ANOVA followed by Tukey's *post hoc* test was used to determine the *P* values. N.D., not detected.

Table 4. Stereological analysis of lungs from miR-34a$^{-/-}$ mice maintained under normoxic or hyperoxic conditions compared to wild-type controls.

Parameter	21% O_2		85% O_2			
	WT	miR-34a$^{-/-}$	WT		miR-34a$^{-/-}$	
	mean ± SD	mean ± SD	mean ± SD	*P* value *vs.* WT/21% O_2	mean ± SD	*P* value *vs.* WT/85% O_2
V (lung) [cm^3]	0.24 ± 0.01	0.22 ± 0.02	0.21 ± 0.02	0.81	0.22 ± 0.01	0.62
CV [*V* (lung)]	0.081	0.093	0.104		0.086	
V_V (par/lung) [%]	94.28 ± 1.95	90.87 ± 6.12	92.11 ± 1.56	0.60	91.2 ± 3.82	0.99
V_V (non-par/lung) [%]	5.71 ± 1.95	9.12 ± 6.12	7.89 ± 1.56	0.61	8.7 ± 3.82	0.99
N (alv, lung) 10^6	4.61 ± 0.48	4.35± 0.21	1.32 ± 0.16	0.60	1.9 ± 0.1	0.04
N_V (alv/par) 10^7 [cm^{-3}]	2.04 ± 0.32	2.13 ± 1.14	0.69 ± 0.13	0.94	0.9 ± 0.1	0.009
CV [N (alv/lung)]	0.016	0.053	0.197		0.069	
S_V [cm^{-1}]	865.8 ± 13.6	872.9 ± 36.4	489.1 ± 59.8	0.99	518.7 ± 29.5	0.71
S (alv epi, lung) [cm^2]	195.4 ± 15.7	178.4 ± 11.2	94.1 ± 11.6	0.23	107.2 ± 7.7	0.44
CV [S (alv epi, lung)]	0.08	0.06	0.12		0.07	
V_V (alv air) [%]	52.33 ± 4.31	53.04 ± 7.08	70.4 ± 3.3	0.97	78.1 ± 2.1	0.63
V (alv air, lung) [cm^3]	0.12 ± 0.01	0.11 ± 0.01	0.1 ± 0.02	0.91	0.1 ± 0.01	0.28
CV [*V* (alv air, lung)]	0.09	0.12	0.13		0.05	
V (sep, lung) [cm^3]	0.10 ± 0.01	0.09 ± 0.02	0.1 ± 0.01	0.71	0.04 ± 0.01	0.92
CV [*V* (sep, lung)]	0.14	0.21	0.11		0.12	
τ (sep) [µm]	11.01 ± 0.93	10.77 ± 1.72	12.1 ± 0.1	0.99	8.4 ± 1.1	0.03
CV [τ (sep)]	0.08	0.16	0.01		0.14	
MLI [µm]	24.19 ± 2.17	24.33 ± 3.4	58.5 ± 9.8	0.99	60.3 ± 3.1	0.99
CV [MLI]	0.08	0.14	0.16		0.05	

alv, alveoli; *alv air*, alveolar airspaces; *alv epi*, alveolar epithelium; *CV*, coefficient of variation; MLI, mean linear intercept; *N*, number, N_V, numerical density; *non-par*, non-parenchyma; *par*, parenchyma; *S*, surface area; S_V, surface density; *τ* (sep), arithmetic mean septal wall thickness; *V*, volume; V_V, volume density. Values are presented as mean ± SD; *n*=6 lungs per group. A one-way ANOVA with Tukey's *post hoc* analysis was used to determine *P* values.

8.3 Cellular localization of miR-34a in the mouse lung

In order to understand miR-34a function, the cell compartment expression of the miR-34a was essential to determine. Thus, miR-34a::*lacZ* mouse pups were exposed to 21% or 85% O_2 from P1.5 until P14.5. Lungs were harvested at P14.5 to obtain cryosections which were stained for β-galactosidase activity indirectly revealing miR-34a expressed in septal cells (**Fig. 9A**). Between these septal cells, those septal

cells located in the tips of the developing septa are reported to be myofibroblasts expressing PDGFRα, which are known to lead the growth of the secondary crests during secondary septation (52). Therefore, in order to confirm and quantify miR-34a gene expression levels in PDGFRα$^+$ cells, PDGFRα$^+$ cells were sorted from whole-lung cell suspensions from WT newborn mice that were exposed to either 21% or 85% O_2 immediately after birth. At P5.5, mouse lungs were harvested and the PDGFRα$^+$ cell populations of both groups were sorted by FACS (**Fig. 9B**) for miR-34a amplification by qPCR. As a result, PDGFRα$^+$ cells from mice exposed to 85% O_2 expressed remarkable up-regulated miR-34a expression levels at P5.5 compared to PDGFRα$^+$ cells from mice exposed to 21% O_2 (**Fig. 9C**). Taken together, miR-34a is highly expressed in PDGFRα$^+$ cells from developing mouse lungs exposed to hyperoxia, suggesting a key role for miR-34a during aberrant lung alveolarization caused by hyperoxia.

8.4 miR-34a interacts with *Pdgfra* mRNA in the bronchopulmonary dysplasia animal model

Taking into account that PDGFRα$^+$ cells transcribed high levels of miR-34a under hyperoxic conditions (**Fig. 9**), the next question to be addressed was to explore whether miR-34a could potentially interact with any mRNA expressed in PDGFRα$^+$ cells. Interestingly, searching in the TargetScan database, a database containing informatically predicted miR-mRNA interactions, miR-34a was predicted to bind to the 3' UTR of the *Pdgfra* mRNA in two different binding sites (**Fig. 10A**). An experimental proof of this miR-34a-*Pdgfra* interaction was reported by another group (24) in a lung cancer cell line. However, it was important to validate this interaction in a cell system close to the mesenchymal PDGFRα$^+$ cells which expressed miR-34a under hyperoxic conditions *in vivo*. Thus, mouse lung primary fibroblasts were transfected in order to overexpress miR-34a which resulted in a decrease of the PDGFRα protein levels *in vitro* (**Fig. 10B**), validating, thus, the interaction between miR-34a and *Pdgfra* mRNA in primary lung fibroblasts. The next hypothesis was that PDGFRα protein levels were down-regulated due to the interaction between miR-34a and *Pdgfra* mRNA since miR-34a is up-regulated in the BPD animal model (**Fig. 7**). Therefore, the relative gene expression and protein levels of PDGFRα were analysed in whole-lung homogenates from WT newborn mice that were exposed to 21% or 85% O_2. The results suggested that *Pdgfra* mRNA levels and PDGFRα protein levels were

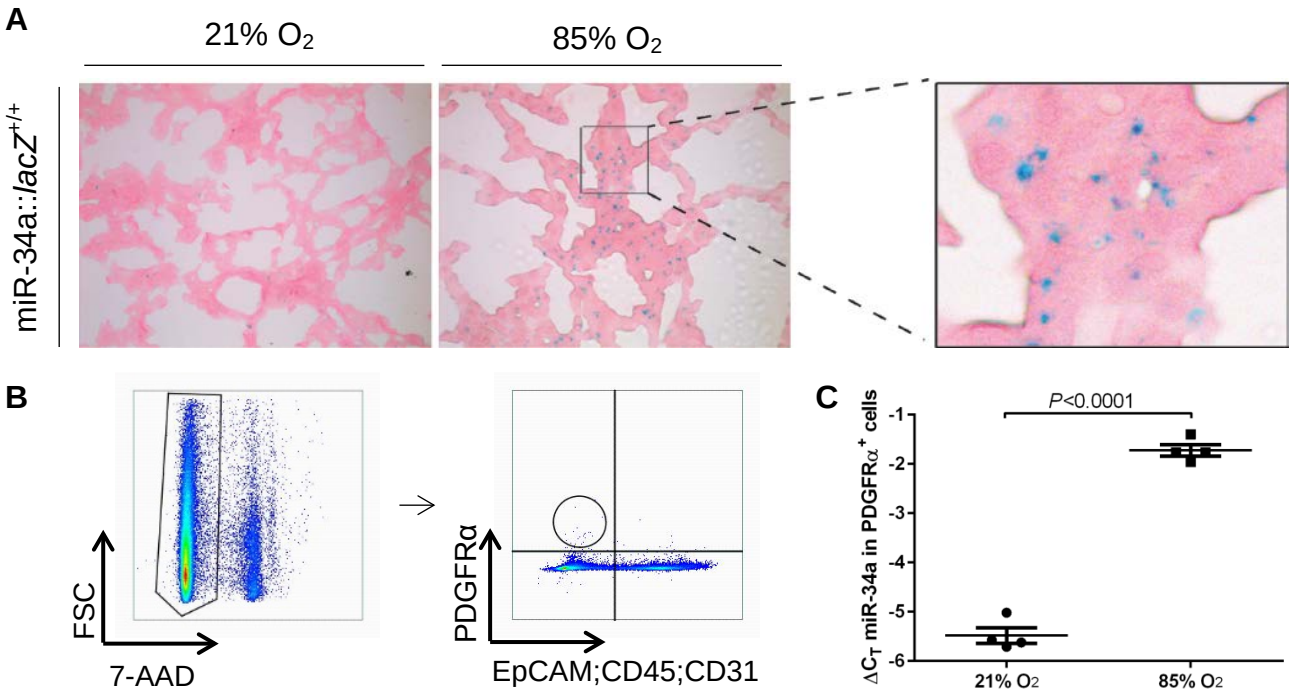

Figure 9. miR-34a is highly expressed in PDGFRα$^+$ cells *in vivo* in mouse lungs under hyperoxic conditions. (**A**) The β-galactosidase activity (revealed by blue colour) was performed on miR-34a::*lacZ*$^{+/+}$ cryosections from P14.5 newborns exposed to 21% or 85% O_2 from the day of birth. Scale bars, 800 µm. (**B**) Illustrations of the gating strategy in order to sort the PDGFRα$^+$ cell population from other lung cell-types in whole-lung cell suspensions from P5.5 newborn mice exposed to 21% or 85% O_2. From the PDGFRα$^+$ sorted cells, the RNA was extracted followed by cDNA synthesis to amplify miR-34a by real-time qPCR (**C**). Values are mean ± SD. An unpaired Student's *t*-test was used to determine the *P* values.

down-regulated from P2.5 to P5.5, just before the peak of the secondary crest formation, in mouse lungs under hyperoxic conditions (**Fig. 10C** and **10D**). To sum up, these data supported that miR-34a interacts with *Pdgfra* mRNA, downregulating the PDGFRα protein levels, and this could explain the decreased PDGFRα abundance observed in developing mouse lungs exposed to 85% O_2.

8.5 The role of miR-34a in PDGFRα$^+$ cells in the bronchopulmonary dysplasia animal model

To explore the hypothesis that miR-34a impairs lung growth under hyperoxic conditions through mesenchymal PDGFRα$^+$ cells, transgenic mice harbouring a tamoxifen-inducible miR-34a deletion only in the PDGFRα$^+$ cell lineage (miR34a$^{i\Delta PC/i\Delta PC}$) were employed (**Fig. 11A**). Firstly, PDGFRα$^+$ cells were isolated by

FACS followed by miR-34a amplification to validate the efficiency of the Cre system in deleting the floxed miR-34a. Those miR34a$^{i\Delta PC/i\Delta PC}$ mice which received tamoxifen injection expressed low miR-34a levels in PDGFRα^{+} cells under hyperoxic conditions (**Fig. 11B**). To evaluate the impact of the miR-34a deletion in PDGFRα^{+} cells on the lung structure, miR34a$^{i\Delta PC/i\Delta PC}$ newborn mice were exposed to 21% or 85% O_2 for two weeks. Lung parameters were assessed from the images of the plastic-embedded lungs (**Fig. 11C**). The stereological analysis revealed that the tamoxifen-inducible miR-34a deletion in PDGFRα^{+} cells did not impact the septal wall thickness (**Fig. 11E**) but the total number of alveoli was remarkably increased in miR34a$^{i\Delta PC/i\Delta PC}$ mice exposed to 85% O_2 compared to miR34a$^{wt/wt}$ mice exposed to 21% O_2 (**Fig. 11D**) (**Table 5**). These results revealed a pivotal role for miR-34a in PDGFRα^{+} cells as a negative regulator of alveologenesis during aberrant late lung development caused by hyperoxia.

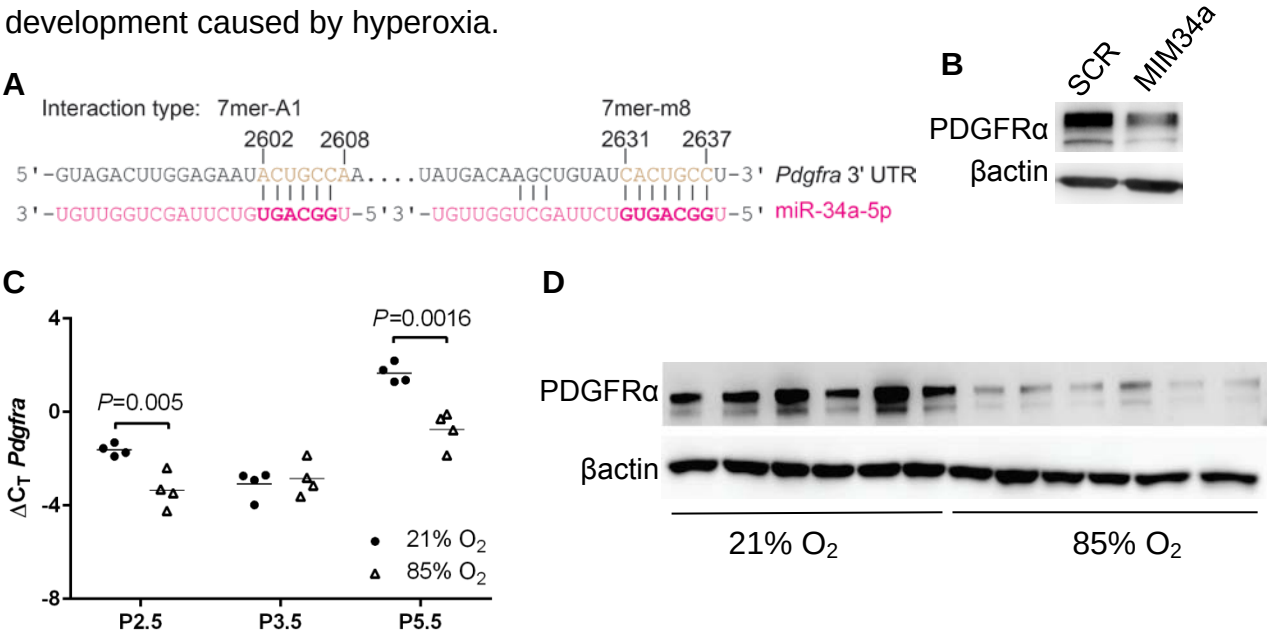

Figure 10. *Pdgfra* expression is down-regulated in mouse lungs under hyperoxic conditions. (**A**) miR-34a (in pink) interacts with *Pdgfra* mRNA in the conserved predicted binding sites 2602-2608 and 2631-2637 (in brown), according to the TargetScan database of informatically predicted miR-mRNA interactions. (**B**) PDGFRα (190 kDa) protein levels were evaluated by immunoblot after primary mouse lung fibroblast transfection with scrambled mimic (SCR) (80 nM) or miR-34a mimic (MIM34a) (80 nM) for 24 h. (**C**) *Pdgfra* gene amplification by real-time qPCR in whole-lung homogenates from mice exposed to 21% or 85% O_2. Values are means ± SD; *n*=5. An unpaired Student's *t*-test was applied to determine *P* values. (**D**) PDGFRα protein levels were evaluated in whole-lung homogenates from P5.5 mice exposed to 21% or 85% O_2 by immunoblot.

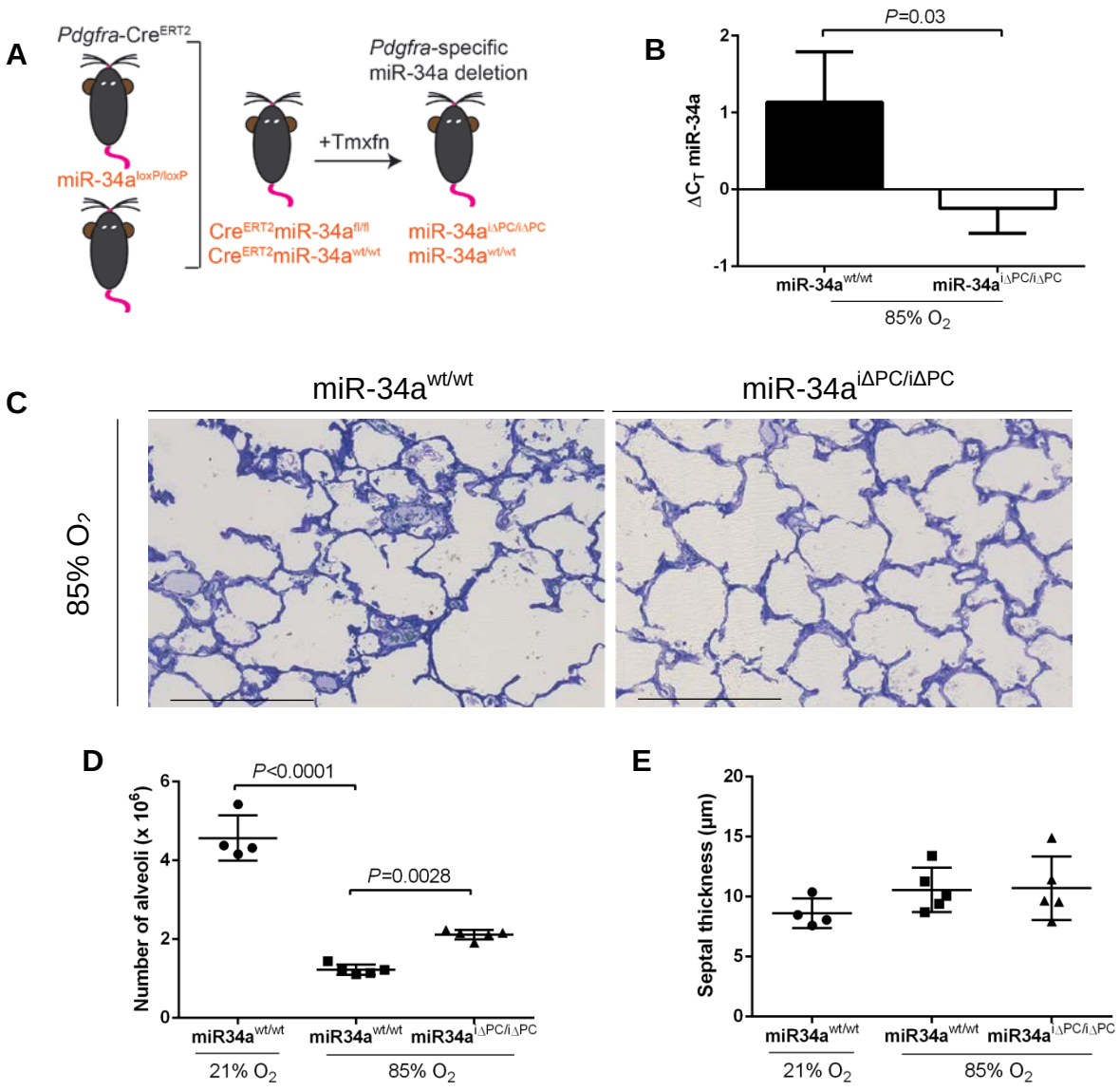

Figure 11. Deletion of miR-34a enhanced alveologenesis in the lungs of mice maintained under hyperoxic conditions. (**A**) Experimental scheme of the study of the effects of miR-34a deletion in PDGFRα^{+} cells on the lung structure of newborn mice exposed to 21% or 85% O_2. A miR-34a$^{fl/fl}$ mouse was mated with a *Pdgfra*-Cre driver mouse and the newborn mice were injected with tamoxifen (Tmxfn) (0.2 mg/mouse) resulting in a deletion of miR-34a only in PDGFRα^{+} cells (miR34a$^{iΔPC/iΔPC}$). (**B**) miR-34a amplification by real-time qPCR in FACS-sorted PDGFRα^{+} cells from miR34a$^{iΔPC/iΔPC}$ compared to miR-34a$^{wt/wt}$ P5.5 newborns exposed to 85% O_2. An unpaired Student's *t*-test was used to determine the *P* values. (**C**) The miR34a$^{iΔPC/iΔPC}$ and miR-34a$^{wt/wt}$ newborn mice were exposed to 21% or 85% O_2 and lungs were harvested at P14.5 for plastic-embedding. Scale bars, 800 µm. The total number of alveoli (**D**) and mean septal wall thickness (**E**) were assessed by stereological analysis. Values are means ± SD. A one-way ANOVA followed by Tukey's *post hoc* test was employed to determine *P* values.

Table 5. Structural parameters of mouse lungs carrying a deletion of miR-34a in PGDFRα^{+} cells in the bronchopulmonary dysplasia animal model.

Parameter	21% O_2	85% O_2			
	miR34a$^{wt/wt}$	miR34a$^{wt/wt}$		miR34a$^{i\Delta PC/i\Delta PC}$	
	mean ± SD	mean ± SD	*P* value *vs.* miR34a$^{wt/wt}$/21% O_2	mean ± SD	*P* value *vs.* miR34a$^{wt/wt}$/85% O_2
V (lung) [cm^3]	0.22 ± 0.01	0.19 ± 0.02	0.32	0.22 ± 0.02	0.16
CV [*V* (lung)]	0.06	0.11		0.09	
V_V (par/lung) [%]	90.26 ± 2.89	89.16 ± 1.11	0.83	91.18 ± 2.41	0.48
V_V (non-par/lung) [%]	9.73 ± 2.89	10.83 ± 1.11	0.83	8.81 ± 2.41	0.48
N (alv, lung) 10^6	4.70 ± 0.62	1.25 ± 0.15	< 0.0001	2.11 ± 0.12	0.01
N_V (alv/par) 10^7 [cm^{-3}]	2.34 ± 0.18	0.71 ± 0.16	< 0.0001	1.02 ± 0.76	0.03
CV [N (alv/lung)]	0.07	0.22		0.07	
S_V [cm^{-1}]	788.33 ± 51.87	500.14 ± 49.11	0.0003	561.76 ± 48.21	0.26
S (alv epi, lung) [cm^2]	158.41 ± 25.67	87.06 ± 0.76	0.002	115.83 ± 16.26	0.11
CV [S (alv epi, lung)]	0.161	0.008		0.142	
V_V (alv air) [%]	68.41 ± 2.22	72.61 ± 3.23	0.58	70.18 ± 6.58	0.79
V (alv air, lung) [cm^3]	0.14 ± 0.01	0.12 ± 0.01	0.58	0.14 ± 0.01	0.17
CV [*V* (alv air, lung)]	0.08	0.06		0.09	
V (sep, lung) [cm^3]	0.06 ± 0.01	0.04 ± 0.01	0.42	0.06 ± 0.01	0.42
CV [*V* (sep, lung)]	0.144	0.219		0.122	
τ (sep) [µm]	8.01 ± 0.44	11.11 ± 2.35	0.26	10.68 ± 2.65	0.96
CV [τ (sep)]	0.05	0.21		0.24	
MLI [µm]	34.85 ± 3.26	58.29 ± 3.33	0.0009	50.25 ± 6.01	0.11
CV [MLI]	0.09	0.05		0.11	

alv, alveoli; *alv air*, alveolar airspaces; *alv epi*, alveolar epithelium; *CV*, coefficient of variation; MLI, mean linear intercept; *N*, number, N_V, numerical density; *non-par*, non-parenchyma; *par*, parenchyma; *S*, surface area; S_V, surface density; *τ* (sep), arithmetic mean septal wall thickness; *V*, volume; V_V, volume density. Values are presented as mean ± SD; *n*=3-5 lungs per group. A one-way ANOVA with Tukey's *post hoc* analysis was used to determine *P* values.

8.6 miR-34a, interacting with *Pdgfra* mRNA, is capable of partially impairing alveoli formation

Exploring further the miR-34a mechanism of action, the next question to be addressed was whether the unique interaction between miR-34a and *Pdgfra* mRNA was responsible for the aberrant lung structure seen in the BPD animal model. For this purpose, two TSBs designed to protect the *Pdgfra* mRNA from miR-34a were tested, firstly, *in vitro*. A co-transfection of a miR-34a mimic together with TSB1 and TSB2, individually or in combination, in MLg cells resulted in an increase in PDGFRα protein levels (**Fig. 12A**), validating the prevention of the interaction between miR-34a and *Pdgfra* mRNA by TSB1 and TSB2. Then, WT mouse newborns were exposed to 85% O_2 and treated with SCR or a mixture of TSB1 and TSB2 (TSB1,2) for two weeks. The images of control mouse lungs, injected with SCR, and experimental mouse lungs, injected with TSB1,2, (**Fig. 12B**) were subjected to stereological analysis. Remarkably, TSB1,2 administration significantly increased the total number of alveoli (**Fig. 12E**) and decreased the mean septal wall thickness (**Fig. 12D**) in the lungs of mice maintained under hyperoxic conditions, compared to SCR-treated mice exposed to 85% O_2 (**Table 6**). In conclusion, although miR-34a may interact with many targets, the prevention of the interaction between miR-34a and *Pdgfra* mRNA is sufficient to observe a partial improvement at the lung structure in mice maintained under hyperoxic conditions.

8.7 Therapeutic intervention to block miR-34a function in the bronchopulmonary dysplasia animal model

The next approach aimed to inhibit miR-34a in newborn mice from P1.5 in order to test a therapeutic approach that could potentially be developed in the clinic. For this purpose, AntmiR34a, which would block miR-34a-5p *in vivo*, was employed in the experiment. Newborn mice were exposed to 21% or 85% O_2 from P1.5 until P14.5 and concomitantly injected with SCR or AntmiR34a twice, at P1.5 and at P3.5, at a dose of 10 mg/kg per injection. The AntmiR34a not only blocked miR-34a with high efficiency until the end of the experiment (P14.5) (**Fig. 13A**) but miR-34b and miR-34c as well, although to a lesser extent, revealing the AntmiR34a as a general miR-34 family repressor (**Fig. 13B** and **13C**). This therapeutic intervention by means of AntmiR34a resulted in a remarkable improvement of the lung structure (**Fig. 13D**)

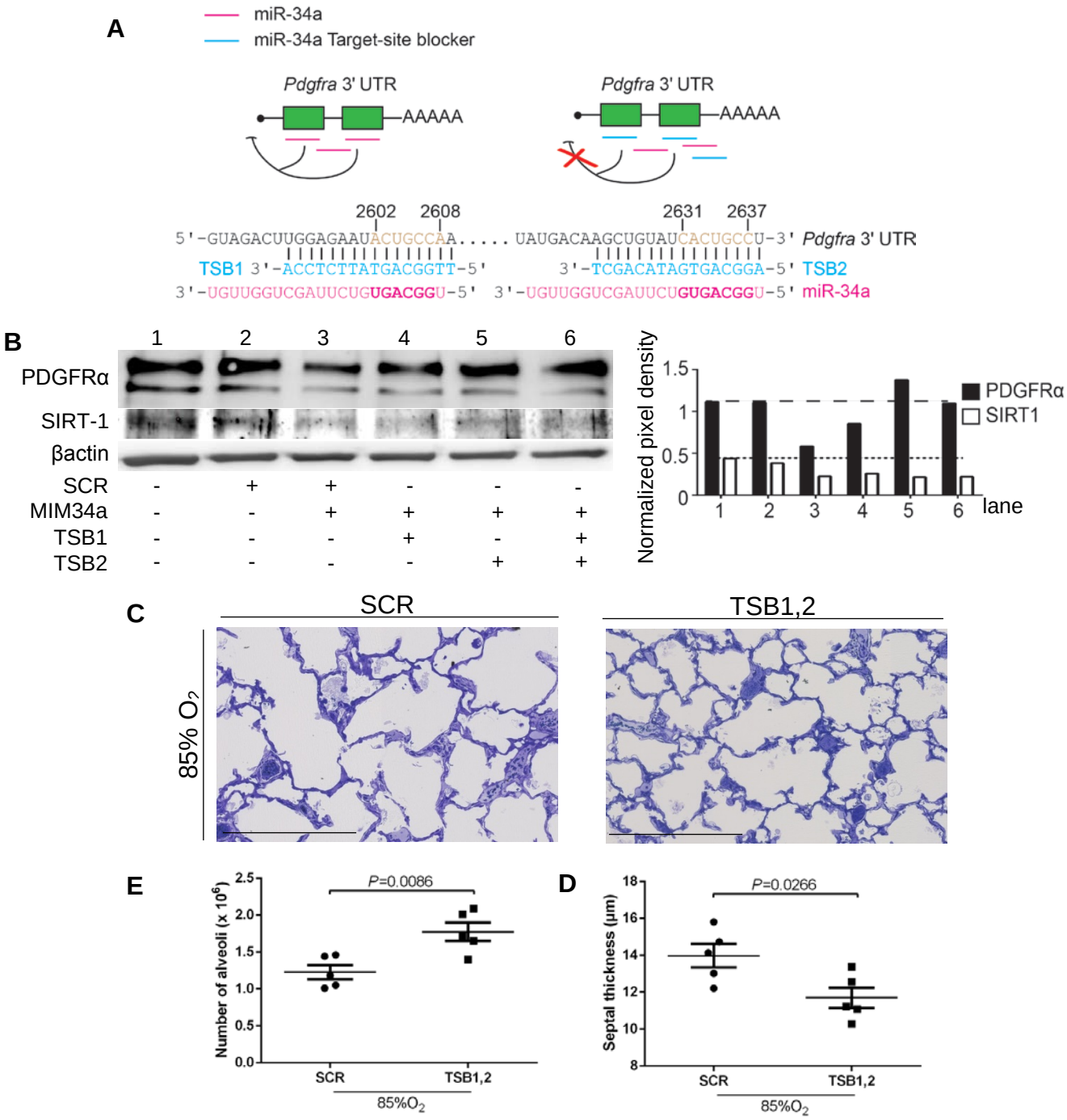

Figure 12. The miR-34a-*Pdgfra* mRNA interaction is partially responsible for the worsening of the lung structure in mouse pups maintained under hyperoxic conditions. (**A**) Scheme of the prevented *Pdgfra* mRNA 3′ UTR from miR-34a by target-site blocker (TSB) 1 and TSB2. (**B**) PDGFRα (190 kDa) and sirtuin-1 (SIRT1) (135 kDa) levels were evaluated by immunoblot after mouse lung fibroblast (MLg) cell line transfection with a scrambled mimic (SCR) (80 nM) or a miR-34a mimic (MIM34a) (80 nM) combined with TSB1 and TSB2 (80 nM). (**C**) Newborns were injected with SCR or TSB1,2 to a final dose of 10 mg/kg and exposed to 85% O_2 from P1.5. Scale bars, 800 µm. Lungs were harvested for plastic-embedding and were cut into slices which were subjected to stereological analysis to assess total number of alveoli (**D**) and mean septal wall thickness (**E**). Values are means ± SD; *n*=5. An unpaired Student's *t*-test was used to determine the *P* values.

Table 6. Structural parameters of lungs from mice treated with scrambled target-site blocker or target-site blockers maintained under hyperoxic conditions.

Parameter	85% O_2		
	SCR	TSB1,2	
	mean ± SD	mean ± SD	*P* value *vs.*SCR/85% O_2
V (lung) [cm^3]	0.24 ± 0.01	0.22 ± 0.02	0.096
CV [*V* (lung)]	0.044	0.110	
V_V (par/lung) [%]	92.35 ± 4.62	90.66 ± 2.78	0.502
V_V (non-par/lung) [%]	7.65 ± 4.62	9.34 ± 2.78	0.502
N (alv, lung) 10^6	1.32 ± 0.17	1.77 ± 0.27	0.017
N_V (alv/par) 10^7 [cm^{-3}]	0.60 ± 0.07	0.90 ± 0.09	0.001
CV [N (alv/lung)]	0.116	0.102	
S_V [cm^{-1}]	498.71 ± 49.86	536.89 ± 32.61	0.189
S (alv epi, lung) [cm^2]	110.37 ± 12.89	105.28 ± 14.41	0.572
CV [S (alv epi, lung)]	0.11	0.136	
V_V (alv air) [%]	65.31 ± 3.46	68.75 ± 1.63	0.079
V (alv air, lung) [cm^3]	0.144 ± 0.01	0.13 ± 0.01	0.167
CV [*V* (alv air, lung)]	0.04	0.098	
V (sep, lung) [cm^3]	0.07 ± 0.01	0.06 ± 0.01	0.012
CV [*V* (sep, lung)]	0.12	0.095	
τ (sep) [µm]	13.97 ± 1.41	11.69 ± 1.23	0.026
CV [τ (sep)]	0.100	0.105	
MLI [µm]	52.91 ± 7.04	51.32 ± 2.39	0.646
CV [MLI]	0.13	0.046	

alv, alveoli; *alv air*, alveolar airspaces; *alv epi*, alveolar epithelium; *CV*, coefficient of variation; MLI, mean linear intercept; *N*, number, N_V, numerical density; *non-par*, non-parenchyma; *par*, parenchyma; *S*, surface area; SCR, scrambled antagomiR; S_V, surface density; TSB1,2, target-site blockers 1 and 2; *τ* (sep), arithmetic mean septal wall thickness; *V*, volume; V_V, volume density. Values are presented as mean ± SD; *n*=5 lungs per group. A one-way ANOVA with Tukey's *post hoc* analysis was used to determine *P* values.

since the stereological analysis revealed an increase in the number of alveoli (**Fig. 13E**) and a decrease in the mean septal wall thickness (**Fig. 13F**) compared to the SCR-treated mice exposed to 85% O_2 (**Table 7**). Interestingly, the blockade of the miR-34a in mice exposed to 21% O_2 did not alter the lung structure, providing evidence that the miR-34 family is not required for normal late lung development. These data demonstrated that blocking miR-34a by means of AntmiR34a had the same effect on lung structure previously observed in transgenic mice deficient for miR-34a (**Fig. 8**) exposed to 85% O_2. In conclusion, the miR-34 family (mainly

miR-34a) is involved in the mechanisms which lead to the failure of alveologenesis in mice under hyperoxic conditions.

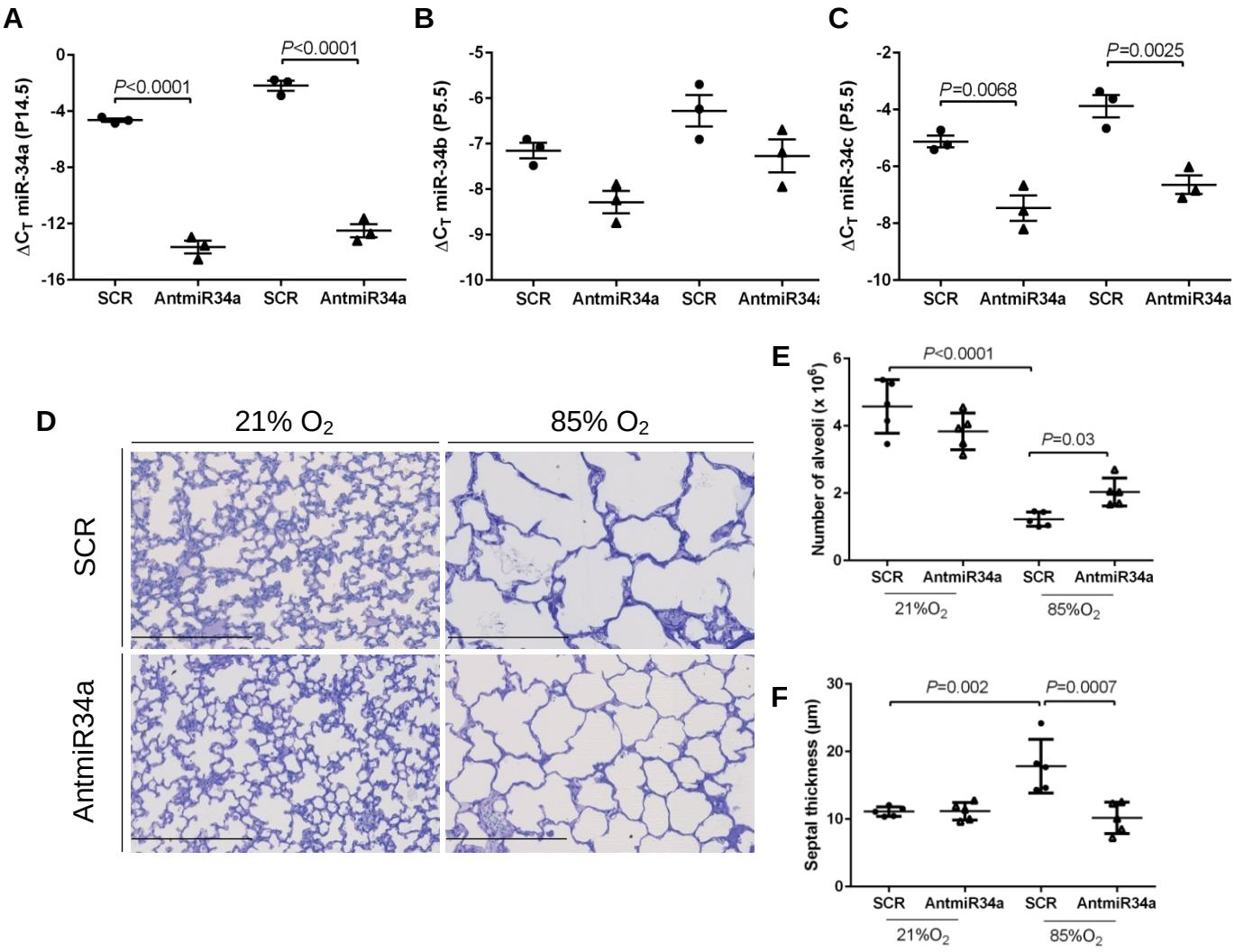

Figure 13. The miR-34 family is involved in the blunted secondary septation in the lungs of mice maintained under hyperoxic conditions. Newborn mice were treated with scrambled antagomiR (SCR) or antagomiR-34a (AntmiR34a) and exposed either to 21% or 85% O_2. (**A**) miR-34a was amplified by means of real-time qPCR in experimental mouse lungs harvested at P14.5. From the same experimental mouse lungs, miR-34b (**B**) and miR-34c (**C**) expression levels were assessed by real-time qPCR. Values are means ± SD; *n*=3. One-way ANOVA followed by Tukey's *post hoc* test was used to determine the *P* values. (**D**) Representative images of mouse lungs treated with SCR or AntmiR34a and exposed either to 21% O_2 or 85% O_2 embedded in plastic. Scale bars, 800 µm. From the stereological analysis, the total number of alveoli (**E**) in the lung and the septal wall thickness (**F**) were quantified. Values are means ± SD; *n*=5. A one-way ANOVA followed by Tukey's *post hoc* test was used to determine the *P* values.

Table 7. Structural parameters of lungs from mice treated with scrambled antagomiR or antagomiR-34a in the bronchopulmonary dysplasia animal model.

Parameter	21% O_2		85% O_2			
	SCR	AntmiR34a	SCR		AntmiR34a	
	mean ± SD	mean ± SD	mean ± SD	*P* value *vs.* SCR/21% O_2	mean ± SD	*P* value *vs.* SCR/85% O_2
V (lung) [cm^3]	0.23 ± 0.04	0.23 ± 0.04	0.24 ± 0.01	0.952	0.27 ± 0.02	0.448
CV [*V* (lung)]	0.189	0.185	0.044		0.079	
V_V (par/lung) [%]	89.54 ± 2.36	93.65 ± 3.91	89.30 ± 7.11	0.486	91.11 ± 3.46	0.932
V_V (non-par/lung) [%]	11.10 ± 2.36	6.39 ± 3.91	10.74 ± 7.11	0.409	1.60 ± 3.46	0.926
N (alv, lung) 10^6	4.57 ± 0.79	3.83± 0.54	1.22 ± 0.09	0.165	2.03 ± 0.4	0.118
N_V (alv/par) 10^7 [cm^{-3}]	1.94 ± 0.39	1.51 ± 0.31	0.57 ± 0.03	0.639	0.87 ± 0.08	0.901
CV [N (alv/lung)]	0.173	0.141	0.172		0.203	
S_V [cm^{-1}]	940.4 ± 53.44	849.86 ± 72.18	450.6 ± 9.98	0.056	501.2 ± 48.1	0.426
S (alv epi, lung) [cm^2]	193.48 ± 42.09	179.51 ± 22.96	96.15 ± 4.84	0.805	123.24 ± 9.6	0.335
CV [S (alv epi, lung)]	0.217	0.127	0.050		0.078	
V_V (alv air) [%]	47.80 ± 4.51	52.89 ± 3.37	59.85 ± 8.93	0.501	74.93 ± 4.01	0.003
V (alv air, lung) [cm^3]	0.099 ± 0.01	0.112 ± 0.02	0.12 ± 0.01	0.751	0.184 ± 0.01	0.002
CV [*V* (alv air, lung)]	0.272	0.197	0.136		0.087	
V (sep, lung) [cm^3]	0.10 ± 0.01	0.10 ± 0.01	0.08 ± 0.02	0.951	0.06 ± 0.01	0.205
CV [*V* (sep, lung)]	0.174	0.191	0.263		0.190	
τ (sep) [μm]	11.10 ± 0.72	11.15 ± 1.3	17.81 ± 3.97	>0.999	10.15 ± 2.32	0.001
CV [τ (sep)]	0.064	0.117	0.223		0.229	
MLI [μm]	20.44 ± 2.84	25.01 ± 1.35	53.15 ± 8.26	0.474	60.03 ± 3.74	0.159
CV [MLI]	0.13	0.09	0.15		0.06	

alv, alveoli; *alv air*, alveolar airspaces; *alv epi*, alveolar epithelium; AntmiR34a, antagomiR-34a; *CV*, coefficient of variation; MLI, mean linear intercept; *N*, number, N_V, numerical density; *non-par*, non-parenchyma; *par*, parenchyma; *S*, surface area; SCR, scrambled antagomiR; S_V, surface density; *τ* (sep), arithmetic mean septal wall thickness; *V*, volume; V_V, volume density. Values are presented as mean ± SD; *n*=5 lungs per group. A one-way ANOVA with Tukey's *post hoc* analysis was used to determine *P* values.

8.8 miR-34a negatively regulates the PDGFRα$^+$ cell population in the lungs of mice maintained under hyperoxic conditions

Since miR-34a interacts with *Pdgfra* mRNA and down-regulates PDGFRα protein levels, the next hypothesis to test was that PDGFRα expression levels were restored after blocking miR-34a in mice exposed to 85% O_2. For this purpose, FACS analysis (**Fig. 14A**) was employed to determine PDGFRα$^+$ cells revealing that mice lacking a functional miR-34a had a significant increase in the PDGFRα$^+$ cell population which was decreased under hyperoxic conditions (**Fig. 15A** and **15B**). Since αSMA and PDGFRα are two robust markers of myofibroblasts (41), the double positive αSMA$^+$ and PDGFRα$^+$ cell population was included in the FACS analysis. Interestingly, the αSMA$^+$/PDGFRα$^+$ cell population was clearly increased in those mice injected with AntmiR34a compared to a control group maintained under hyperoxic conditions (**Fig. 15C** and **15D**). Consistent with this finding, a higher number of alveolar αSMA$^+$ cells were observed in the septa in lungs of P14.5 mice treated with AntmiR34a and exposed to 85% O_2 (**Fig. 16A**). This observation confirmed the increased alveolar myofibroblast abundance after AntmiR34a injection under hyperoxic conditions. In addition, an important myofibroblast function during late lung development is the production of ECM components such as collagen or elastin (8) which are disturbed under hyperoxia stress (3, 46). Elastin staining was then carried out on the P14.5 lung paraffin sections revealing a better deposition and distribution of the elastin (**Fig. 16B**), particularly in the tips of the growing secondary

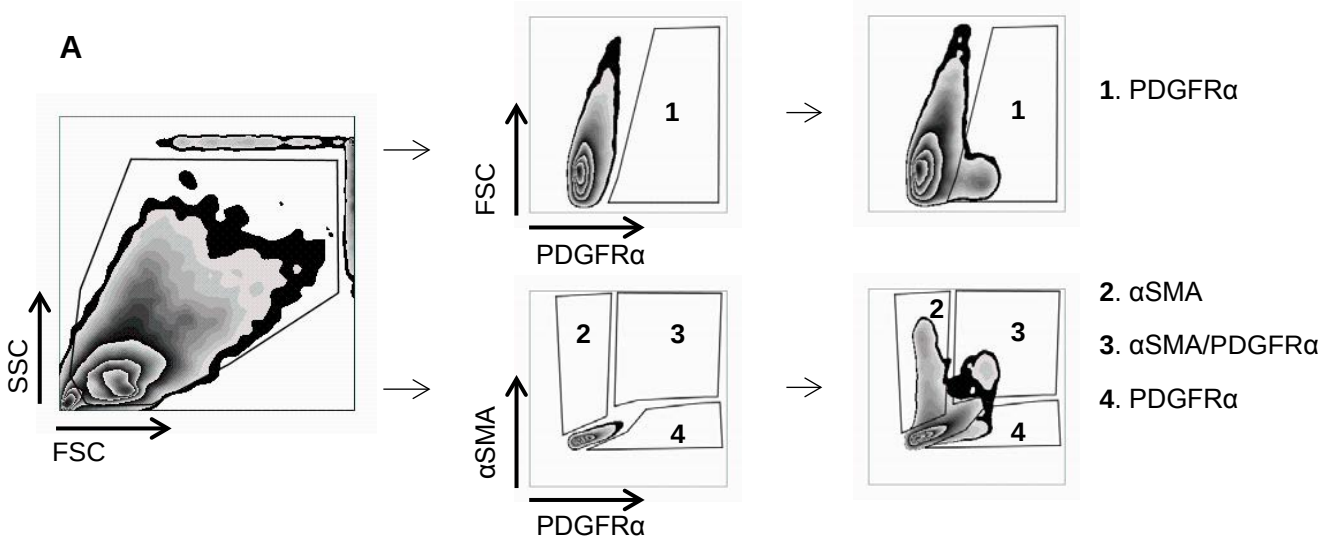

Figure 14. Analysis of mesenchymal cells by FACS. Gating of platelet-derived growth factor receptor (PDGFR)α$^+$, α smooth muscle actin (SMA)$^+$ or double-positive αSMA$^+$/PDGFRα$^+$ cells by FACS. FSC, forward scatter; SSC, side scatter.

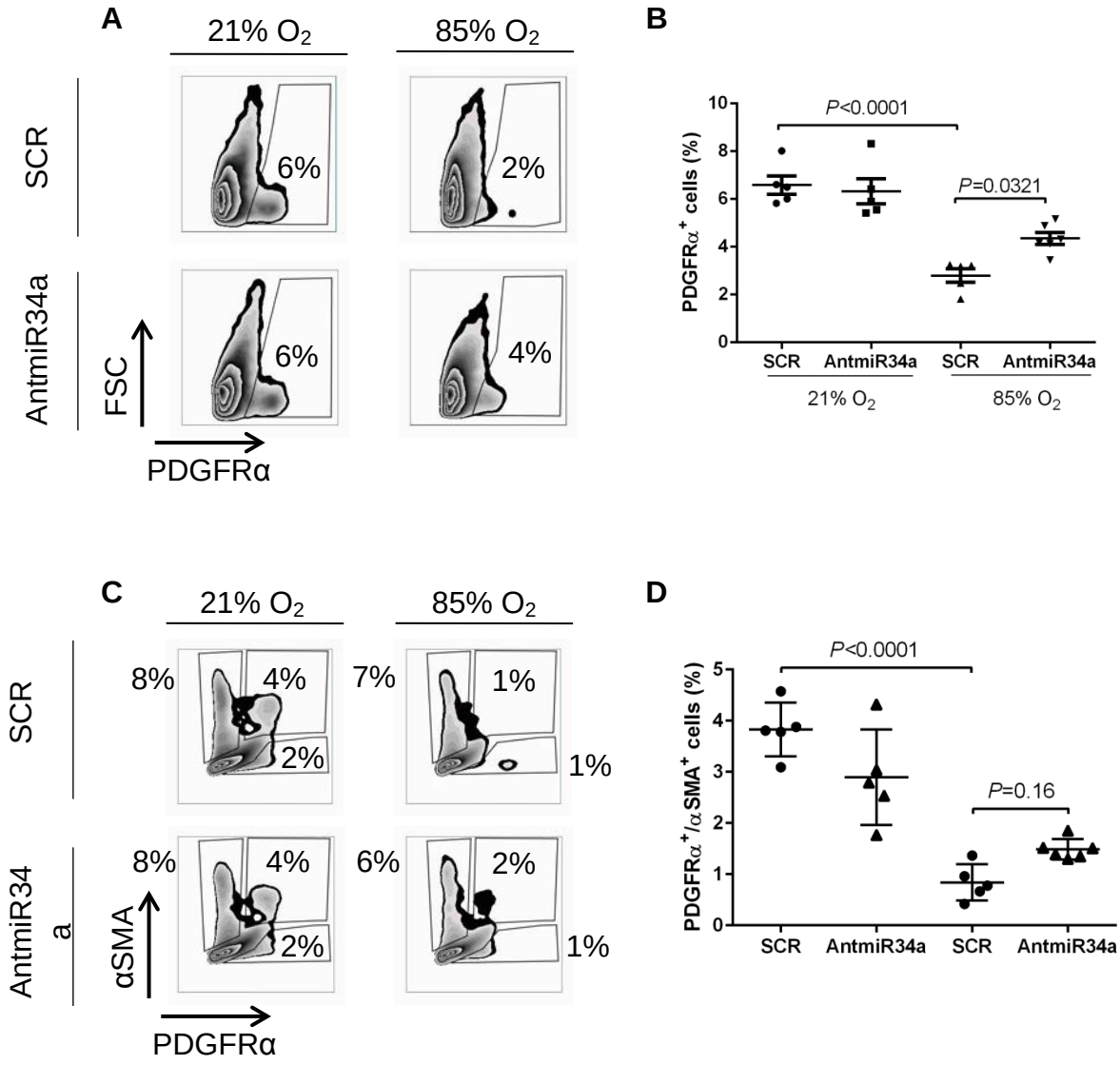

Figure 15. Myofibroblast abundance in the lung is partially restored in mice treated with antagomiR-34a in the bronchopulmonary dysplasia animal model. Newborn mice were injected with scrambled antagomiR (SCR) or antagomiR-34a (AntmiR34a) and exposed to 21% or 85% O_2. Lungs were isolated and homogenized at P5.5 and the cell suspension stained for PDGFRα and αSMA for FACS analysis. (**A**) Illustration of the gating strategy for PDGFRα$^+$ cell analyse. (**B**) Quantification of the PDGFRα$^+$ cells analysed by FACS. (**C**) Illustration of the gating strategy for αSMA$^+$/PDGFRα$^+$ cell analyse. (**D**) Quantification of the αSMA$^+$/PDGFRα$^+$ cell population analysed by FACS. Values are means ± SD. A one-way ANOVA followed by Tukey's *post hoc* test was used to determine the *P* values.

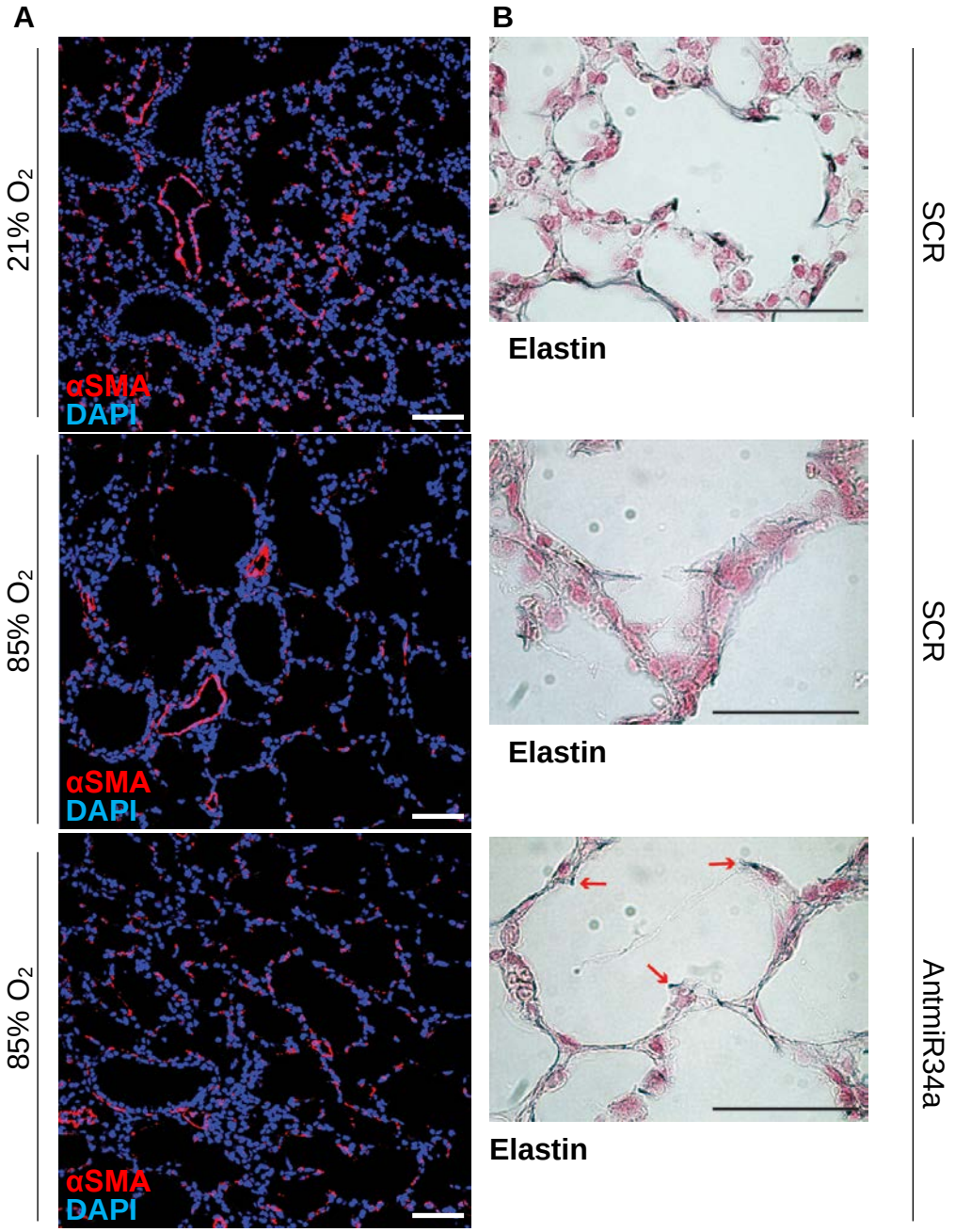

Figure 16. Better organised elastin foci were observed in the developing lungs of mice treated with antagomiR-34a in the bronchopulmonary dysplasia animal model. To study the presence of and the elastin production by myofibroblasts, pups were treated with scrambled antagomiR (SCR) or antagomiR-34a (AntmiR34a) and exposed to 21% or 85% O_2 from P1.5 until P14.5. Lungs embedded in paraffin were cut into sections for αSMA (red) (**A**) and elastin staining (black dots and fibres; pointed out by red arrows) (**B**). Scale bars, 50 µm.

crests after AntmiR34a injection in mice exposed to 85% O_2. Summing up, these findings suggested that miR-34a negatively regulates the myofibroblast transdifferentiation through PDGFRα modulation during aberrant late lung development caused by hyperoxia.

8.9 miR-34a is partially responsible for the increased apoptosis observed in the bronchopulmonary dysplasia animal model

Since miR-34a is reported to target molecules involved in regulating the cell cycle (17, 55), and the miR-34a blockade reduced apoptosis in the heart (4, 9), the amount of cell apoptosis and proliferation were evaluated to understand the mechanisms that thinned the septa in hyperoxic mouse lungs treated with AntmiR34a. Thus, pups were treated with SCR or AntmiR34a and exposed to 21% or 85% O_2. Whole-cell lung suspensions from P5.5 lungs were stained for annexin V (**Fig. 17A**) and for Ki67 (**Fig. 17B**), robust markers for apoptosis and proliferation, respectively. The FACS analysis revealed an increased apoptotic cell number in the SCR-treated mice exposed to 85% O_2 compared to pups under normoxic conditions (**Fig. 18A** and **18C**). Notably, the level of cell apoptosis was almost normalized in the lungs of AntmiR34a-treated mice under hyperoxic conditions. On the other hand, the AntmiR34a did not improve the severely diminished number of proliferative cells observed in the SCR-treated mice exposed to 85% O_2 (**Fig. 18B** and **18D**). In conclusion, miR-34a was mainly involved in triggering apoptosis rather than decreasing proliferation in lung cells from mouse developing lungs under hyperoxic conditions.

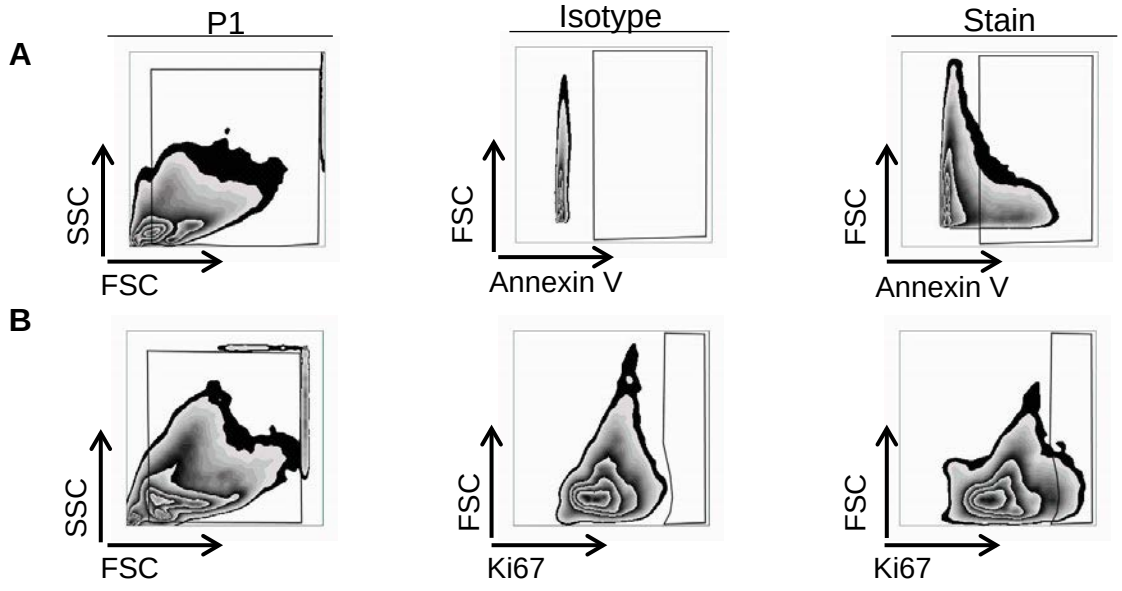

Figure 17. Gating strategy for annexin V^+ or $Ki67^+$ cells by FACS analysis. (**A**) Representative illustrations of the gates to assess the number of annexin V^+ (**A**) and $Ki67^+$ cells (**B**). Inside the population 1 (P1), within which cells with a FSC < 30 are excluded, a plot of FSC (y-axes) *versus* APC or PE is employed to assess stained cells compared to the correspondent isotype control. FSC, forward scatter; SSC, side scatter.

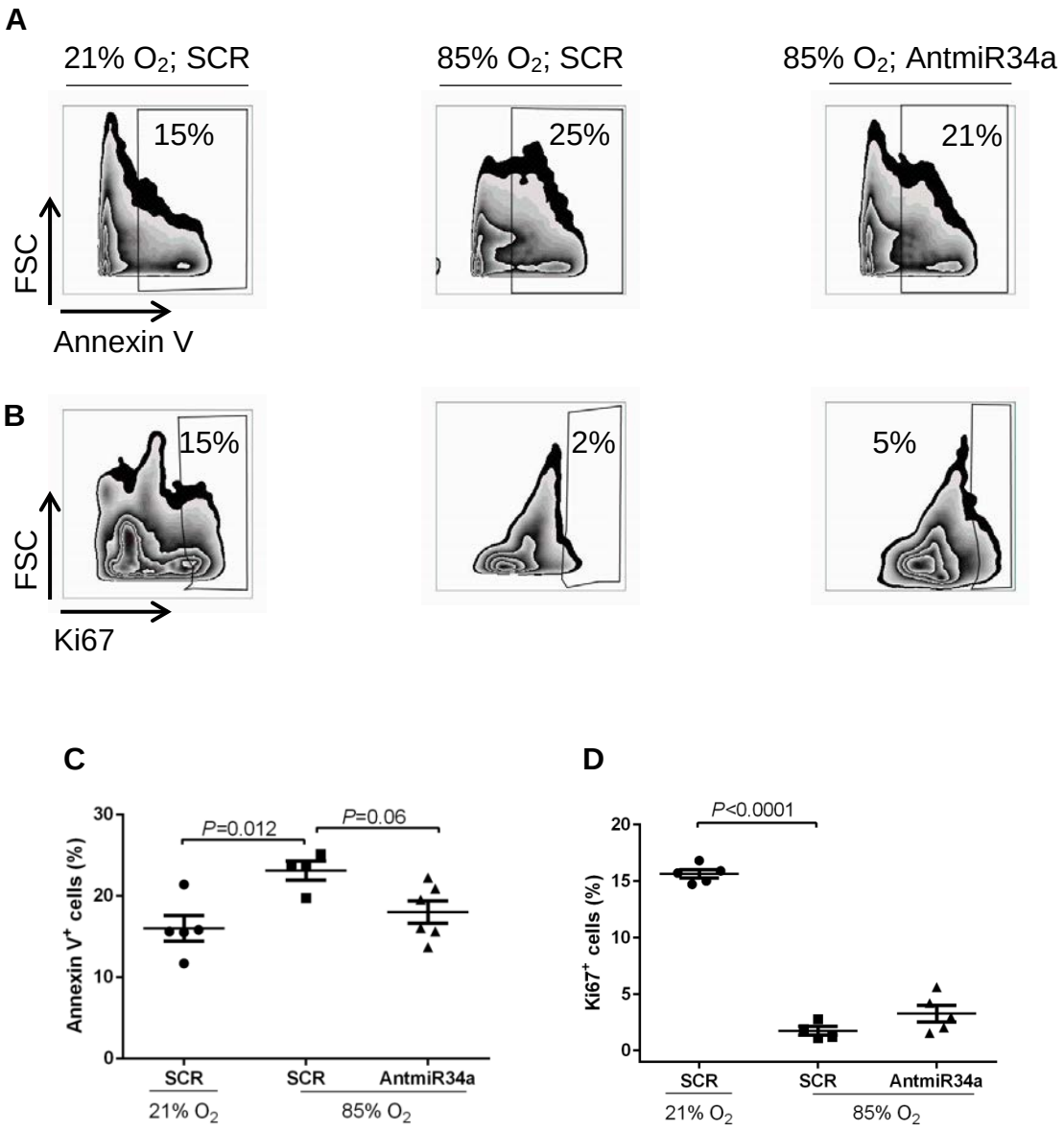

Figure 18. AntagomiR-34a administration reduced apoptosis but not cell proliferation levels in mouse lungs in the bronchopulmonary dysplasia animal model. Newborn mice were exposed to 21% or 85% O_2 and treated with scrambled antagomiR (SCR) or antagomiR-34a (AntmiR34a) since P1.5. Mice lungs were harvested at P5.5 and whole-lung cell suspensions were stained with annexin V for measuring apoptosis (**A**) or with Ki67 for measuring proliferation (**B**). Quantification of cells positive for apoptosis (**C**) and for proliferation (**D**) was carried out. Values are means ± SD; *n*=4-5. A one-way ANOVA followed by Tukey's *post hoc* test was applied to determine the *P* values. FSC, forward scatter.

8.10 Dysfunctionality of miR-34a under hyperoxic conditions leads to a decrease in apoptosis in almost every cell-type evaluated.

Since epithelial cells are one of the cell population largely present in the lung parenchyma, and since PDGFRα$^+$ cells have a great relevance during secondary septation, to assess whether miR-34a promoted apoptosis of AEC1 cells under hyperoxic conditions was a priority in order to understand the decreased mean septal wall thickness. For this purpose, WT pups were treated with SCR or AntmiR34a and concomitantly exposed either to 21% or 85% O_2. Then, mice were sacrificed at P5.5 for FACS analysis of the apoptotic epithelial (**Fig. 19A**-**C**). Firstly, the numbers of each cell population were assessed in order to later determine the number of apoptotic cells. Gated frequencies of epithelial lung cells (EpCAM$^+$), including epithelial cells from airway and alveolar epithelium, were slightly diminished under hyperoxic conditions (from 22% in the normoxic control group to 16% in the hyperoxic control group) and were not significantly changed after miR-34a blockade (from 16% in the hyperoxic control group to 18% in the AntmiR34a treated mice) under hyperoxic conditions (**Fig. 20A**). From the EpCAM$^+$ cell population, AEC1 cells were quantified (T1α$^+$ cells of EpCAM$^+$ cell population). Interestingly, the hyperoxia stimulus significantly increased the AEC1 cell proportion inside the epithelial cell population (from 36% in the normoxic control group to 43% in the hyperoxic control group) which was partially restored when miR-34a was blocked (38% in the AntmiR34a-treated group) (**Fig 20C**). Regarding the apoptotic cell number, neither the EpCAM$^+$ cell population (9% in the normoxic control group to 10% in the hyperoxic control group) (**Fig. 20B**) nor the AEC1 cell population (28% in the normoxic control group to 28% in the hyperoxic control group) was affected under hyperoxic conditions (**Fig. 20D**). However, the apoptotic cells decreased in cell number when miR-34a was blocked under hyperoxic conditions in both EpCAM$^+$ (from 10% in the SCR-treated mice to 9% in the AntmiR34a-treated mice) and AEC1 cells (from 28% in the SCR-treated mice to 21% in the AntmiR34a-treated mice). Taken together, AEC1 cell population, which increased in number in mouse lungs treated with SCR and exposed to hyperoxia, was partially normalized after miR-34a blockade by AntmiR34a injection because miR-34a reduced the number of apoptotic cells of AEC1 cell population in mouse lungs maintained under hyperoxic conditions.

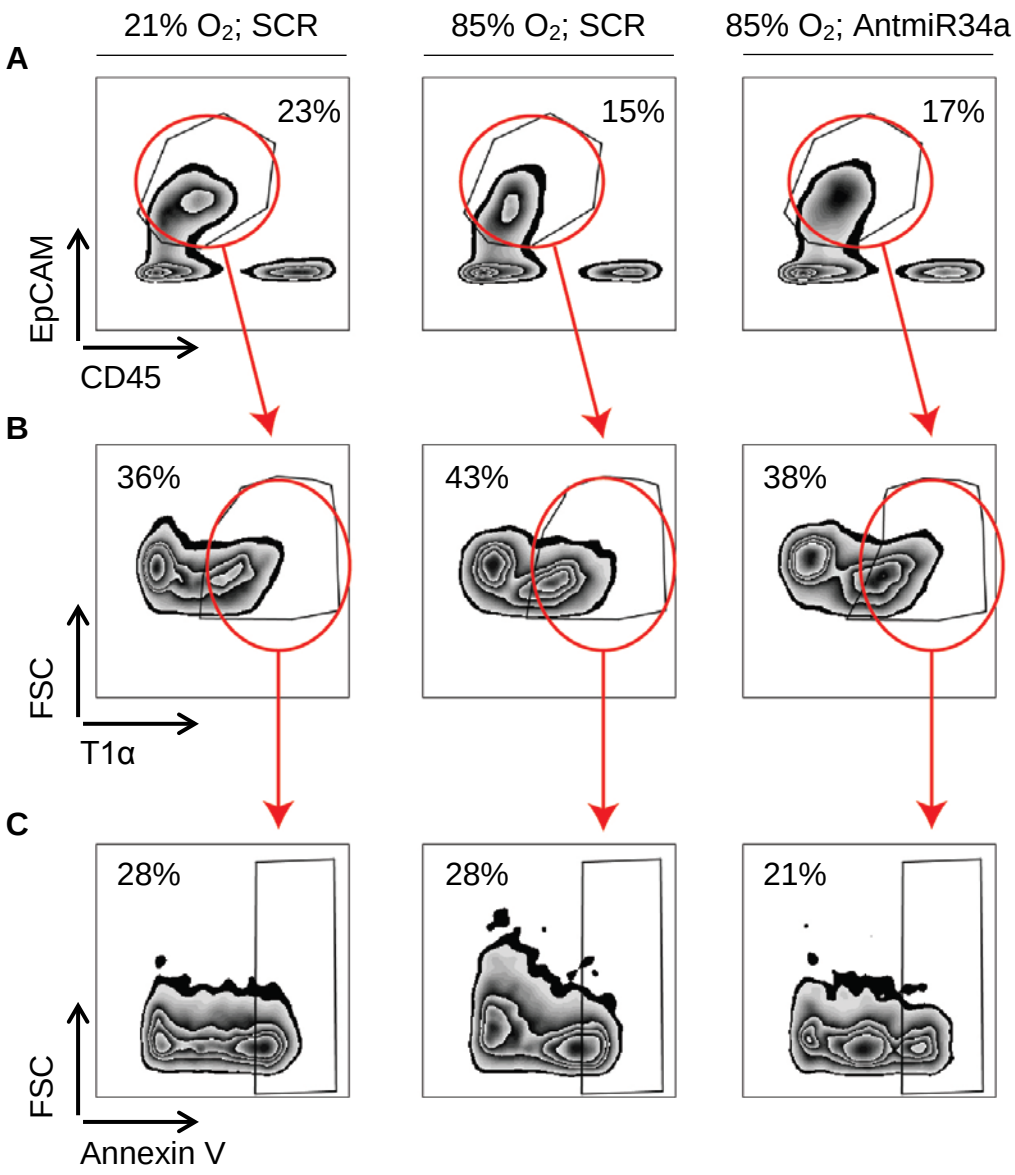

Figure 19. Reduction of apoptosis in different cell-types of the lung after blockade of miR-34a in mice maintained under hyperoxic conditions. Wild-type newborn mice were treated with scrambled antagomiR (SCR) or antagomiR-34a (AntmiR34a) and concomitantly exposed to either 21% or 85% O_2, and euthanized at P5.5. The whole-lung cell suspensions prepared from the different experimental groups were stained for several cell markers, and annexin V to measure apoptosis. EpCAM (**A**) is gated in the graph by $CD45^+$ cell exclusion and, following the red arrow, $T1\alpha^+$ cells are gated from the $EpCAM^+$ cell population (**B**). Indicated by the red arrow, annexin V^+ cells from the $EpCAM^+/T1\alpha^+$ cell population were assessed (**C**). Following the same procedure, the annexin V^+ cell population was discriminated from the $EpCAM^+$ cell population. FSC, forward scatter.

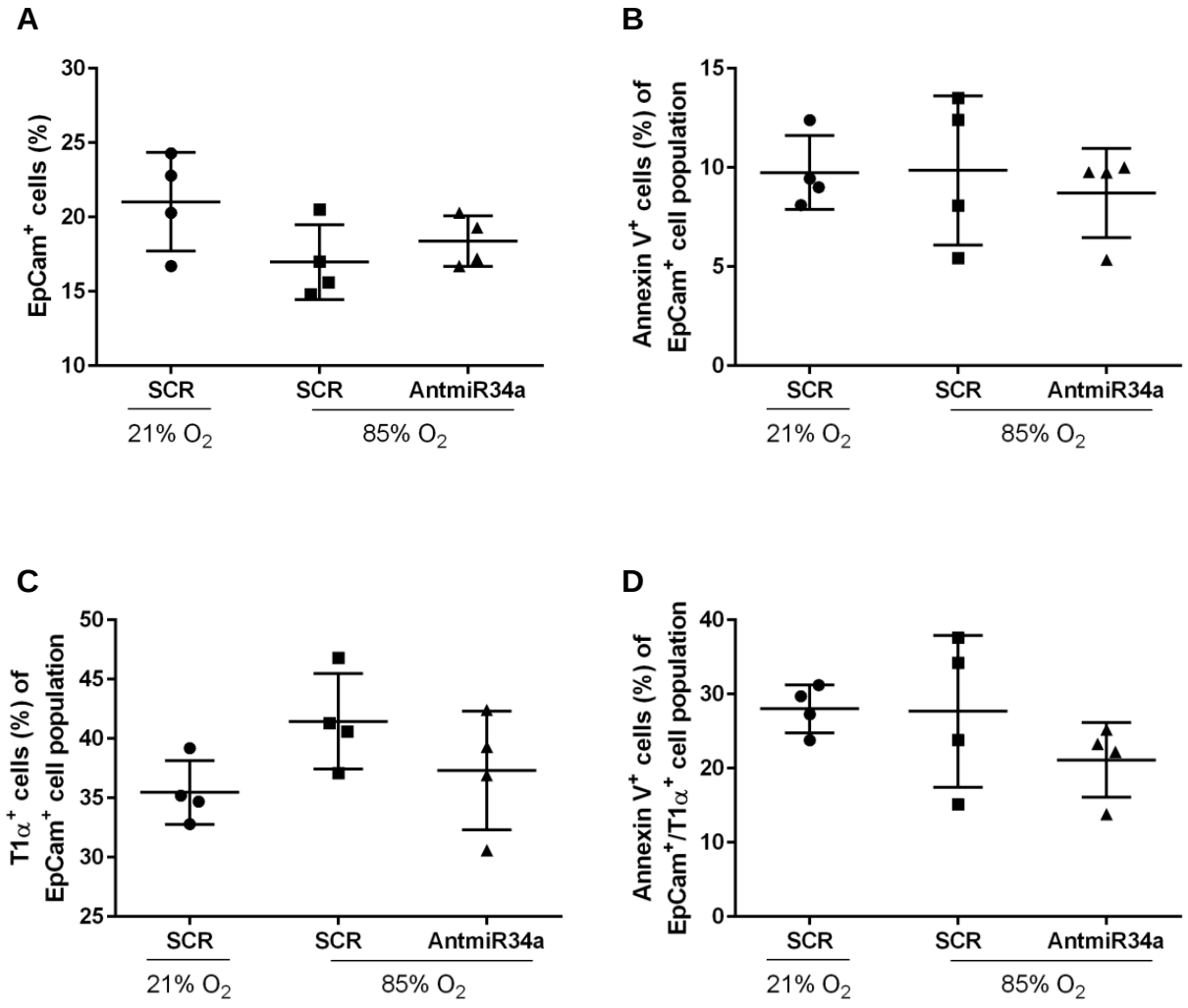

Figure 20. Quantification of apoptotic epithelial and myofibroblast cells in the lungs of mice treated with antagomiR-34a under hyperoxic conditions. Mouse pups were treated with scrambled antagomiR (SCR) or antagomiR-34a (AntmiR34a) and exposed to 21% O_2 or 85% O_2. At P5.5, lungs were harvested and whole-lung cell suspension was stained for EpCAM, CD45, T1α and annexin V for FACS analysis. After FACS analysis, every cell-type and the annexin V^+ cells within each cell-type were quantified for statistical analysis. $EpCAM^+$ cells (**A**) and $T1\alpha^+$ cells of $EpCAM^+$ cell population (**C**) were quantified together with the corresponding level of apoptosis (**B** and **D**, respectively). Values are means ± SD; *n*=4. A one-way ANOVA followed by Tukey's *post hoc* test was applied to determine the *P* values.

8.11 miR-34a is responsible for the thickened septa: what cells constitute the thickened alveolar septum?

In an attempt to better understand whether a change in a specific cell-type is responsible for the diminishing of the mean septal wall thickness after AntmiR34a administration, several immunofluorescent stainings for different cell-markers were carried out. Newborn mice were injected with SCR or AntmiR34a and exposed to either 21% or 85% O_2. After two weeks, paraffin sections of mouse lungs were stained with 4',6-diamidino-2-phenylindole (DAPI) revealing an accumulation of cells in the growing septa in the SCR-treated mouse group which was not observed in the AntmiR34a-treated mouse group maintained under hyperoxic conditions (**Fig. 21A**). In order to explore whether epithelial cells are forming the observed thickened septa since epithelial cells are one of the most abundant cell-type in the lung, AEC1 cells and AEC2 cells were analysed by immunofluorescence staining. After analysis under confocal microscopy, both AEC1 cell (**Fig. 21B**) and AEC2 cell (**Fig. 21C**) populations did not exhibit any apparent change in the cell abundance, comparing the SCR-treated mice with AntmiR34a-treated mice exposed to 85% O_2. Taken together, hyperoxia exposure drove an accumulation of epithelial cells in the septal wall, resulting in an increased septal wall thickness, which was partially decreased because the epithelial cells in septal wall cells were distributed in a single layer without changing the cell abundance after AntmiR34a administration.

.

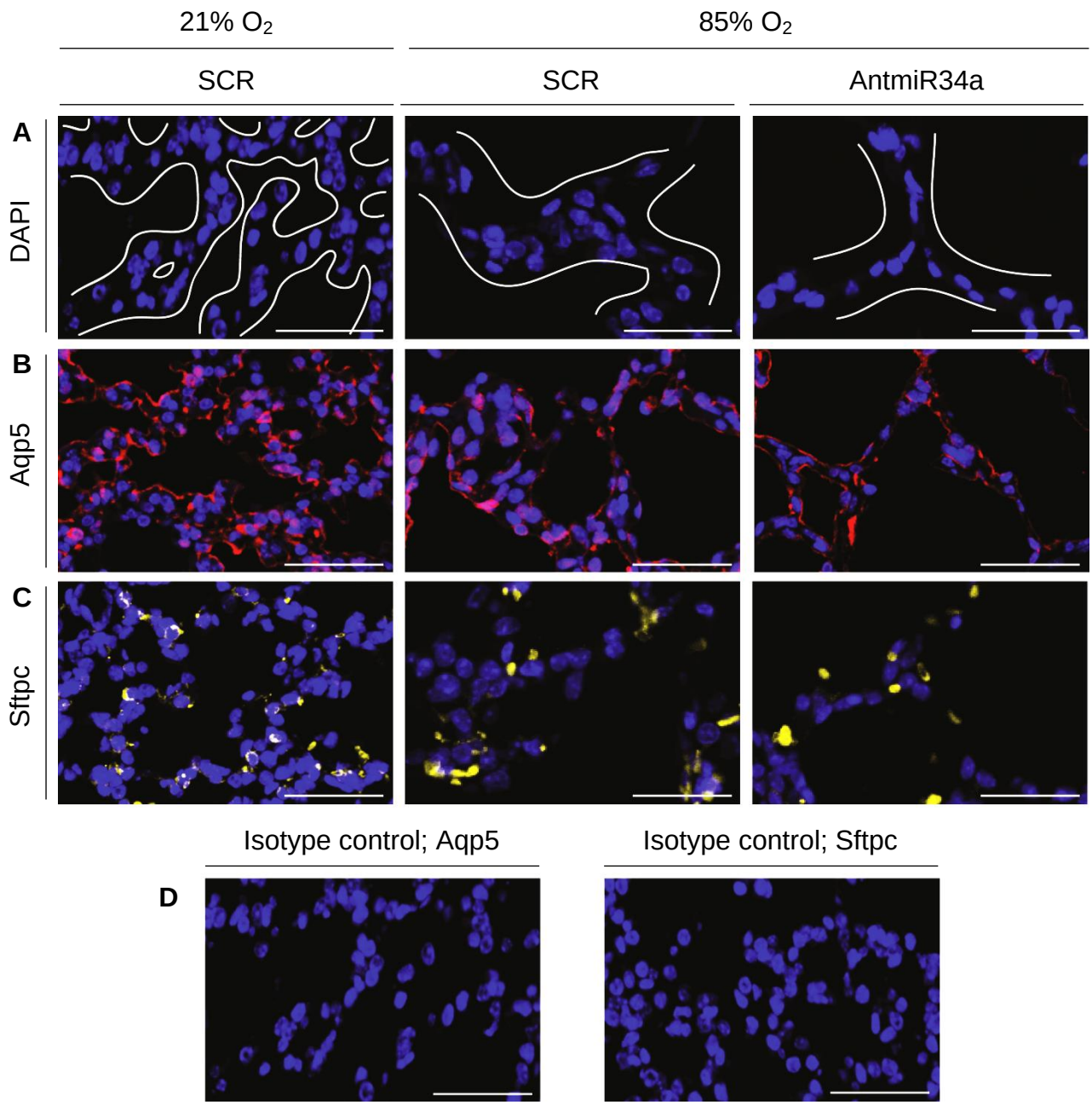

Figure 21. The cell composition of the septa after antagomiR-34a injection in mice maintained under hyperoxic conditions. Newborn mice were treated with scrambled antagomiR (SCR) or antagomiR-34a (AntmiR34a) and exposed to 21% or 85% O_2. Mouse lungs were harvested at P14.5 to obtain paraffin sections which were stained with 4',6-diamidino-2-phenylindole (DAPI) (**A**) in the SCR-treated mice and AntmiR34a-treated mice maintained under hyperoxic conditions. Representative images of paraffinized lung sections stained for Aquaporin-5 (Aqp5; in red) (**B**), and proSurfactant protein-C (Sftpc; in yellow) (**C**), in order to observe the cell abundance in the lungs of mice exposed to 85% O_2. Note the isotype control stainings for both Aqp5 and Sftpc in **D**. Scale bars, 50 µm.

9. Discussion

Previous studies have highlighted the dysregulation of several miRs in different BPD animal models (49). However, the causal role for these dysregulated miRs in aberrant late lung development caused by hyperoxia is not well understood. This is the first study supporting miR-34a as a key regulator of lung alveolarization in mice maintained under hyperoxic conditions.

The initial question posed in this study was whether any miR was involved in late lung development under normal or hyperoxic conditions. A starting point to address this question was the validation of several dysregulated miRs after hyperoxia insult that were identified in a miR microarray previously carried out in the laboratory. The miR-34a-5p (referred to as miR-34a) (**Fig. 7**) was the most up-regulated member of the miR-34 family in aberrant late lung development caused by hyperoxia. This finding was consistent with a previous study that identified miR-34a as being amongst the up-regulated miRs in hyperoxic rat lungs (7).

Several stereological approaches that aimed at studying a global or cell-specific miR-34a loss-of-function were performed in order to investigate the role of miR-34a during late lung development. In first instance, a global deletion of miR-34a increased the total number of alveoli (from $1.32 \pm 0.16 \times 10^6$ alveoli in WT mice to $1.94 \pm 0.17 \times 10^6$ alveoli lungs in miR-34a$^{-/-}$ exposed to 85% O_2); and, decreased the mean septal wall thickness, (from 12.09 ± 0.18 µm in WT mice to 8.47 ± 1.19 µm in miR-34a$^{-/-}$ mice exposed to 85% O_2) (**Fig. 8**). However, these increased numbers in the total number of alveoli and mean septal wall thickness still fall short of the $4.61 \pm 0.49 \times 10^6$ alveoli, and, 11.01 ± 0.93 µm mean septal wall thickness observed in healthy pups exposed to 21% O_2. Similar improvements in lung structure were observed when AntmiR34a was administered to pups under hyperoxic conditions. The total number of alveoli increased from $1.22 \pm 0.09 \times 10^6$ alveoli in SCR-treated mice to $2.03 \pm 0.18 \times 10^6$ alveoli in AntmiR34a-treated mice exposed to 85% O_2; whereas, the septal wall thinned out, from 17.81 ± 1.77 µm in SCR-treated mice to 10.15 ± 1.04 µm in AntmiR34a-treated mice and exposed to 85% O_2. Although the total number of alveoli was not fully restored ($4.57 \pm 0.35 \times 10^6$ alveoli in SCR-treated mice exposed to 21% O_2), the septal wall thickness improved reaching values that were noted under conditions of normal lung development (11.10 ± 0.32 µm in SCR-treated mice under normoxic conditions) (**Fig. 13**). These data suggest that

miR-34a is responsible for negatively regulating alveologenesis in the lungs of mice maintained under hyperoxic conditions. Since blocking miR-34a did not fully restore the lung structure in developing mouse lungs exposed to hyperoxia, other experiments targeting other dysregulated miRs might be required to further dissect the molecular basis of BPD.

Concerning the function of miR-34a, little is known in the BPD context. The interaction between miR-34a and *Pdgfra* mRNA has been bioinformatically predicted and has been experimentally validated by another group (24) in a lung cancer cell line. Therefore, it was important to validate the interaction between miR-34a and *Pdgfra* mRNA in primary mouse lung fibroblasts (**Fig. 10B**). In addition, PDGFRα has been reported as a required receptor for a proper lung alveolarization (11). Therefore, to reveal the location of miR-34a in order to know whether miR-34a was exerting the function via repressing *Pdgfra* mRNA was important. A β-galactosidase activity stain revealed that miR-34a is expressed in the developing septa, and the miR-34a expression levels were particularly enriched in PDGFRα^{+} sorted cells from P5.5 newborn mice exposed to 85% O_2 (**Fig. 9**) when compared to the normoxic control group. The importance of these findings resides in that both miR-34a and PDGFRα were co-expressed in the same cell-type and at the same time-point, supporting the idea that miR-34a acts through *Pdgfra* mRNA repression. Thus, following the same experimental set-up of AntmiR34a, a mixture of two TSBs, which blocked the interaction between miR-34a and *Pdgfra* mRNA, was administered to newborn mice exposed to 85% O_2. A similar improvement in the total number of alveoli was observed (from 1.32 ± 0.08 × 10^6 alveoli lungs in SCR-treated mice to 1.77 ± 0.12 × 10^6 alveoli lungs in TSB1,2-treated mice under hyperoxic conditions); whereas, septal wall thickness was decreased [from 13.97 ± 0.63 µm in SCR-treated mice to 11.69 ± 0.55 µm (**Fig. 12**)]. The main conclusion of this experiment is that miR-34a negatively regulates alveologenesis via *Pgdfra* mRNA repression in every cell in which *Pdgfra* and miR-34a were co-expressed in the lungs of mice maintained under hyperoxic conditions.

Since the TSB reagents did not exclusively impact PDGFRα^{+} cells, an experiment to specifically protect PDGFRα^{+} cells from miR-34a in newborn mice was carried out in order to investigate the role of miR-34a within the PDGFRα^{+} cell population in aberrant mouse lung development caused by hyperoxia. The effect of having deleted

miR-34a in PDGFRα^{+} cells (while the other cell populations of the lung were unaffected) under hyperoxic conditions was an increased total number of alveoli (from 1.25 ± 0.09 × 10^6 alveoli in miR-34a$^{wt/wt}$ to 2.11 ± 0.05 × 10^6 alveoli in miR-34a$^{-/-}$ mice exposed to 85% O_2) (**Fig. 11**). However, the mean septal wall thickness was not affected (11.11 ± 1.35 μm in miR-34a$^{wt/wt}$ and 10.68 ± 1.18 μm in miR-34a$^{-/-}$ mice exposed to 85% O_2). A recent study demonstrated that cottonseed oil improved lung structure in developing mouse lungs under hyperoxic conditions (50). Therefore, since Miglyol 812, the solvent of tamoxifen, is a caprylic/capric triglyceride mixture it is possible that septa were prevented from thickening in these mouse lungs treated with tamoxifen and exposed to hyperoxia. Therefore, these data revealed that an aberrant up-regulation of miR-34a expression levels specifically in the mesenchymal PDGFRα^{+} cells negatively regulated alveologenesis in mouse lungs under hyperoxic conditions.

These four separate approaches aimed at modulating miR-34a function revealed a significant enhancement in terms of alveolarization and septal wall thickness in developing mouse lungs under hyperoxic conditions compared to the respective control groups. However, not all four approaches exhibited a similar magnitude of improvement. The alveolar density assessed from mice carrying a cell-specific miR-34a deletion in PDGFRα^{+} cells was the highest amongst the four approaches, which means that miR34a$^{i\Delta PC/i\Delta PC}$ mouse lungs developed the highest number of bridges closing the alveolar sacs (**Fig. 22A**). On the other hand, the total number of alveoli, which is normalized to lung volume, is approximately the same in all four different approaches, except the total number of alveoli assessed in TSB-treated mice and exposed to 85% O_2, which was the lowest of the four (**Fig. 22B**). The septal wall thickness was substantially reduced in every approach, with a minor effect in the TSB-treated mice (**Fig. 22C**). The variability in the observed improvement in developing mouse lungs can be explained by the different effect triggered by the different ways of modulating miR-34a function in mouse pups. For example, the administration of Antmir34a blocked mainly miR-34a but also miR-34b and miR-34c. Thus, the effect produced by AntmiR34a administration in mouse developing lungs was a general blockade of the entire miR-34 family and, as a possibility, this could have protected any mRNA targeted by the members of the miR-34 family in every cell in the lung. Conversely, administration of TSB aimed to block only one interaction, the interaction between miR-34a and *Pdgfra*, while the rest of the

miR-34a targets remained unaffected, explaining why the effect was milder compared to the other approaches. In the case of PDGFRα$^+$ cell-specific miR-34a deletion, the aim was to delete miR-34a and prevent *Pdgfra* mRNA down-regulation in these mesenchymal PDGFRα$^+$ cells. However, the absence of miR-34a likely prevent the down-regulation of other validated miR-34a targets (27, 33, 55), which could have enhanced the performance of the PDGFRα$^+$ cells during lung alveolarization in mice exposed to hyperoxia. Furthermore, the effect of the global deletion of miR-34a involved all the mRNA targeted exclusively by miR-34a exhibiting similar results to the AntmiR34a approach. This might be because the miR-34a expression level is the most up-regulated in mouse lungs under hyperoxic conditions (**Fig. 7**) and the blockade of miR-34b and miR-34c by AntmiR34a might not contribute to such an extent in enhancing alveologenesis in mouse lungs.

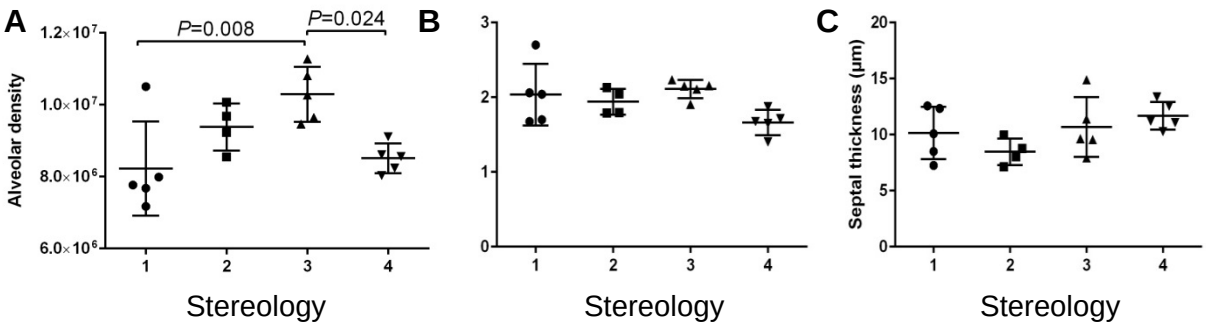

Figure 22. Comparison between the different treatments which blocked miR-34a function in mice maintained under hyperoxic conditions. The effect on lung structure of the four different approaches to modulate miR-34a function under hyperoxic conditions is compared. (**A**) Alveolar density; (**B**) total number of alveoli; and, (**C**) septal wall thickness. 1, antagomiR-34a treatment; 2, global miR-34a deletion; 3, PDGFRα$^+$ cell-specific miR-34a deletion; and, 4, target-site blocker treatment. Values are mean ± SD. A one-way ANOVA with Tukey's *post hoc* test was used to determine *P* values.

In an attempt to investigate the miR-34a-*Pdgfra* interaction, further experiments addressing the abundance of the PDGFRα$^+$ cell population were carried out. Since miR-34a expression was up-regulated *in vivo* (**Fig. 7**), the first question to address was whether PDGFRα protein levels were down-regulated because of miR-34a repression in mouse lungs in the BPD animal model. An initial assessment by western blot was followed by FACS analysis to improve the accuracy of the results which revealed a significant increase of PDGFRα$^+$ cells after AntmiR34a administration in mice under hyperoxic conditions (**Fig. 15A** and **15B**). This strongly

suggested a link between the miR-34a repressor role and the low PDGFRα$^+$ cell abundance in the BPD animal model. However, since blocking miR-34a did not restore PDGFRα$^+$ cell abundance observed in the lungs of healthy pups (**Fig 15A** and **15B**), other stimuli must negatively affect the PDGFRα$^+$ cell abundance. Other experiments addressing the mechanisms negatively regulating such an important mesenchymal cell population during lung alveolarization need to be performed.

The same experiment that revealed the key role of PDGFRα in orchestrating the secondary crest growth (11) reported that the deletion of the PDGFRα ligand, PDGFA, resulted in the loss of myofibroblasts in developing septa of mouse lungs (10). Building on that observation, several studies have focused on the cell biology of myofibroblasts during late lung development in mice, and the resulting consensus was that a cell must express, at least, both PDGFRα and αSMA proteins to be a myofibroblast (41, 42). Therefore, the next question to address was whether myofibroblasts were affected, and whether miR-34a was modulating the myofibroblast fate in aberrant mouse lung development caused by hyperoxia exposure. Thus, whole-lung cell suspensions obtained from P5.5 newborn mice treated with AntmiR34a and placed into the hyperoxia chamber were stained for PDGFRα and αSMA for FACS analysis. The data revealed not only an increased number of PDGFRα$^+$ cells but also an increased number of double-positive PDGFRα$^+$/αSMA$^+$ cells (**Fig. 15C** and **15D**). This evidence supported miR-34a as a negative regulator of alveolar myofibroblast transdifferentiation during aberrant secondary septation caused by hyperoxia. However, this conclusion has a weak point. Although myofibroblasts do express PDGFRα and αSMA protein, [amongst other markers such as CD49e (1)], the location of this cell-type must be taken into account since myofibroblasts are present in both the vasculature and the alveolar septal wall. Thus, while this project aimed at elucidating the events taking place in the septa, using whole-lung cell suspension analysis by FACS did not allow the discrimination between alveolar or vascular myofibroblasts. Therefore, the samples used for the FACS analysis could have been enriched by vascular, not alveolar myofibroblasts. To test this possibility, paraffin-embedded lungs of mice treated with AntmiR34a and exposed to 85% O_2 were cut into slices and then stained for αSMA and for elastin. From these stainings an increased abundance of αSMA$^+$ cells in the septa (**Fig. 16A**) and a better distribution of elastin (**Fig. 16B**) when miR-34a was blocked under hyperoxic conditions, compared to the controls, were observed. In

addition, another line of evidence indirectly supporting an increased myofibroblast abundance in the alveolar region is the increased alveolar number scored by stereological analysis in AntmiR34a-treated mice exposed to 85% O_2 (**Fig. 13C**). Having an increased abundance of alveolar myofibroblasts would likely lead to a higher number of secondary growing crest, giving rise to a larger total number of alveoli in the lung under hyperoxic conditions. Thus, the increased myofibroblast population observed by FACS analysis after the miR-34a blockade under hyperoxic conditions was, most probably, due to an increased alveolar but not vascular myofibroblast abundance.

Another crucial point to address was the reason behind the thinning of the alveolar septa in mouse lungs under hyperoxic conditions. Although this is a well-documented phenomenon which occurs from P12.5 to P14.5 (42), the various stereological approaches revealed an abnormally decreased septal wall thickness. To better understand the reason of the septal wall thinning, total levels of apoptosis and proliferation were assessed, resulting in a clear involvement of miR-34a in triggering apoptosis but not in blocking proliferation in P5.5 mouse lungs under hyperoxic conditions (**Fig. 18A**-**D**). Therefore, an experiment aiming at detecting which cell population changed the number of apoptotic cells in developing mouse lungs treated with AntmiR34a and exposed to hyperoxia was performed. An increased number of AEC1 cells, which are one of the most abundant cell type in the lung, and PDGFRα$^+$ cells together with a decreased number of apoptotic cells in each population AntmiR34a-treated mice exposed to hyperoxia was noted (**Fig. 20**). These observations supported an increased number of epithelial and mesenchymal cell populations which, in turn, would explain a better epithelial-mesenchymal cross-talk as a basis for a better alveolarization and diminished septal wall thickness observed in P14.5 AntmiR34a-treated mice exposed to hyperoxia. Then, in an attempt to better characterize the thinned septa observed when miR-34a was blocked under hyperoxic conditions, several immunofluorescent stainings were performed on P14.5 lung sections from mice treated with SCR or AntmiR34a and exposed either to 21% or 85% O_2. The first observation was a better distribution of the septal wall cells which became distributed in a single layer (**Fig. 21B**) instead of the stacked septal cells observed in the hyperoxic control group (**Fig. 21A**). Regarding the detection of cell types in the septa of mouse lungs treated with AntmiR34a and maintained under hyperoxic conditions, alveolar myofibroblasts abundance, revealed by increase in

αSMA$^+$ (**Fig. 16A**) fluorescent cells, was remarkably more apparent. Additionally, the increased number of double-positive PDGFRα$^+$/αSMA$^+$ cells (**Fig. 15C** and **15D**) further supported alveolar myofibroblasts as the cell-type most affected in the septa of mouse developing lungs treated with AntmiR34a and maintained under hyperoxic conditions. On the other hand, AEC2 cells and endothelial cells did not exhibit any change in the septa of mouse lungs treated with AntmiR34a and maintained under hyperoxic conditions. Therefore, the thinning of the septa observed after AntmiR34a administration is due to an increased myofibroblast cell population and a better cellular organization in mouse lungs. However, the mechanisms behind the thinning of the septa are not clear: a) are the cells distributed in a single layer because AntmiR34a is releasing other miR-34a mRNA targets involved in cell-cell cross-talk and subsequently cells are better organised?; b) are the rescued myofibroblasts enhancing the epithelial-mesenchymal cross-talk and producing more ECM components (**Fig. 16B**), and thus facilitating a better distribution of the cells?; c) there is a reason to suspect that the septa thin out might be due to a higher cell demand for covering the increased parenchymal surface (**table 7**) and, since cell proliferation is not restored after AntmiR34a injection (**Fig. 18B** and **18D**), cells distributed in a single layer to cover the surface area; or, d) all the former speculations combined at once led to the thinning of the septa in the lung.

In addition, an mRNA microarray was performed to evaluate whether any mRNA expression levels were affected in mouse lungs injected with AntmiR34a (data sets available at the GEO database under accession number GSE89730). The aim of this microarray was to identify changes at mRNA level that could highlight signalling pathways related to cellular organization in mouse lungs treated with AntmiR34a and maintained under hyperoxic conditions. Unexpectedly, the analysis and validation of the microarray revealed no change at the mRNA expression level in the AntmiR34a-treated group compared to SCR-treated group at both P5.5 and P14.5 under hyperoxic conditions. This observation has several different possible explanations: a) the changes that AntmiR34a triggered were reflected at protein level, not detected by the mRNA microarray; or, b) the mRNA differential expression might be happening in particular cell-types not detected by the microarray since the microarray was performed in whole-lung homogenates which could mask events taking place in particular cell-types. The last possibility being the case, single-cell sequencing would be a better approach to evaluate the differential gene expression.

This study unravelled a mechanism of action for miR-34a through a specific interaction with *Pdgfra* mRNA, as hinted at by the data collected from the TSB-treated mice exposed to 85% O_2 (**Fig. 12**). Nevertheless, the possibility that miR-34a exerted the function through other mRNA targets exists. For example, previous studies related to heart research reported that blocking miR-34a by AntmiR34a injection protected cardiac cells from apoptosis [consistent with the findings of this study (**Fig. 18A** and **18C**)] and, subsequently, improved heart function after disease (4, 9, 65). However, the reported mechanism of action of miR-34a was through a different target than *Pdgfra*, such as protein phosphatase 1 regulatory subunit 10 (4). A different study reported that miR-34a delayed the cell cycle through interaction with retinoic acid-inducible gene 1 in cervical cancer cells (63). This evidence indicates that miR-34a most likely interacted with other mRNA species to perform other functions in the lungs of mice maintained under hyperoxic conditions, since the effect of the TSB administration was milder than the AntmiR34a injection. Thus, further experiments based on a TSB intervention protecting other miR-34a mRNA targets might be required to further characterize the miR-34a mechanism of action.

In conclusion, these findings support miR-34a as an important negative regulator of alveologenesis in aberrant late lung development caused by hyperoxia exposure in mice. These experiments unravel a new pathway for miR-34a through *Pdgfra* mRNA which, in turn, reduced the PDGFRα$^+$ and double-positive PDGFRα$^+$/αSMA$^+$ cell population which are myofibroblasts. In every experiment involving transgenic or WT mice which involved a global or cell-specific deletion of miR-34a, the lung structure improved in terms of alveolarization and septal wall thickness. Here, strong evidence supporting miR-34a as a part of the intricate dysregulated gene network, which disturbs secondary septation under hyperoxia injury, is reported. Since recent articles highlighted the importance of miR-34a in humans (45), miR-34a should be considered to study in samples from infants suffering from BPD to potentially propose miR-34a as a candidate for future BPD treatment.

10. Summary

Bronchopulmonary dysplasia (BPD) is a chronic lung disease of preterm newborns characterized by a simplification of the distal lung structure because of a lack of alveoli formation. The receptor platelet-derived growth factor receptor (PDGFR)α, expressed by α smooth muscle actin $(SMA)^+$ myofibroblasts, is critical for a proper epithelial-mesenchymal cross-talk required for the formation of alveoli during secondary septation. In BPD, PDGFRα is found down-regulated but the reason for this is unknown.

In a study of mouse lungs exposed to a hyperoxia-based BPD animal model, a microRNA (miR) microarray revealed the up-regulation of miR-34a expression levels. Therefore, the aim was to reduce miR-34a levels *in vivo* and, for this, an experiment based on a global miR-34a deletion was carried out, resulting in an improvement of the alveolarization and decrease of the septal wall thickness in mice under hyperoxic conditions. As *Pdgfra* mRNA was found to be a miR-34a target, another experiment blocking the miR-34a-*Pdgfra* interaction by means of TSBs was performed and resulted in an increased total number of alveoli and decreased mean septal wall thickness in mouse lungs under hyperoxic conditions. The same improved lung structure was observed when either miR-34a was deleted specifically in $PDGFR\alpha^+$ cells or blocked by an antagomiR-34a (AntmiR34a) in mice under hyperoxic conditions. Regarding the mechanism, miR-34a was expressed in cells located in the developing septa and showed a surprising up-regulated miR-34a expression level in $PDGFR\alpha^+$ sorted cells from P5.5 newborn mice under hyperoxic conditions. The receptor PDGFRα is important for the transdifferentiation of myofibroblasts which are placed in the growing septal tips and producing extracellular matrix (ECM) compounds such as elastin under normal conditions. After blocking miR-34a by AntmiR34a, both $PDGFR\alpha^+$ cells and double-positive $PDGFR\alpha^+/\alpha SMA^+$ cells were partially rescued in the BPD animal model assessed by FACS. Additionally, a higher number of αSMA^+ was observed in the septa together with a better deposition and distribution of elastin revealing a better myofibroblast function. In addition, AntmiR34a administration decreased the level of generalized apoptosis and contributed to a better cell organization in the septa. These data suggested a novel role of miR-34a as a new negative regulator of alveologenesis through *Pdgfra* in a BPD animal model.

11. Zusammenfassung

Bronchopulmonale Dysplasie (BPD) ist eine chronische Lungenerkrankung frühgeborener Kinder. Ein Hauptmerkmal der BPD ist eine Vereinfachung der distalen Anteile der Lungenstruktur aufgrund einer Fehlbildung der Lungenbläschen, der Alveolen. Der platelet-derived growth factor receptor (PDGFR) α ist wesentlich an der epithelialen-mesenchymalen Interaktion, die für eine korrekte Bildung von Alveolen notwendig ist beteiligt und wird unter anderem in α smooth muscle actin (SMA) positiven Myofibroblasten exprimiert. Während der BPD wurde eine Herunterregulation von PDGFRα gezeigt. Die zu Grunde liegenden Mechanismen sind derzeit jedoch nicht bekannt.

In Studien an postnatalen Mauslungen aus dem Hyperoxie basierten Tiermodel der BPD zeigten microRNA (miR) microarray Analysen eine Hochregulation von miR-34a. Die Zielsetzung dieser Arbeit war die Reduzierung der Expression von miR-34a *in vivo* und die Analyse der Auswirkung auf die Veränderung der Lungenstruktur im Hyperoxie basierten BPD Model. Diesbezüglich wurde in Mäusen eine globale Gendeletion von miR-34a *in vivo* durchgeführt. Es zeigte sich eine verbesserte Alveolarisierung und eine Verdünnung der Alveolarsepten unter Deletion von miR-34a in den der Hyperoxie ausgesetzten Mauslungen. Ein Zielgen von miR-34a ist die mRNA von *Pdgfra*. Um eine spezifische Blockade der Interaktion von miR-34a und der mRNA von *Pdgfra* zu erzielen, wurde ein *target-site blocker in vivo* appliziert. Dies führte zu einer Erhöhung der Anzahl der Alveolen und einer Reduzierung der Wanddicke der Alveolarsepten. Gleiche Effekte auf die Anzahl der Alveolen und die Wanddicke der Alveolen wurden durch Deletion von miR-34a in PDGFRα-positiven ($PDGFR\alpha^+$) Zellen als auch durch die Blockade von miR-34a durch antagomiR-34a (AntmiR34a) Applikation *in vivo* ausgelöst. Analysen in neu geborenen Mäusen an postnatal Tag (P)5.5 im Hyperoxie basierten BPD Model zeigten, dass miR-34a in Zellen der sich entwickelnden Alveolarsepten lokalisiert ist und in $PDGFR\alpha^+$ Zellen, welche an P5.5 isoliert wurden heraufreguliert ist. Der PDGFRα ist wesentlich für die Transdifferenzierung von Myofibroblasten. Myofibroblasten befinden sich in den sich entwickelnden Alveolarsepten und bilden extrazelluläre Matrix Komponenten wie beispielsweise Kollagen und Elastin unter physiologischen Bedingungen. Eine Blockade von miR-34a durch AntmiR34a im Hyperoxie basierten BPD Model zeigte in FACS Analysen eine teilweise Aufhebung

der Reduzierung sowohl der PDGFRα^{+} Zellen als auch der PDGFRα^{+} und αSMA^{+} doppelpositiven Zellen in den der Hypoxie ausgesetzten Mäusen. Darüber hinaus zeigten sich mehr αSMA^{+} Zellen in den Alveolarsepten, sowie eine besser organisierte Ablagerung und Verteilung von Elastin als Zeichen einer verbesserten Funktion der Myofibroblasten. Zudem zeigte sich der Grad der allgemeinen Apoptose vermindert und führte zu einer verbesserten Organisation der Alveolarsepten.

Diese Ergebnisse deuten auf eine neue Rolle von miR-34a als negativer Regulierer der Bildung von Alveolarsepten über PDGFRα im Hyperoxie basierten Tiermodel der BPD hin.

12. Bibliography

1. **Akamatsu T, Arai Y, Kosugi I, Kawasaki H, Meguro S, Sakao M, Shibata K, Suda T, Chida K, and Iwashita T**. Direct isolation of myofibroblasts and fibroblasts from bleomycin-injured lungs reveals their functional similarities and differences. *Fibrogenesis & Tissue Repair* 6: 15-21, 2013.

2. **Ali Z, Schmidt P, Dodd J, and Jeppesen DL**. Bronchopulmonary dysplasia: a review. *Archives of Gynecology and Obstetrics* 288: 325-333, 2013.

3. **Berg JT, Breen EC, Fu Z, Mathieu-Costello O, and West JB**. Alveolar hypoxia increases gene expression of extracellular matrix proteins and platelet-derived growth factor-B in lung parenchyma. *American Journal of Respiratory and Critical Care Medicine* 158: 1920-1928, 1998.

4. **Bernardo BC, Gao XM, Winbanks CE, Boey EJ, Tham YK, Kiriazis H, Gregorevic P, Obad S, Kauppinen S, Du XJ, Lin RC, and McMullen JR**. Therapeutic inhibition of the miR-34 family attenuates pathological cardiac remodeling and improves heart function. *Proceedings of the National Academy of Sciences of the United States of America* 109: 17615-17620, 2012.

5. **Betsholtz C**. Insight into the physiological functions of PDGF through genetic studies in mice. *Cytokine & Growth Factor Reviews* 15: 215-228, 2004.

6. **Betsholtz C**. Role of platelet-derived growth factors in mouse development. *The International Journal of Developmental Biology* 39: 817-825, 1995.

7. **Bhaskaran M, Xi D, Wang Y, Huang C, Narasaraju T, Shu W, Zhao C, Xiao X, More S, Breshears M, and Liu L**. Identification of microRNAs changed in the neonatal lungs in response to hyperoxia exposure. *Physiological Genomics* 44: 970-980, 2012.

8. **Bitterman PB, Rennard SI, Adelberg S, and Crystal RG**. Role of fibronectin as a growth factor for fibroblasts. *The Journal of Cell Biology* 97: 1925-1932, 1983.

9. **Boon RA, Iekushi K, Lechner S, Seeger T, Fischer A, Heydt S, Kaluza D, Treguer K, Carmona G, Bonauer A, Horrevoets AJ, Didier N, Girmatsion Z, Biliczki P, Ehrlich JR, Katus HA, Muller OJ, Potente M, Zeiher AM, Hermeking H, and Dimmeler S**. MicroRNA-34a regulates cardiac ageing and function. *Nature* 495: 107-110, 2013.

10. **Bostrom H, Gritli-Linde A, and Betsholtz C**. PDGF-A/PDGF alpha-receptor signaling is required for lung growth and the formation of alveoli but not for early lung branching morphogenesis. *Developmental Dynamics: an official publication of the American Association of Anatomists* 223: 155-162, 2002.

11. **Bostrom H, Willetts K, Pekny M, Leveen P, Lindahl P, Hedstrand H, Pekna M, Hellstrom M, Gebre-Medhin S, Schalling M, Nilsson M, Kurland S, Tornell J, Heath JK, and Betsholtz C**. PDGF-A signaling is a critical event in lung alveolar myofibroblast development and alveogenesis. *Cell* 85: 863-873, 1996.

12. **Bruce MC, and Honaker CE**. Transcriptional regulation of tropoelastin expression in rat lung fibroblasts: changes with age and hyperoxia. *The American Journal of Physiology* 274: L940-950, 1998.

13. **Burri PH**. Fetal and postnatal development of the lung. *Annual Review of Physiology* 46: 617-628, 1984.

14. **Bursuker I, Rhodes JM, and Goldman R**. Beta-galactosidase--an indicator of the maturational stage of mouse and human mononuclear phagocytes. *Journal of Cellular Physiology* 112: 385-390, 1982.

15. **Cardarelli F, Digiacomo L, Marchini C, Amici A, Salomone F, Fiume G, Rossetta A, Gratton E, Pozzi D, and Caracciolo G**. The intracellular trafficking mechanism of Lipofectamine-based transfection reagents and its implication for gene delivery. *Scientific Reports* 6: 512-519, 2016.

16. **Chao CM, El Agha E, Tiozzo C, Minoo P, and Bellusci S**. A breath of fresh air on the mesenchyme: impact of impaired mesenchymal development on the pathogenesis of bronchopulmonary dysplasia. *Frontiers in Medicine* 2: 27-35, 2015.

17. **Chen F, and Hu SJ**. Effect of microRNA-34a in cell cycle, differentiation, and apoptosis: a review. *Journal of Biochemical and Molecular Toxicology* 26: 79-86, 2012.

18. **Choi YJ, Lin CP, Ho JJ, He X, Okada N, Bu P, Zhong Y, Kim SY, Bennett MJ, Chen C, Ozturk A, Hicks GG, Hannon GJ, and He L**. miR-34 miRNAs provide a barrier for somatic cell reprogramming. *Nature Cell Biology* 13: 1353-1360, 2011.

19. **Concepcion CP, Han YC, Mu P, Bonetti C, Yao E, D'Andrea A, Vidigal JA, Maughan WP, Ogrodowski P, and Ventura A**. Intact p53-dependent responses in miR-34-deficient mice. *PLoS Genetics* 8: 121-130, 2012.

20. **de Antonellis P, Medaglia C, Cusanelli E, Andolfo I, Liguori L, De Vita G, Carotenuto M, Bello A, Formiggini F, Galeone A, De Rosa G, Virgilio A, Scognamiglio I, Sciro M, Basso G, Schulte JH, Cinalli G, Iolascon A, and Zollo M**. MiR-34a targeting of Notch ligand delta-like 1 impairs CD15+/CD133+ tumor-propagating cells and supports neural differentiation in medulloblastoma. *PLOS ONE* 6: 541-552, 2011.

21. **Dong J, Carey WA, Abel S, Collura C, Jiang G, Tomaszek S, Sutor S, Roden AC, Asmann YW, Prakash YS, and Wigle DA**. MicroRNA-mRNA interactions in a murine model of hyperoxia-induced bronchopulmonary dysplasia. *BMC Genomics* 13: 204-213, 2012.

22. **El Agha E, and Bellusci S**. Walking along the Fibroblast Growth Factor 10 Route: A Key Pathway to Understand the Control and Regulation of Epithelial and Mesenchymal Cell-Lineage Formation during Lung Development and Repair after Injury. *Scientifica* 2014: 469-477, 2014.

23. **Garcia DM, Baek D, Shin C, Bell GW, Grimson A, and Bartel DP**. Weak seed-pairing stability and high target-site abundance decrease the proficiency of lsy-6 and other microRNAs. *Nature Structural & Molecular Biology* 18: 1139-1146, 2011.

24. **Garofalo M, Jeon YJ, Nuovo GJ, Middleton J, Secchiero P, Joshi P, Alder H, Nazaryan N, Di Leva G, Romano G, Crawford M, Nana-Sinkam P, and Croce CM**. MiR-34a/c-Dependent PDGFR-alpha/beta Downregulation Inhibits Tumorigenesis and Enhances TRAIL-Induced Apoptosis in Lung Cancer. *PLOS ONE* 8: 812-820, 2013.

25. **Griffiths-Jones S, Grocock RJ, van Dongen S, Bateman A, and Enright AJ**. miRBase: microRNA sequences, targets and gene nomenclature. *Nucleic Acids Research* 34: D140-144, 2006.

26. **Harris KS, Zhang Z, McManus MT, Harfe BD, and Sun X**. Dicer function is essential for lung epithelium morphogenesis. *Proceedings of the National Academy of Sciences of the United States of America* 103: 2208-2213, 2006.

27. **He L, He X, Lim LP, de Stanchina E, Xuan Z, Liang Y, Xue W, Zender L, Magnus J, Ridzon D, Jackson AL, Linsley PS, Chen C, Lowe SW, Cleary MA, and Hannon GJ**. A microRNA component of the p53 tumour suppressor network. *Nature* 447: 1130-1134, 2007.

28. **Herriges M, and Morrisey EE**. Lung development: orchestrating the generation and regeneration of a complex organ. *Development (Cambridge, England)* 141: 502-513, 2014.

29. **Hogan BL, Barkauskas CE, Chapman HA, Epstein JA, Jain R, Hsia CC, Niklason L, Calle E, Le A, Randell SH, Rock J, Snitow M, Krummel M, Stripp BR, Vu T, White ES, Whitsett JA, and Morrisey EE**. Repair and regeneration of the respiratory system: complexity, plasticity, and mechanisms of lung stem cell function. *Cell Stem Cell* 15: 123-138, 2014.

30. **Hsia CC, Hyde DM, Ochs M, and Weibel ER**. An official research policy statement of the American Thoracic Society/European Respiratory Society: standards for quantitative assessment of lung structure. *American Journal of Respiratory and Critical Care Medicine* 181: 394-418, 2010.

31. **Rivers LE, Young KM, Rizzi M, Jamen F, Psachoulia K, Wade A, Kessaris N, Richardson WD.** PDGFRA/NG2 glia generate myelinating oligodendrocytes and piriform projection neurons in adult mice. *Nature Neuroscience* 11: 1392-1401, 2008.

32. **Kotton DN, and Morrisey EE**. Lung regeneration: mechanisms, applications and emerging stem cell populations. *Nature Medicine* 20: 822-832, 2014.

33. **Li Y, Guessous F, Zhang Y, Dipierro C, Kefas B, Johnson E, Marcinkiewicz L, Jiang J, Yang Y, Schmittgen TD, Lopes B, Schiff D, Purow B, and Abounader R**. MicroRNA-34a inhibits glioblastoma growth by targeting multiple oncogenes. *Cancer Research* 69: 7569-7576, 2009.

34. **Lizé M, Herr C, Klimke A, Bals R, and Dobbelstein M**. MicroRNA-449a levels increase by several orders of magnitude during mucociliary differentiation of airway epithelia. *Cell Cycle* 9: 4579-4583, 2014.

35. **Lize M, Pilarski S, and Dobbelstein M**. E2F1-inducible microRNA 449a/b suppresses cell proliferation and promotes apoptosis. *Cell Death and Differentiation* 17: 452-458, 2010.

36. **Lu J, Qian J, Chen F, Tang X, Li C, and Cardoso WV**. Differential expression of components of the microRNA machinery during mouse organogenesis. *Biochemical and Biophysical Research Communications* 334: 319-323, 2005.

37. **Lu Y, Okubo T, Rawlins E, and Hogan BL**. Epithelial progenitor cells of the embryonic lung and the role of microRNAs in their proliferation. *Proceedings of the American Thoracic Society* 5: 300-304, 2008.

38. **Madurga A, Mizikova I, Ruiz-Camp J, and Morty RE**. Recent advances in late lung development and the pathogenesis of bronchopulmonary dysplasia. *American Journal of Physiology-Lung Cellular and Molecular Physiology* 305: L893-905, 2013.

39. **Madurga A, Mizikova I, Ruiz-Camp J, Vadasz I, Herold S, Mayer K, Fehrenbach H, Seeger W, and Morty RE**. Systemic hydrogen sulfide administration partially restores normal alveolarization in an experimental animal model of bronchopulmonary dysplasia. *American Journal of Physiology-Lung Cellular and Molecular Physiology* 306: L684-697, 2014.

40. **Maniscalco WM, Watkins RH, Roper JM, Staversky R, and O'Reilly MA**. Hyperoxic ventilated premature baboons have increased p53, oxidant DNA damage and decreased VEGF expression. *Pediatric Research* 58: 549-556, 2005.

41. **McGowan SE, Grossmann RE, Kimani PW, and Holmes AJ**. Platelet-derived growth factor receptor-alpha-expressing cells localize to the alveolar entry ring and have characteristics of myofibroblasts during pulmonary alveolar septal formation. *Anatomical Record (Hoboken)* 291: 1649-1661, 2008.

42. **McGowan SE, and McCoy DM**. Fibroblasts expressing PDGF-receptor-alpha diminish during alveolar septal thinning in mice. *Pediatric Research* 70: 44-49, 2011.

43. **McGowan SE, and Torday JS**. The pulmonary lipofibroblast (lipid interstitial cell) and its contributions to alveolar development. *Annual Review of Physiology* 59: 43-62, 1997.

44. **Metzger RJ, Klein OD, Martin GR, and Krasnow MA**. The branching programme of mouse lung development. *Nature* 453: 745-750, 2008.

45. **Misso G, Di Martino MT, De Rosa G, Farooqi AA, Lombardi A, Campani V, Zarone MR, Gulla A, Tagliaferri P, Tassone P, and Caraglia M**. Mir-34: a new weapon against cancer? *Molecular Therapy Nucleic acids* 3: 387-398, 2014.

46. **Mizikova I, Ruiz-Camp J, Steenbock H, Madurga A, Vadasz I, Herold S, Mayer K, Seeger W, Brinckmann J, and Morty RE**. Collagen and elastin cross-linking is altered during aberrant late lung development associated with hyperoxia. *American Journal of Physiology-Lung Cellular and Molecular Physiology* 308: L1145-1158, 2015.

47. **Mosca F, Colnaghi M, and Fumagalli M**. BPD: old and new problems. *The Journal of Maternal-Fetal and Neonatal Medicine* 24 Supplement 1: 80-82, 2011.

48. **Nana-Sinkam SP, Karsies T, Riscili B, Ezzie M, and Piper M**. Lung microRNA: from development to disease. *Expert Review of Respiratory Medicine* 3: 373-385, 2009.

49. **Nardiello C, and Morty RE**. MicroRNA in late lung development and bronchopulmonary dysplasia: the need to demonstrate causality. *Molecular and Cellular Pediatrics* 3: 19-28, 2016.

50. **Nardiello C, Mižiková I, Silva DM, Ruiz-Camp J, Mayer K, Vadász I, Herold S, Seeger W, and Morty RE**. Standardisation of oxygen exposure in the development of mouse model for bronchopulmonary dysplasia. *Disease Models and Mechanisms* 10: 185-196, 2017.

51. **Northway WH, Jr., Rosan RC, and Porter DY**. Pulmonary disease following respirator therapy of hyaline-membrane disease. Bronchopulmonary dysplasia. *The New England Journal of Medicine* 276: 357-368, 1967.

52. **Ntokou A, Klein F, Dontireddy D, Becker S, Bellusci S, Richardson WD, Szibor M, Braun T, Morty RE, Seeger W, Voswinckel R, and Ahlbrecht K**. Characterization of the platelet-derived growth factor receptor-alpha-positive cell lineage during murine late lung development. *American Journal of Physiology-Lung Cellular and Molecular Physiology* 309: L942-958, 2015.

53. **Olave N, Lal CV, Halloran B, Pandit K, Cuna AC, Faye-Petersen OM, Kelly DR, Nicola T, Benos PV, Kaminski N, and Ambalavanan N**. Regulation of alveolar septation by microRNA-489. *American Journal of Physiology-Lung Cellular and Molecular Physiology* 310: L476-487, 2016.

54. **Popova AP, Bentley JK, Cui TX, Richardson MN, Linn MJ, Lei J, Chen Q, Goldsmith AM, Pryhuber GS, and Hershenson MB**. Reduced platelet-derived growth factor receptor expression is a primary feature of human bronchopulmonary dysplasia. *American Journal of Physiology-Lung Cellular and Molecular Physiology* 307: L231-239, 2014.

55. **Rock JR, and Hogan BL**. Epithelial progenitor cells in lung development, maintenance, repair, and disease. *Annual Review of Cell and Developmental Biology* 27: 493-512, 2011.

56. **Rokavec M, Li H, Jiang L, and Hermeking H**. The p53/miR-34 axis in development and disease. *Journal of Molecular Cell Biology* 6: 214-230, 2014.

57. **Ruiz-Camp J, Rodriguez-Castillo JA, Herold S, Mayer K, Vadasz I, Tallquist MD, Seeger W, Ahlbrecht K, and Morty RE**. Tamoxifen dosing for Cre-mediated recombination in experimental bronchopulmonary dysplasia. *Transgenic Research* 1:165-170, 2016.

58. **Silva DM, Nardiello C, Pozarska A, and Morty RE**. Recent advances in the mechanisms of lung alveolarization and the pathogenesis of bronchopulmonary dysplasia. *American Journal of Physiology-Lung Cellular and Molecular Physiology* 309: L1239-1272, 2015.

59. **Stein CA, Hansen JB, Lai J, Wu S, Voskresenskiy A, Hog A, Worm J, Hedtjarn M, Souleimanian N, Miller P, Soifer HS, Castanotto D, Benimetskaya L, Orum H, and Koch T**. Efficient gene silencing by delivery of locked nucleic acid antisense oligonucleotides, unassisted by transfection reagents. *Nucleic Acids Research* 38: 410-419, 2010.

60. **Torday JS, Torres E, and Rehan VK**. The role of fibroblast transdifferentiation in lung epithelial cell proliferation, differentiation, and repair in vitro. *Pediatric Pathology & Molecular Medicine* 22: 189-207, 2003.

61. **Treutlein B, Brownfield DG, Wu AR, Neff NF, Mantalas GL, Espinoza FH, Desai TJ, Krasnow MA, and Quake SR**. Reconstructing lineage hierarchies of the distal lung epithelium using single-cell RNA-seq. *Nature* 509: 371-375, 2014.

62. **Universities of Fribourg LaB**. Embryology, http://www.embryology.ch/anglais/rrespiratory/phasen07.html, 2008.

63. **Wang JH, Zhang L, Ma YW, Xiao J, Zhang Y, Liu M, and Tang H**. microRNA-34a-Upregulated Retinoic Acid-Inducible Gene-I Promotes Apoptosis and Delays Cell Cycle Transition in Cervical Cancer Cells. *DNA and Cell Biology* 35: 267-279, 2016.

64. **Winter J, Jung S, Keller S, Gregory RI, and Diederichs S**. Many roads to maturity: microRNA biogenesis pathways and their regulation. *Nature Cell Biology* 11: 228-234, 2009.

65. **Yang Y, Cheng HW, Qiu Y, Dupee D, Noonan M, Lin YD, Fisch S, Unno K, Sereti KI, and Liao R**. MicroRNA-34a Plays a Key Role in Cardiac Repair and Regeneration Following Myocardial Infarction. *Circulation Research* 117: 450-459, 2015.

66. **Zeltner TB, and Burri PH**. The postnatal development and growth of the human lung. II. Morphology. *Respiration Physiology* 67: 269-282, 1987.

13. Acknowledgements

My first words of gratitude are for my supervisor Dr. Rory Morty giving me the opportunity to experience the PhD adventure and to join MBML PhD programme. Thank you for your guidance along the project, your professionalism, for giving me the critical point of view of the well performed science and for the good moments.

I would like to thank Prof. Dr. Werner Seeger for all the internal lab meeting of the Department IV and his enthusiastic suggestions for every project. His scientific dedication is very inspiring. Also, I would like to thank Prof. Dr. Thomas Braun for his interesting suggestions that helped me to develop the project.

Thanks to all my lab members as together we could solve lots of problems with a charming environment. Thanks to Dr. Wujak for his advices, to Dr. Niess for the help with the car insurance, to Dr. Sakkas for the funny moments in the lab, to Dr. Likhoshvay for sharing with me her technical knowledge, Dr. Madurga for all the help and the good moments, to Ivana for the help and competition, to Diogao for the funny moments, to Claudio who always supported me, to Lina for all the help and coffees under the sun, to Alberto for his support and collaboration, to David for the interesting political chats, to Agnieszka for the great moments, Ettore (il romano) for your absolute support and to Francesco, the artisan of science. Thank you Philip, my first student, for your hard-working attitude and will for learning. Also, I would like to thank Dr. Ahlbrecht for the support and the technicians Diana and Nilifer for the help in the laboratory tasks and, thanks to our lovely secretary Monica (I will meet you in Roses).

Obviously, I could not forget my collaborator Dr. Quantius. Thanks for the long days in front of the Diva sorter which at the end were for something good.

Special thanks to my wife, Luciana. I do not think that going through this adventure named life and PhD would have been possible without you. I love you!

“No digas no puedo es no quiero”, esta ha sido la frase que siempre retumba en mi cabeza. Gracias a mis hermanos del barrio, gràcies als amics rabiolini i amigues pel vostre suport incondicional, gràcies a tots vosaltres! Mai ens hem separat.

Gracias papoia i gràcies mamoia, aquesta tesis us la dedico. Sou els millors, us estimo!

14. Declaration

I declare that I have completed this dissertation single-handedly without the unauthorized help of a second party and only with the assistance acknowledged therein. I have appropriately acknowledged and referenced all text passages that are derived literally from or are based on the content of published or unpublished work of others, and all information that relates to verbal communications. I have abided by the principles of good scientific conduct laid down in the charter of the Justus Liebig University of Giessen in carrying out the investigations described in the dissertation.

“This happens because this happens”

15. Appendix

List of peer-reviewed publications:

I. Madurga A, Mizikova I, **Ruiz-Camp J**, and Morty RE. Recent advances in late lung development and the pathogenesis of bronchopulmonary dysplasia. *American Journal of Physiology-Lung Cellular and Molecular Physiology* 305: L893-905, 2013.

II. Madurga A, Mizikova I, **Ruiz-Camp J**, Vadasz I, Herold S, Mayer K, Fehrenbach H, Seeger W, and Morty RE. Systemic hydrogen sulfide administration partially restores normal alveolarization in an experimental animal model of bronchopulmonary dysplasia. *American Journal of Physiology-Lung Cellular and Molecular Physiology* 306: L684-697, 2014.

III. Mizikova I, **Ruiz-Camp J**, Steenbock H, Madurga A, Vadasz I, Herold S, Mayer K, Seeger W, Brinckmann J, and Morty RE. Collagen and elastin cross-linking is altered during aberrant late lung development associated with hyperoxia. *American Journal of Physiology-Lung Cellular and Molecular Physiology* 308: L1145-1158, 2015.

IV. **Ruiz-Camp J** and Morty RE. Divergent fibroblast growth factor signaling pathways in lung fibroblast subsets: where do we go from here? *American Journal of Physiology-Lung Cellular and Molecular Physiology* 309(8): L751-5, 2015.

V. **Ruiz-Camp J**, Rodriguez-Castillo JA, Herold S, Mayer K, Vadasz I, Tallquist MD, Seeger W, Ahlbrecht K, and Morty RE. Tamoxifen dosing for Cre-mediated recombination in experimental bronchopulmonary dysplasia. *Transgenic Research* 1: 165-170, 2016.

VI. Nardiello C, Mižiková I, Silva DM, **Ruiz-Camp J**, Mayer K, Vadász I, Herold S, Seeger W, and Morty RE. Standardisation of oxygen exposure in the development of mouse model for bronchopulmonary dysplasia. *Disease Models and Mechanisms* 10: 185-196, 2017.